ANI

Analysis and **N**onparametric **I**nference in High Energy Physics and Astrophysics Experiments

Reference Manual

Version 98.5

Ashot Chilingarian
Yerevan Physics Institute, 2 Alikhanian Brothers, Yerevan 36, Armenia,
e-mail - chili@yerphi.am, ANI home-page: crdlx5.yerphi.am

June 10, 2000

Contents

List of Figures

List of Tables

Foreword

What ANI is Intended to Do.

The program represents an unified methodology of multivariate data analysis and physical inference for the high energy astroparticle physics experiments. It represents a novel approach to data analysis consisted of:

- optimal utilization of information contained in simulation (calibration) trials and experimental data;
- best feature subsets selection and initial dimensionality reduction;
- optimized methods of multivariate probability density estimation;
- scanning of multivariate distributions to investigate embedded nontrivial structures;
- nonparametric estimation of regression function;
- Neural and Bayesian classification and background rejection;

The main physical problems to be solved are:

- event -by - event (shower-by-shower) analysis of Extensive Air Shower (EAS) data;
- determination of the type and the energy of primary particles;
- hadronic background rejection in detection of very high energy gamma - quanta with imaging Cherenkov telescopes;
- determination of energy spectra of Primary Cosmic Radiation (PCR).
- estimation of the energy dependence of PCR;

What ANI is not Intended to Do.

- Simulation of nuclear - electromagnetic cascade in the atmosphere;
- estimation of the detector response;
- ANI is not intended also for the repeated solution of identically parameterized problems (such as shower size reconstruction) where a specialized program will be in general much more efficient.

Notation

d	Dimensionality
L	Number of classes
M	Number of experimental events
$\mathbf{v}_i$	Vector of measured variables
$\mathbf{u}_i$	Vector of simulated events
$(\mathcal{A}, \mathcal{P})$	Stochastic mechanism which generates experimental data
$(\mathcal{A}, \tilde{\mathcal{P}})$	"Controlled" stochastic mechanism, simulation program
$\mathcal{V}$	Event (measurement, feature) space
$\mathcal{A}$	Basic states space
$P_{\mathcal{A}}$	Prior measure
$\mathcal{C}_{\mathcal{A}\tilde{\mathcal{A}}}$	Losses (cost) measure
$p(\mathbf{v}/\mathcal{A}_k)$	Conditional probability density function
$\hat{p}(\mathbf{v}/\mathcal{A}_k)$	Estimate of conditional density
$\hat{p}(\mathcal{A}_i/\mathbf{v})$	Posterior density.

References

The basic idea of applied Bayesian statistics, that the probability is orderly opinion, and that inference from data is nothing other that the revision of such opinion in the light of relevant new information, was presented in [1, 2].

The posterior robustness of Bayesian decisions, as a key issue for applied statistical analysis was discussed and illustrated in [3, 4].

Among the current books on Bayesian statistics one of the best ones is [5].

Though simulation in data analysis in high energy physics is widely used, we can aware of a very few systematic investigations of theoretical aspects about how data may be compared with their simulated counterpart [6, 7, 9, 10].

The development of the Monte Carlo statistical inference for high energy astroparticle physics experiments data analysis is presented in [11, 12, 13, 14, 15, 16, 17, 18, 19, 20, 21].

The references on another key problem of applied Bayesian inference- nonparametric multivariate density estimation, could be found in tutorial section.

Further Remarks

This manual consists of four chapters:

- Introduction
- A reference guide explaining the concepts and ANI user interface;
- A tutorial about mathematical foundations of the Bayesian nonparametric statistical inference;
- Two tutorials on the ANI implementation and interpretation of results for the samples from Gaussian populations and for for KASCADE experiment data [22].

Acknowledgments

I am grateful to Prof. Dr. G. Schatz and Prof. Dr. H. Rebel and all members of KASCADE collaboration for the stimulating scientific atmosphere and supporting the interest in the development of the ANI program for KASCADE data analysis.

Dipl. Phys. M.Roth prepared full simulations of KASCADE experimental data used as a priory information for ANI, and he was instrumental in implementing different modes of ANI for KASCADE data analysis. Dipl. Phys. A.Vardanyan achieved several improvements of the neural modes of ANI and participated in testing ANI in various regimes. He wrote the description of ANI graphical interface.

Both M.Roth and A.Vardanyan have been very helpful in preparation of this manual.

The chapter 5 of this manual concerning KASCADE data analysis was prepared in collaboration with Prof. Dr. H.Rebel, Dipl. Phys. M.Roth and Dipl. Phys. A.Vardanyan.

I'm grateful to Dr. J.Knapp and Dr. M.Cowley for useful discussions and valuable remarks concerning new methods of data analysis. I thank the Wipple collaboration for the permission of the use of the Crab Nebula database.

The ANI graphical interface and genetic algorithm were designed and programmed by S.Chilingaryan. The calculations presented on figure (4.5) were prepared by E.Sevinian.

This work is part of a WTZ project (X131.2) of scientific cooperation between Forschungszentrum Karlsruhe, Germany and Yerevan Physics Institute, Armenia. It has been partly supported by the research grant number 94694 of Armenian government and by A116 ISTC grant.

Copyright notice

Yerevan Physics Institute undertakes no obligations for maintenance of the programs, nor responsibility for their correctness, and accepts no liability whatsoever resulting from the use of its programs.

All trademarks appearing in this user's manual are acknowledged as such.

Chapter 1

Introduction

1.1 Problems of Data Analysis in CR Physics

No model is true, only useful

Modern arrays of particle detectors covering a large area are measuring different parameters of numerous secondary products of the primary cosmic ray interactions with the atmosphere. Only a simultaneous measurement of a large number of independent parameters in each individual Extensive Air Shower can yield reliable information to reconstruct the Primary Cosmic Radiation particle mass and its energy as well as the phenomenological characteristics of strong interaction with atmosphere nuclei.

The ambiguity of interpretation of the results of experiments with cosmic rays is connected with both significant gaps in our knowledge of the characteristics of hadron - nuclear interaction at superaccelerator energies and indefiniteness of the primary cosmic ray composition, as well as - with strong fluctuations of all shower parameters. The extra difficulties are due to indirect experiments and hence, due to the use of Monte - Carlo simulations of development and detection of different components of nuclear electromagnetic cascade.

To make the conclusions about the investigated physical phenomenon more reliable and significant, it is necessary to develop a unified theory of statistical inference, based on nonparametric models, in which various nonparametric approaches (density estimation, Bayesian decision making, error rate estimation, feature extraction, sample control during handling, neural net models, etc...) would be incorporated.

The most important part of the presented approach is the quantitative comparison of multivariate distributions and use of a nonparametric technique to estimate the probability density in the multidimensional feature space. As compared to the earlier used methods of inverse problem solution, in ANI the object of analysis is each particular event (a point in the multivariate space of measured parameters - feature space) rather than alternative distributions of model and experimental data.

By considering all measured EAS parameters simultaneously we are able to incorporate important information about their relationship and outline in multidimensional feature space nonlinear regions where events of definite type mostly grouped. That is why, along with the averaged characteristics, the belonging of each experimental event to a certain class (primary nuclei group, energy interval) is determined.

The advocated approach was used to estimate the upper limit of the iron nuclei fraction according to the gamma - family characteristics, registered by PAMIR collaboration [23, 24, 25, 26, 27] . It was the first attempt to make PCR studies on event-by-event basis.

A multidimensional analysis was applied for classification of the Cherenkov light images of air showers registered by the Whipple observatory. It was shown that the use of several image parameters together with their correlations can lead to a reduction of the background rejection down to a few tenths of a percent while retaining about 50% of useful (gamma-rays induced) events. The application of multivariate technique to the famous Crab detection data file (Whipple observatory - 1988-1989) [29], proves the advantage of the new background suppression technique and - achievement of considerable enhancement of source detection significance [31, 32, 33, 34, 35, 36, 37, 38, 39, 40, 41, 42, 43, 44, 45].

From recently ANI is intensively used for KASCADE experiment data analysis [46, 47, 48, 49, 50, 51, 52, 53]. Already obtained preliminary results on the energy dependence of elemental composition, give hope for conducting the "mass spectroscopy" in "knee" region, and, therefore, addressing the PCR origin and acceleration problems.

1.2 Simulation for CR Physics Experiments

The most difficult and most important part of high energy physics data analysis is the comparison of competitive hypotheses and decision making on the nature of the investigated physical phenomenon.

In the cosmic ray physics the main technique of statistical inference, connected the with problem of determination of initial physical parameters (such as mass composition and energy spectrum of PCR, strong interaction characteristics, flux of very high energy gamma - quanta from point sources, etc...), - is the direct problem solution with detailed simulation of the cosmic ray traversal through the atmosphere and the experimental installation with a following comparison of the multivariate simulation and experimental data. Actually, an algorithm is constructed, which describes EAS development and registration of its different components on the observation level, which is based on a certain model of the process investigated, i.e. the set of the parameters that characterize the PCR flux and interaction of incident hadrons with the air nuclei.

By simulations with different models and comparing the experimental and model data, a class of models is selected, which describe the experimental data satisfactorily. Such an approach allows us to discard a certain class of non-satisfactory models, but the available experimental data do not allow one to select the only model among the many proposed.

For almost all problems of inference, the crucial question is whether the used models are in fact consistent with data.

Of course, any inference is conditioned on the model used, and, if the model is oversimplified, so that essential details are ever omitted, or improperly defined, at best only qualitative conclusions may be done.

The actual need of a a reliable reference M.C.code can be just illustrated by contradicting results of physical inferences on elemental composition, presented in the literature on basis of different simulation procedures.

Based on the measured intensity of gamma-families detected by emulsion chamber experiments at high mountain altitudes [56], the Fuji-Kanbala group concluded that beyond the knee iron nuclei are dominating in the primary flux [57]. On the other hand, using nearly the same data, the Chacaltaya and Pamir collaborations [58] insist that the origin of the knee is due to a change of the character of the hadronic interaction, while the elemental composition remains approximately unaltered.

Using an alternative observation technique the Fly's Eye group propagates in a number of papers [59] a significant change of primary composition towards approximately pure proton content at energies larger than $10^{17} eV$, in contrast to the Akeno group which could not find a significant change in composition at these energies [60]. These cases of conflicting results reflect essentially the different basis of the theoretical "calibration" of the data, in addition to inadequate simplifications of the analysis techniques.

There is a general agreement [55] about the vital importance to develop a reference simulation program that invokes the actually best and most detailed treatments of all physical processes, relevant to EAS development, in order to be used, tested and cross checked for consistency by different groups, without adapting the model parameters for each actual case in different way. What concerns such a program for simulations of the air shower development in the atmosphere, with the CORSIKA [54] program developed in context of the KASCADE experiment there is a modern code available, using efficient Monte-Carlo techniques. It includes various options of alternative interaction models, generally accepted to be valid up to $10^{16} - 10^{17}$ eV.

Similarly there is an established code: The CERN detector simulation package GEANT [61] for the simulation of detector response function of complex detector setups in presence of various different radiation sources. This widely used program and its procedures can be used to transform the theoretical EAS variables into the form they are potentially registered by the actual apparatus and can be compared with the real data. Both programs CORSICA and GEANT are published, freely accessible and matter of continuous refinements by concerned study groups.

In the interface of developing such a tool, providing significant reference samples of the observables, including realistically all types of fluctuations, and of the experimental task to setup a detector installation measuring with high fidelity as many as possible EAS parameters, a "comparator" is necessary, based on coherent statistical methods for the analysis of nonparametric multivariate distributions with hidden nonlinear dependences.

What we need is a well defined technique, what one can call Monte - Carlo Inference. The presented approach to develop such techniques considers the classification and hypothesis testing problems in the framework of Bayesian paradigm and the main steps of the unified data analysis methodology are as following.

1.3 ANI Strategy

1.3.1 Selection of the best subset of measured variables

The data preprocessing is a first step in data analysis.

Both experimental and simulation event are checked for "outliers" - events with very big descrepances according to "expected" values.

Then the "best subset of measurements" (in the sense of great discriminative value in heavy-light nuclei dilemma, or - of strong correlation with primary energy) is selected from a variety of potentially useful variables. Proceeding from the initial dimensionality, on each step of backward elimination a ”worst” feature is selected, according to reduction of Bhatacharya distance, calculated for all variants of the reduced subsets.

The quantitative comparison of variables is done by means of the so called P-values of statistical test, showing the relative discriminative value of the variable. The greater this value, the smaller the probability of the H_0 hypothesis to be correct. H_0 consists in the statement, that the two independent samples come from the one and the same population. The smaller this probability, one can reject this hypothesis with greater confidence and accept the alternative hypothesis: that two samples come from different populations. And the ”distance” between populations is proportional to the P-value. Three different tests are used: the parametric Student test, the nonparametric Kolmogorov - Smirnov and Mahn - Whitney tests. The last two does not require any assumptions about the shape of the underlying distributions.

Since interdependencies among the variables affect most of multivariate analyses procedures, it is worth examining the correlation matrix of EAS parameters.

The correlation analysis can help in the selection of the ”best” feature pairs . The calculated Fisher matrix values point on significant difference of pair-wise correlation in different classes.

1.3.2 Bayesian Analysis

Bayesian approach provides the general method of incorporating of prior and experimental information. Decision rule, that assigns observable $\mathbf{v}$ to the class with the highest a posterior density, takes into account all useful information and all possible losses due to any decision.

The posterior density is basis of statistical decisions on particle type and on simulation and experimental data closeness. The term closeness refers to the degree of coincidence, similarity, correlation, overlapping or any such measure. Bayes classifier provides minimum probability of error among all classifiers for the same feature set.

However, the Bayes classification meets several difficulties, as the analytic expressions of conditional densities and, hence, the posterior ones, are unknown. Therefore, we are obliged to use their nonparametric estimates.

Nonparametric in the sense, that density function is not a particular member of a previously chosen parametric distribution family, but an estimate based only on sample information and - on very mild conditions on the underlying density (usually only continuity). The well known Parzen and K Nearest Neighbors (KNN) estimators are used in ANI

The nonparametric regression is used for energy estimation . The peculiarity of solution of the regression problem in the cosmic - ray physics is the fact that neither the true spectrum $f(E)$ nor the conditional density $P(\mathbf{v}/E)$ are known in the general case.

The method is based on the obvious fact that the events close to each other in some metric in the feature space have similar energy - the geometrical consistence.

1.3.3 Neural Net Solutions

The alternative very powerful classification and estimation technique is connected with the development of mathematical models of Feed-Forward Neural Nets (FFNN). The input layer of the feed - forward network have one node for each feature, signal processing is performed layer by layer beginning from the input. Neurons of successive layers receive input only from neurons of the previous layer and each neuron in a given layer sends it's output to all nodes in the next layer. The neurons of the output layer produce the values of the the discriminant function.

The training is performed with simulated data or/and calibration results. The initial values of net parameters are chosen randomly from Gaussian population with zero mean and not large variance. The training of FFNN consists in multiple processing of all training samples with iterative modifications of connection coefficients (weights).

The quality function minimization is usually done by the "so called" back propagation method, the gradient descend is performed on the quality function with respect to the weights in order to minimize the deviations of the network response from the desired "goal" response. The main drawback of such methods is their convergence to local minimum, in contrast, implemented in ANI different scenario's of minima random search allows to escape from the local minimum region and continue the search.

A common complaint about these techniques is the dependence of the final classification scheme on the purity and finiteness of training sets (small training samples effects). However, due to the inherent robust characteristics of FFNN, classifiers results from neural analyses are relatively insensitive to modest impurities in the training sets.

1.3.4 Robustness Conception

In general, referring to a statistical estimator robustness means the insensitiveness to small departures from the idealized assumptions for which the estimator is optimized [63, 64]. The word "small" refers to both: small departures for all data, or large departures for a small number of data.

For example, the particular nonparametric density estimator have to be tuned according to the unknown distribution function. Our modification of estimators - the so called probability density L-estimator didn't require determination of the unique "best" parameter for the whole data set, rather a wide interval of parameters, one of which will be automatically chosen for the appropriate data point.

1.3.5 Visualization

For such abstract procedures as multivariate mapping and classification in multidimensional spaces, the visualization is of crucial importance.

After classifying experimental data according to training sample classes, a necessary analysis step is to examine the initial feature space for outlining the regions of acception of one or another hypotheses.

Usually there are physical arguments about location of such "clusters".

For example, "heave-nuclei" initiated events in $N_e - N_\mu$ coordinates tend to occupy left–top quarter; the Cherenkov images, initiated from primary γ–quanta, have very specific shape in Hillas parameter space, etc...

A special "DENCURVE" key word of ANI provide possibility to store the multidimensional (of course one-dimensional density estimates also) clusters in CERN PAW ntuples.

A special Bayesian scanning of multivariate space produces nonlinear multidimensional clusters corresponding to EAS, initiated from chosen primary nuclei group.

One can easily examine nonlinear interdependencies between EAS variables using wide possibilities of PAW utility.

1.3.6 Limitations and Perspectives of Development

The potential difficulties and limitations of the ANI package are connected with model dependence of statistical inference. The question of correctness of the model itself is always open and we need a more general procedure to check the model validity and obtain physical results not so crucially depending on the pre chosen models.

One possibility of model - independent inference is connected with cluster analysis - to scan the multidimensional feature space to find singularities of probabilistic measure - but difficulties will encounter with physical interpretation of embedded structures.

The second one is connected with the idea of integration over plausible models. Proceeding from a list of acceptable models - an model-integration procedure (committee method) can be defined for tuning both astrophysical parameters (composition, spectra) and strong interaction parameters.

Chapter 2

How to Use ANI

2.1 Program Summary

Title of program - *A*NI - Analysis and Nonparametric Inference

Computers - DEC-ALPHA, SGI, PENTIUM based UNIX workstations.
Operating system - UNIX, LINUX
N of bits in a word - 32
Programming language used - FORTRAN 77
Number of code lines 7800

2.2 Key Words

- Monte-Carlo Statistical Inference;
- Nonparametric Methods;
- Pattern Recognition;
- Multivariate Statistical Techniques;
- Bayes Risk estimation;
- Probability Density estimation;
- Classification;
- Artificial Neural Networks in Data Analysis;
- Sampling methods;
- Genetic Algorithms;
- Evolutionary Programming.

2.3 Source Code

The source code is written in standard FORTRAN77 including several routines from CERN program library. The "structure-creating" style of Fortran programming was used. Any function or procedure are represented by separate units (subroutines, or IF loops), provided with lines of explanations.

The CMZ source code management system is used for bookkeeping and version archiving [65]. The same source code is available for the all platforms mentioned. The automatically check of platform will activate the appropriate to this platform translators, linkers and program libraries. The modifications of code performed on one platform are fully available for others, of course, if there is no significant difference in translators.

For installation on a new platform the paths to system and CERN libraries have to be mentioned explicitly in CMZ KUIP files.

2.4 History of ANI Versions

There exist several versions of ANI package developed for different computers and operation systems.

YerPhI BESM-6 VERSION - 1985.5
CERN IBM 3090 (VM) VERSION - 1986.6
FIAN PDP 11/70 1987.2
FIAN VAX VERSION - 1989.1
YerPhI EC 1045 VERSION - 1989.2
PATCHY VERSION - 1990.6
DUBLIN VAX (UNIX) VERSION - 1990.7
KfK IBM 3090 (MVS) VERSION 1993.5
MPI VAX (VMS) Version 1993.6
KfK UNIX version 1994.5
YerPhI LINUX version 1994.8
CERN NOMAD version 1995.4
YerPhI Silicon Graphics version 1995.10
YerPhI Pentium version 1996.1
YerPhI CMZ alpha-97 version 1997.03

2.5 Restrictions on Data Size

Depending on platform used and memory available different restrictions on possible sizes of executed data files and formats are made by following declarations of Fortran PARAMETER command:

```
 parameter (in=8, imb=50000, il=5, imp=50000, ikcl=11, ipr=5)
 parameter (maxley=5, maxnod=13)
```

Current parameter settings available on FZK ALFA's are as follows:

IL	maximal number of classes	5
IN	maximal data dimensionality	8
IMB	maximal number of events in training sample	50000
IMP	maximal number of experimental events	50000
IKCL	maximal number of nuclei width variants	11
MAXLEY	maximal number of neural net layer	5
MAXNOD	maximal number of nodes in each layer	13
IPR	number of cost function variants	5

All array declarations in ANI are made implicitly using above mentioned restrictive values.

The declaration of arrays in subroutines also is made implicitly via transfered list of the formal parameters.

This restrictions helps to avoid main obstacle of Fortran programming – absence of the utilities controling the structures.

If any erroneous array dimension request encounters in input stream, detailed error report message is send and execution of program stopped.

2.6 The Main ANI Procedures (Modes)

The most important Key word is Analysis MODE, specifying the particular statistical procedure or estimator to be used.

The selected operation **MODE** is printed in the first line of analysis passport, containing also description of all data subsets executed, and parameters of data analysis procedures. Usually data analysis started with determination of intrinsic dimensionality of data - **DIMDIM** mode, the two figures used for dimensionality estimates: the average of local dimensionality, and the global correlation dimensionality .

Then a best data subset (in sense of discriminative value) is selected by the **BHATA** mode: proceeding from the initial dimensionality , on each step of dimensionality reduction a "worst" feature is selected and eliminated, according to the value of Bhatacharya distance, calculated for each variant of obtained subsamples.

The **ONE DIMEN.** mode is examining single variables and evaluated their discriminative power.

The **COVCOR** mode can help in the selection of the best pairs of the featurs.

The comparison of the multidimensional samples and Bayes risk estimation are performed in **ONE-LEAVE-OUT-** mode.

The **CLASSIFICATION** mode performs the attributing of the experimental events according to training sample classes (a priory knowledge) using Bayesian decision rules. The true fraction of different types of events in mixture distribution is estimated if RECONSTRUCT key word is selected.

The **REGRO** mode is used for energy and mass estimation.

The alternative very powerful classification and estimation techniques represent the Neural Networks models.. The parameters of **LEARNING and CLASSIFI** mode are specifying the topology of net the number of neurons (nodes) and layers.

2.7 Data Files

ASCII format files with standard headers are supported. Also PAW NTUPLES could be used. Data files are defined and refered by their names. The procedure of data reading can be checked line-by-line. Different selections, according to variables subsets, variables cuts, events numbers can be introduced.

Special data files with fixed names, provide possibility of information excange between different ANI modes. Several ANI modes are using statistical parameters and estimates calculated in previous runs. The Neural Net training scenarios implemented in ANI provided possibilities of multi step search with changing from one search algorithm to another.

The Bayes error estimates, calculated in **ONE-LEAVE-OUT-** mode are used in **CLASSIFICATION** mode for fraction estimation.

Therefore following files with fixed names connected to particular mathematical numbers, provided possibility of data exchange between different ANI modes:

b.tem - for Bayes risk estimates;
learn.dat - current values of neural net weights;

For user interface following files are used:
b.in - input stream;
b.out - output stream;
b.sys - error reporting.

A new installed user-friendly graphical interface is intended to make running jobs with ANI much more comfortable and easy.

2.8 ANI-SETUP

The *ANISETUP* graphic interface is designed for **ANI** (*Analysis and Nonparametric Inference*) statistical analysis package. It is written on *TCL.7.6* script language 7.6 and *TK.4.2* toolkit, which are available on most of **UNIX** platforms. The interface consists of two main parts:

- bookkeeping of input and output information (Figure 2.1).
- main input script setup for running the **ANI** program (Figure 2.2).

2.8.1 Bookkeeping Setup

Select b.in - Click on the icon and select “b.in” (input file). If it is the first run, the default file, named “b” will be downloaded.

Save b.in to... - Specify the name for current “b.in” to be saved. Different input files corresponding to the various operating modes will be archived under different names. By the default the “b” is saving with the same name.

Delete button - One can select and delete the input file from the archive.

Run button - Runs the main input setup.

Next part is for viewing run results. Variants of red color message: *New running, Program terminated correctly, Error detected.* If the second message is printed, one can view the current results. In case of third message one have to view the *"b.sys"* file for error report.

Run PAW++ - Interface to CERN PAW++

View b.out - View the output ASCII file, which is available in each running and contains the resulting information on current run.

View b.sys - Detected errors during current running.

Run CMZ - Run CMZ, change the source code and recompile the program.

At each new run all output files, besides the b.tem file (*"b.hbook", "b.out", "learn.dat"*) will be overwritten.

File to save b.out - Specify the name for *"b.out"*, write comments if necessary (next icon) and press *Save.*

Save PAW output - Specify the name for *"b.hbook"* and press *Save.*

Select learn.dat - from first icon of this line one can select the archived *"learn.dat"* file, which contains the trained *neural network* parameters and *Restore* it for continuing net training from the point reached at the previous training cycle. After net training one can specify the file name to save the obtained "learn.dat" file.

PAW file: - Select saved hbook file and run paw++(*View PAW Arc.*), or delete it(*delete PAW Arc.*).

OUT file: - Select saved output file and and *View...*, or *Delete...* it.

EXIT button - Exit from ANI-SETUP.

2.8.2 Main Input Setup

Number of classes - Number of categories in data analysis.

Bootstrap replicas - Number of bootstrap replicas.

Set names : (Figure 2.3)

- *Control name* - control or experimental sample name.
- *Dump name* - name of the file to store current training sample with applied cuts and selections.
- *Ntuple name* - hbook file name (in the current version of ANI it is fixed to be 'b.hbook').

- **Training sample names** - data files containing a priory information to be used in current run .

Set Ntuple - *Ntuple Write Options*: (Figure 2.4)

- *code* - if code is 1 hbook file will be created, if it is equal to 0 no hbook will be created.
- *id* - identification number of ntuple.
- *memory* - required memory for ntuples.
  item *hbook* - mathematical number associated with hbook file.

The same key words are specified for *Ntuple Read Options.*

Bank dimension - dimensionality of training and control samples (number of variables).

Size of control - the relative coordinate of the first event of control (experimental) sample and number of events.

Relational shifts - relative coordinate of the first event for each training sample (Figure 2.5).

Number of events - Number of events for each training sample to be downloaded (Figure 2.6).

Access - The formats of data files: (Figure 2.7)

- *SEQUENTAL* - sequential access mode (standard ANI files with header);
- *DIRECT* - abandoned;
- *NOMAD* - reading data from PAW ntuples.

Variables to be processed - the number of variables to be processed and the relative number of each variable in variable list (Figure 2.8).

Edit lower bounds - specify the lower bounds for all variables (Figure 2.9).

Edit upper bounds - specify the upper bounds for all variables (Figure 2.10).

Format of input - the format of input stream. (FORTRAN operator) Control and all training samples must be in the same format.

Debugging information - Output information debugging. If it is set to “0” - no output information is send to output file *b.out*, “8” value corresponds to most detailed output.

Data normalization - input data normalization to 0-1.

Operation mode - The main and most important key word in ANI. 19 operating modes are implemented in ANI program, to perform a different statistical procedures: (Figure 2.11)

- *DIMDIM*, *DIMFLAT* - intrinsic dimensionality analyses.

- *BHATA* - Bhattacharyya distance calculation.
- **ONE-DIMEN** - tests for comparing single variables.
- **COVCOR** - covariances analyses.
- *FWRITE* - data subsamples archiving.
- **ONE-LEAVE-OUT-** - Bayesian learning and Bayes error estimation.
- **CLASSIFICATION** - Bayesian classification of experimental data.
- **BOOTSRAP** - Bootstrapization of Bayesian learning and classification, fraction reconstruction.
- **REGRO**, **REGRO-AD** - Nonparametric regression for energy estimation (KNN and Parzen types).
- **LEARNING** - Neural network training for both, classification and estimation.
- **CLASSIFI** - Neural classification and estimation of control events.
- **EXP** - Neural classification and estimation of experimental data.
- *FAST, SUPERCUT, SOBOL-CUT, MULTI-CUT* - for on-line analyses of atmospheric Cherenkov telescope data.
- *SAMEPT* - abandoned.

Set NetConf - Neural network configuration setup (Figure 2.12).

- *Input number of layers* - specify the number of layers in multi-layered feed forward neural network (FFNN).
- *Edit number of nodes* - specify the number of neurons in each layer. For the first (input) layer number of neurons must be equal to number of variables to be processed, the last (output) layer has only 1 node for classification, for estimation - equal to number of regressands (not exceed 2) (Figure 2.13).
- *Edit Quality Function Symmetrization Weights* - control the influence of distinct training sample classes on the quality function (Figure 2.14).
- *Speed and WSpeed* - quality function calculation metric and events weights power.
- *Search mode* - Network training types. Possible strategy's: (Figure 2.15)
    1. *single* - one random net parameter is optimized at each iteration step,
    2. *neuron* - all parameters of random chosen neuron are processing at each iteration step,
    3. *mullti* - all net parameters are processing simultaneously.
- **Quality type** - quality function type:
    - *msd* - mean square deviation
    - *kolm, X**2* - under testing.
- **Begin point** - initial point in multidimensional space of neural net parameters. Variants: *random* - start from random point, *better* - to continue the net training from previously obtained point.

- **Decision point** - the threshold value, determaining decision for two-way classification).
- **Input number of variants for intervals** - the number of alternative intervals defined on net output support (classification into multiple categories).
- **Edit intervals variants** - define the particular intervals for each class. (Figure 2.16).
- **Edit true outputs for each class** - neural network "goal" output values for each class to be compared with actual net output in training process. (Figure 2.17).
- **Number of regressands** - specify the number of variables to be estimated (in case of neural estimation only), and *Edit* - specify the name(s) of regressand(s). (Figure 2.18).
- **Quality function** - submodes of **LEARNING and CLASSIFI**. Possible variants: (Figure 2.19)
  - *montec* - neural network classificator (pattern recognition).
  - *sigmaa* - background rejection in gamma-astronomy.
  - *spectr* - under testing.
  - *estima* - neural regression.
- **Memory type** -
  - *memory* - accumulats all successful steps in training process,
  - *simple* - remember only the last obtained better point.
- **Stop condition** - stop the training process (before the maximum number of training steps is reached) if the quality function is less then the number specified.
- **Set IterConfig** - initialization of training: (Figure 2.20)
  - *Number of iterations* - maximum number of training steps.
  - *Iteration coefficient* - step size in training process.
  - *Symmetrical constraint* - abandoned
  - *Initial spread* - parameter for neural network weights initialization.
  - *Shift* - random number generator shift.

Brief description of other ANI key words:

- Status - Run status: *DENCURVE* - in *CLASSIFICATION* mode stores in PAW ntuples the probability density plots for different classes and multidimensional clusters.
- Weights in REGRO - the type of distance weighting *LINEAR, SQRT, SQUARE* .
- Preference values - number of different variants of a priori loses, *Edit* - set a priori probabilities for each class (Figure 2.21)
- Number of widths - number of different Parzen kernels or number of nearest neighbors for probability density estimation (Figure 2.22)
- Strangeness criteria - threshold value of estimated probability density for triggering outlier report.

- Density estimation - probability density estimation method in Bayesian modes:
  - *PARZ* - Parzen kernels estimation.
  - *KNN* - K nearest neighbors estimation.
- Reconstruct different type events portion? - After making Bayesian learning and classification one can *RECONSTRUCT* the fraction of different classes.
- Maximal exponent in density estimation - Platform depended maximal possible exponent number (the greater values will be truncated).
- Number of nearest neighbors - nearest neighbors number in REGRO mode and in intrinsic dimensionality estimation mode (*DIMDIM*).
- Intrinsic dimension - the minimal dimension data to be reduced in (*BHATA* mode.
- Bhattacharyya distance weights - abandoned.
- Random generator - random number generator type:
  - *lp-tau* - Sobol's quasi-random numbers generator.
  - *pseudo* - pseudo-random generator from CERN program library.
- Scale partitioning - Number of mesh points for scanning multidimensional feature space and constructing nonlinear cluster of "signal" events. (*CLASSIFICATION* - *DENCURVE*).

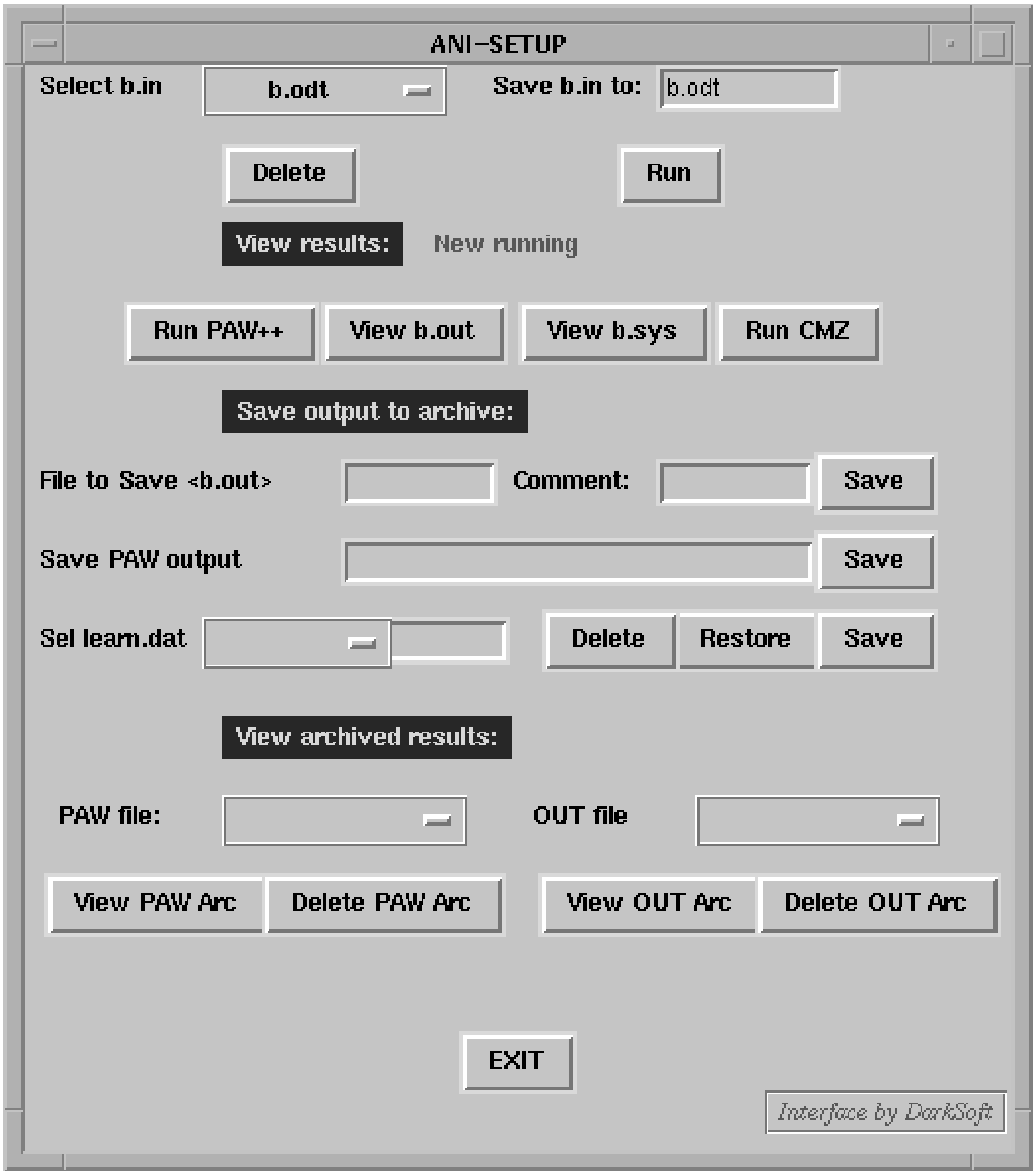

ANI–SETUP

Select b.in: b.odt

Save b.in to: b.odt

Figure 2.1: ANI Setup

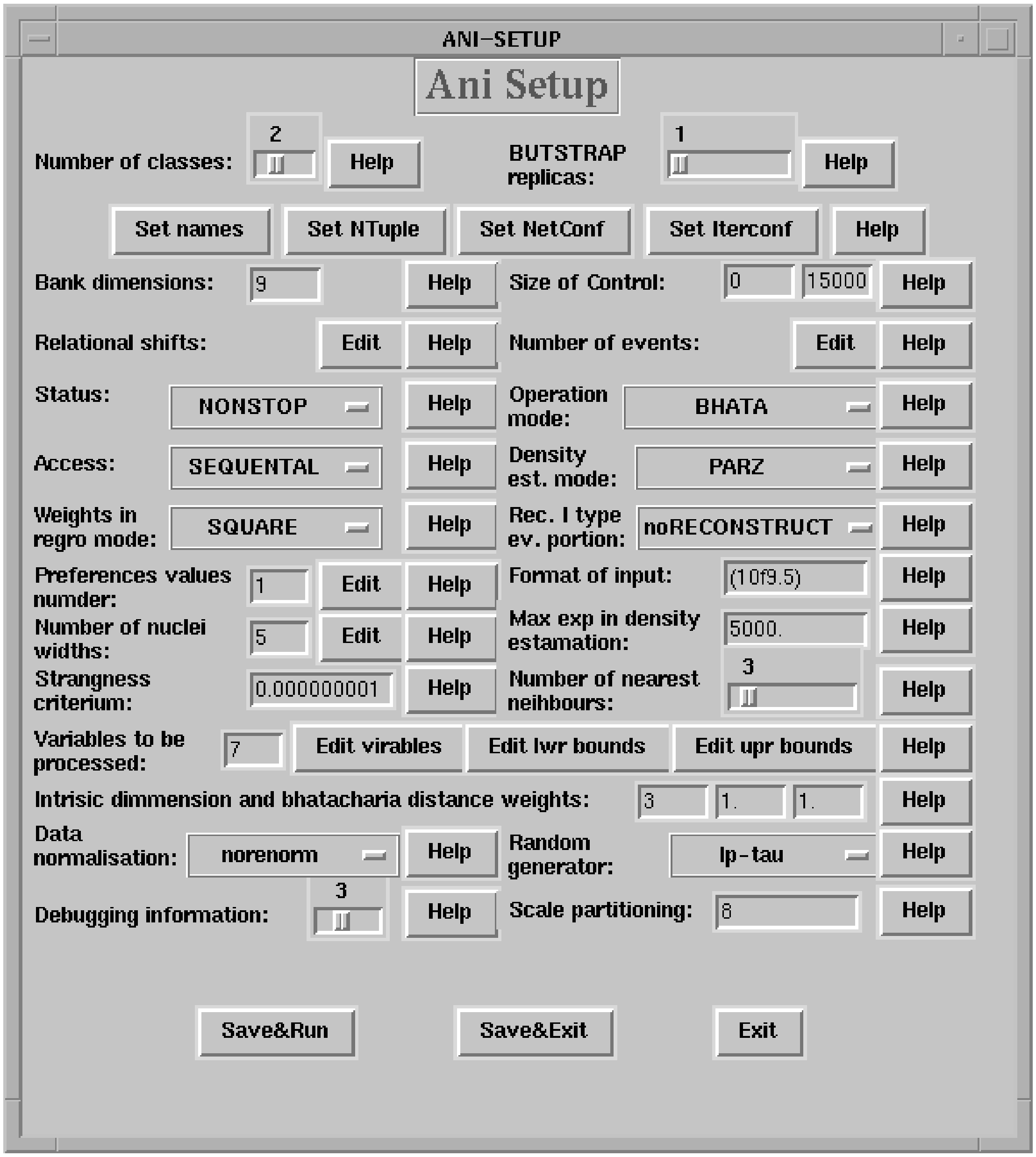

Number of classes: 2

BUTSTRAP replicas: 1

Bank dimensions: 9

Size of Control: 0 15000

Status: NONSTOP

Operation mode: BHATA

Access: SEQUENTAL

Density est. mode: PARZ

Weights in regro mode: SQUARE

Rec. I type ev. portion: noRECONSTRUCT

Preferences values numder: 1

Format of input: (10f9.5)

Number of nuclei widths: 5

Max exp in density estamation: 5000.

Strangness criterium: 0.000000001

Number of nearest neihbours: 3

Variables to be processed: 7

Intrisic dimmension and bhatacharia distance weights: 3 1. 1.

Data normalisation: norenorm

Random generator: lp-tau

Debugging information: 3

Scale partitioning: 8

Figure 2.2: Main Input Setup

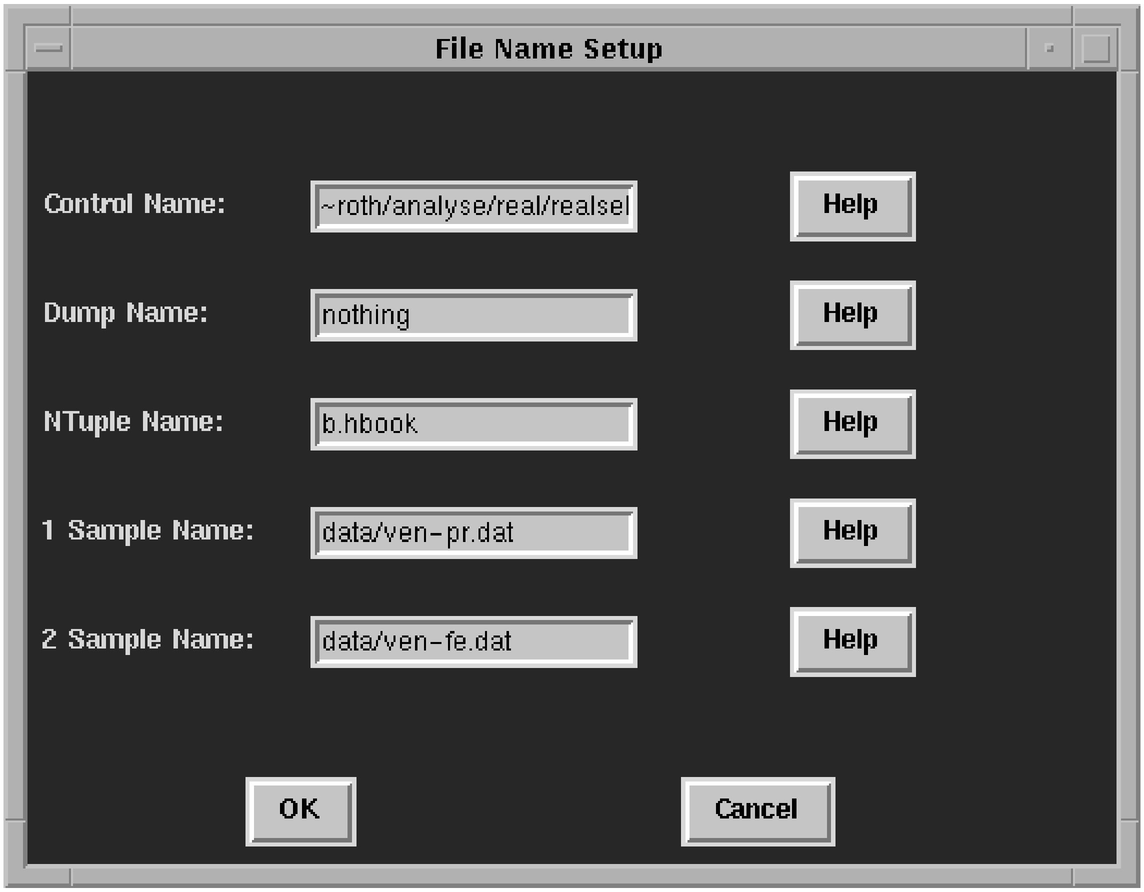

File Name Setup

Control Name: ~roth/analyse/real/realsel

Dump Name: nothing

NTuple Name: b.hbook

1 Sample Name: data/ven-pr.dat

2 Sample Name: data/ven-fe.dat

Figure 2.3: Set the file names

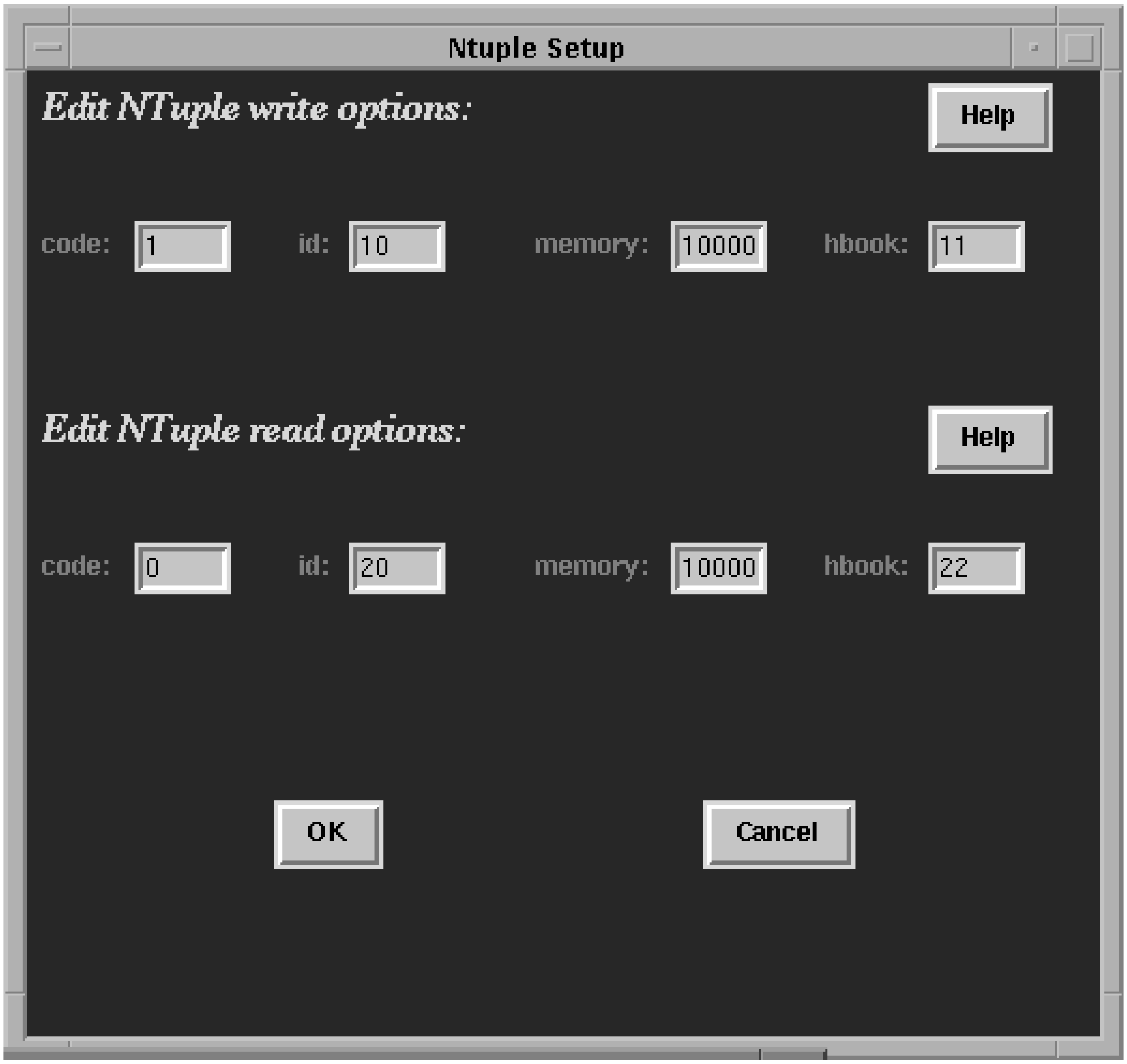

Ntuple Setup

Edit NTuple write options:

code: 1 id: 10 memory: 10000 hbook: 11

Edit NTuple read options:

code: 0 id: 20 memory: 10000 hbook: 22

Figure 2.4: Ntuple options

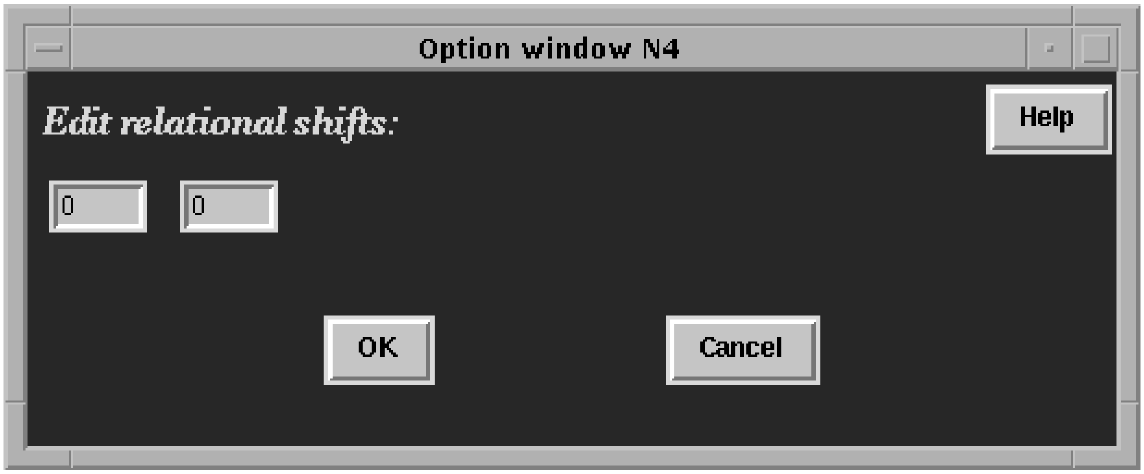

Option window N4

Edit relational shifts:

0 0

Figure 2.5: Relative coordinates

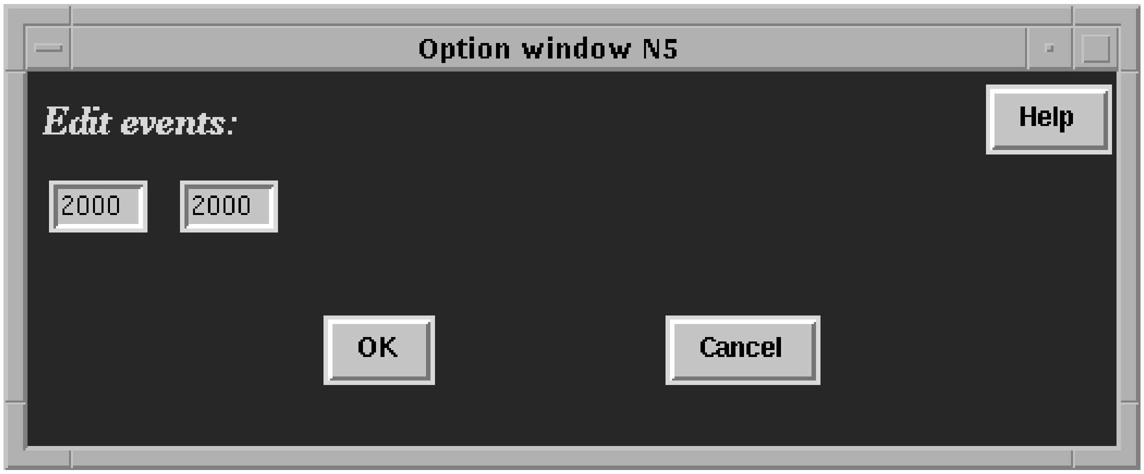

Option window N5

Edit events:

2000 2000

Figure 2.6: Training samples sizes

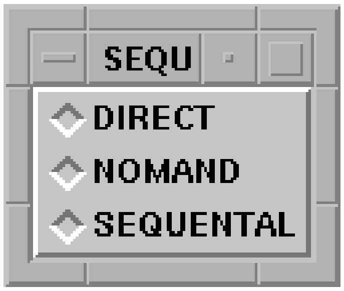

SEQU

◇ DIRECT
◇ NOMAND
◇ SEQUENTAL

Figure 2.7: Access modes

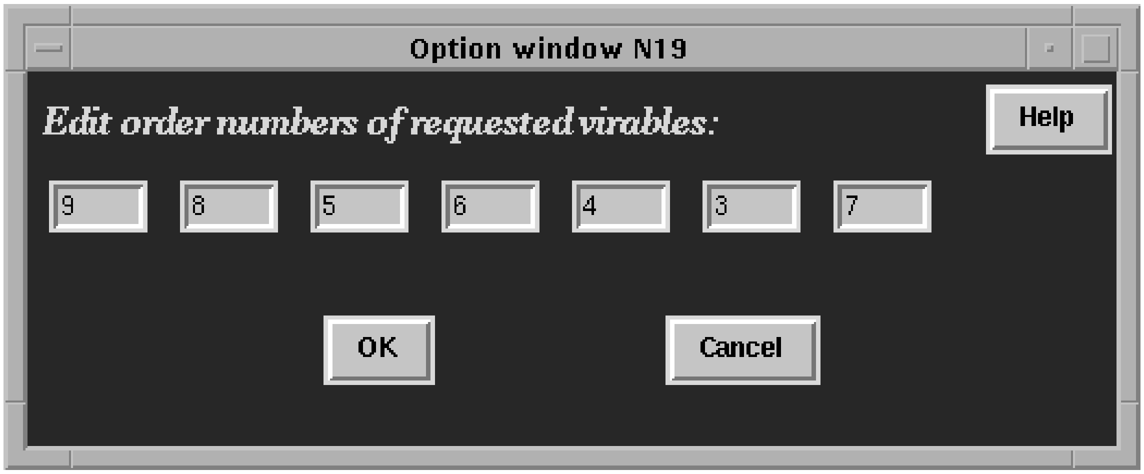

Option window N19

Edit order numbers of requested virables:

9 8 5 6 4 3 7

Figure 2.8: Variables to be processed

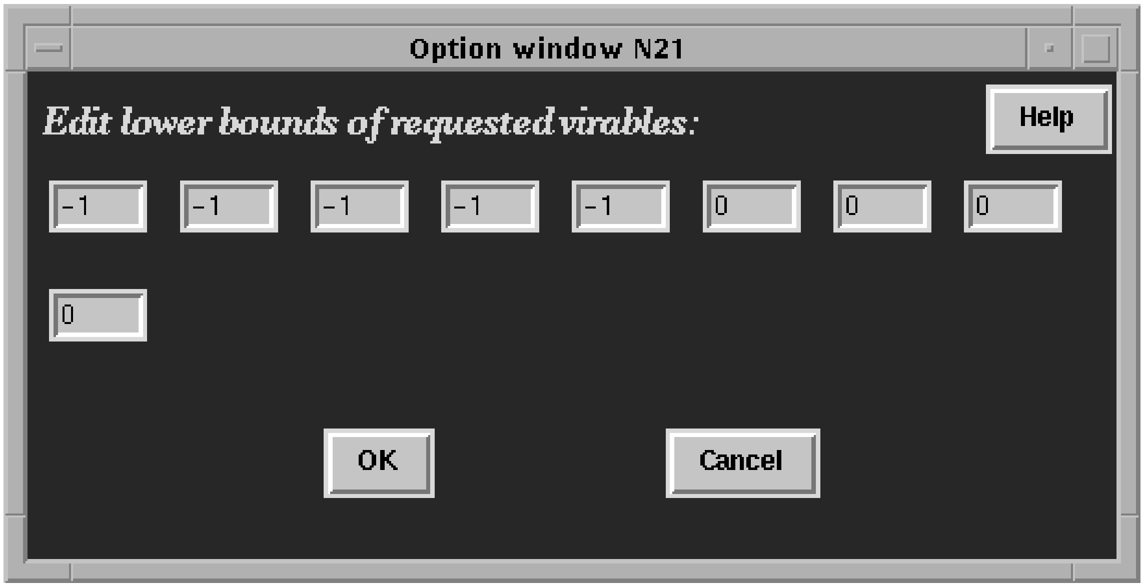

Option window N21

Edit lower bounds of requested virables:

-1 -1 -1 -1 -1 0 0 0

0

Figure 2.9: Set the lower bounds

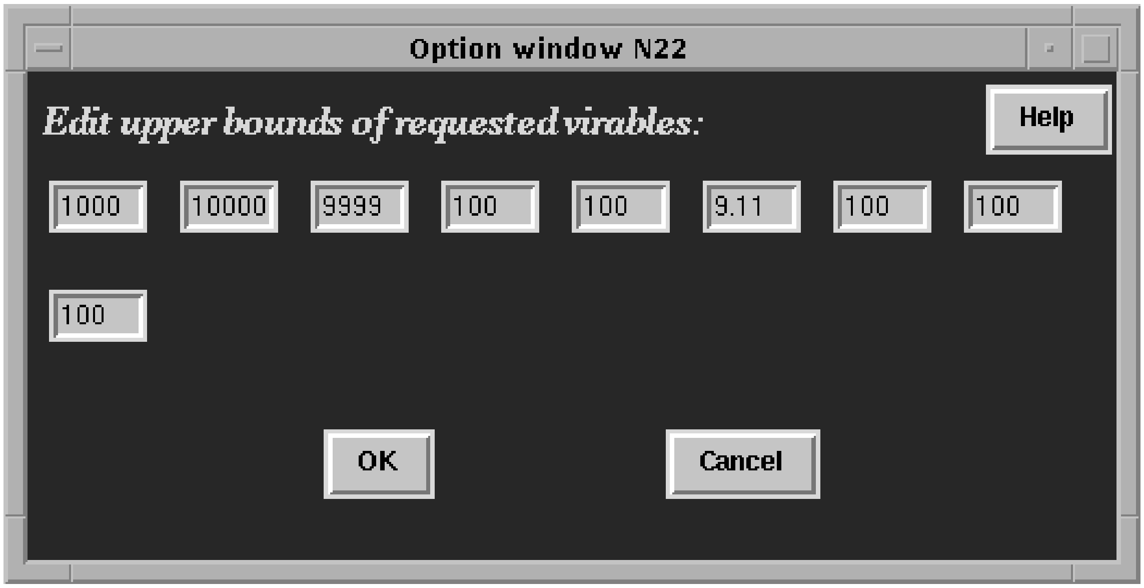

Option window N22

Edit upper bounds of requested virables:

1000 10000 9999 100 100 9.11 100 100

100

Figure 2.10: Set the upper bounds

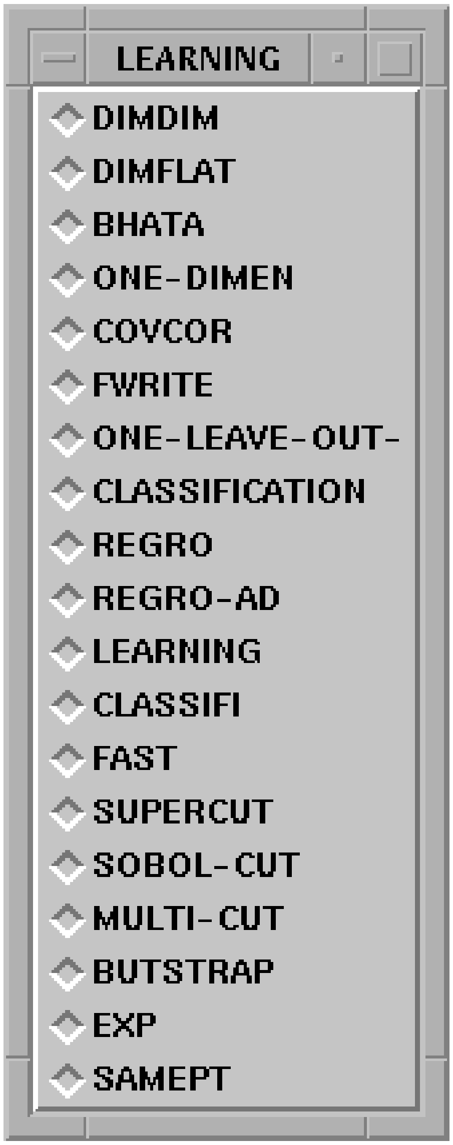

Figure 2.11: Operation modes

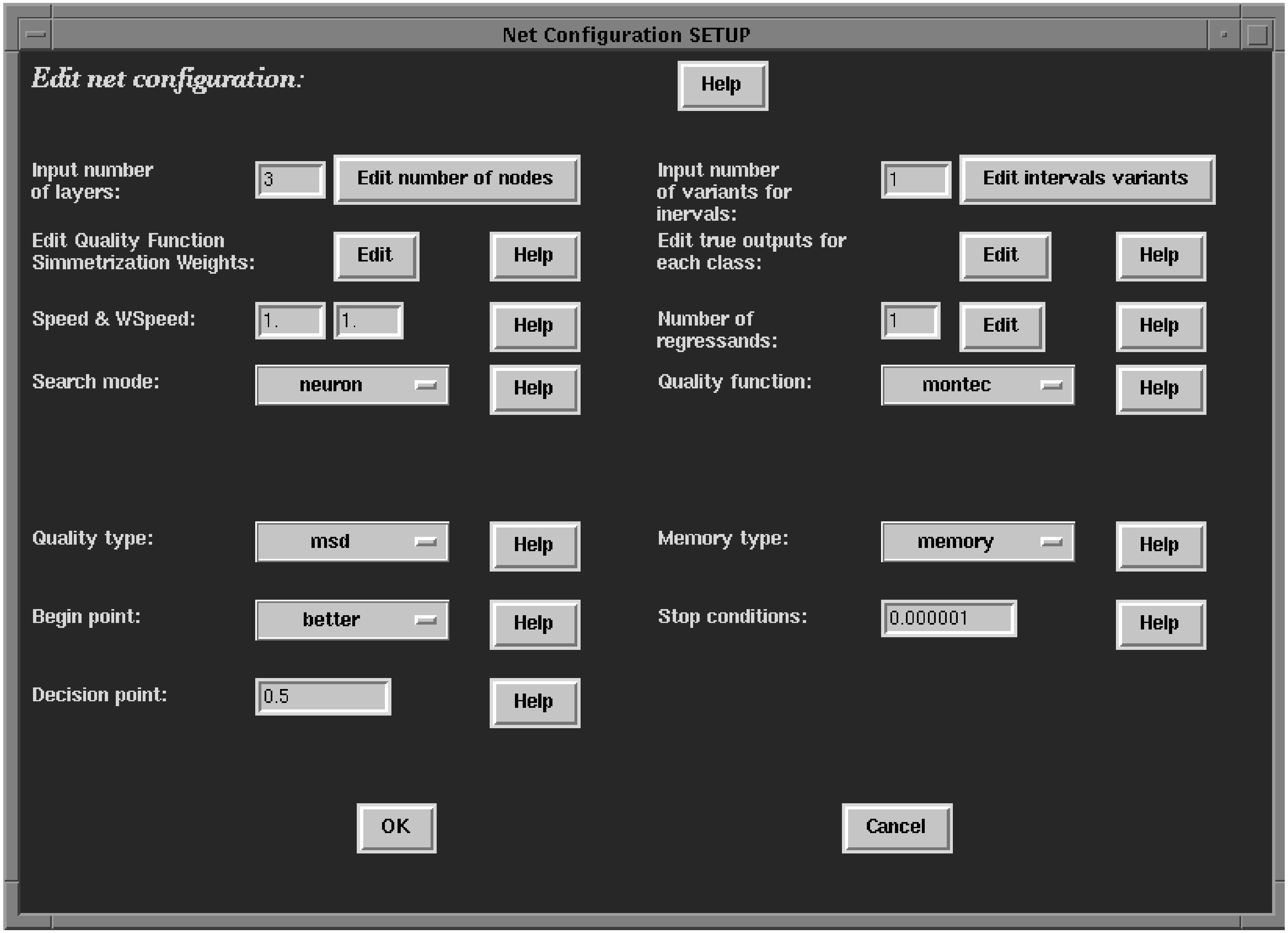

Net Configuration SETUP

Edit net configuration:

Input number of layers: 3

Edit Quality Function Simmetrization Weights:

Speed & WSpeed: 1. 1.

Search mode: neuron

Quality type: msd

Begin point: better

Decision point: 0.5

Input number of variants for inervals: 1

Edit true outputs for each class:

Number of regressands: 1

Quality function: montec

Memory type: memory

Stop conditions: 0.000001

Figure 2.12: Neural network configuration setup

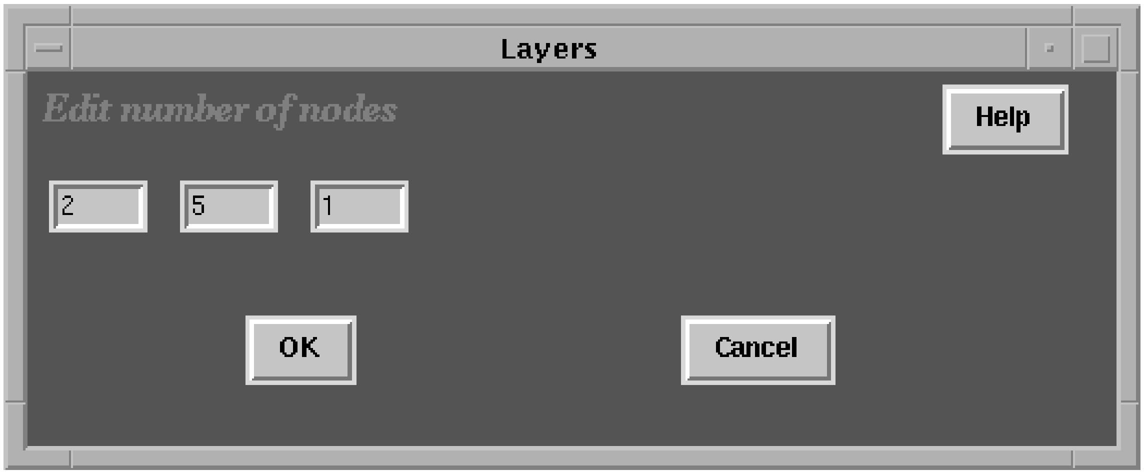

Layers

Edit number of nodes

2 5 1

Figure 2.13: Number of nodes in each layer

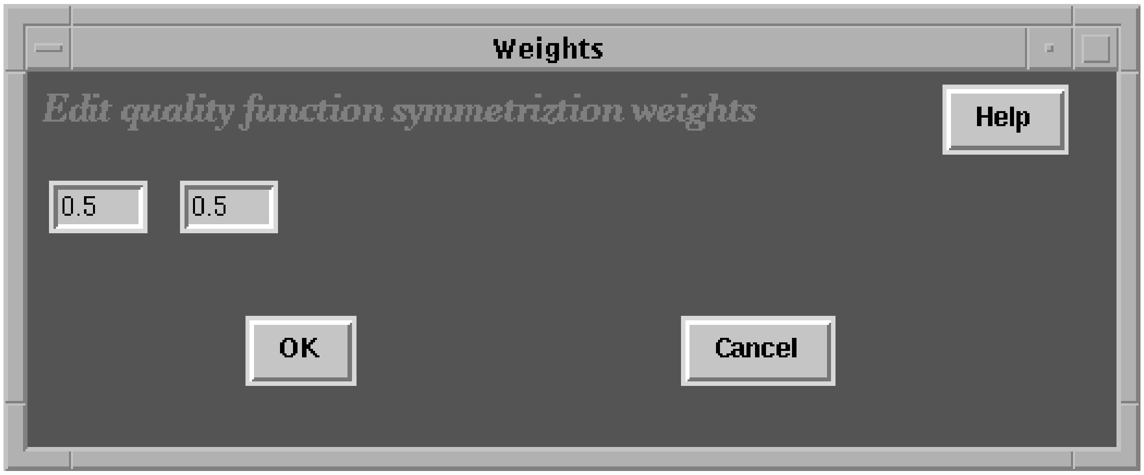

Weights

Edit quality function symmetriztion weights

0.5 0.5

Figure 2.14: Quality function weights

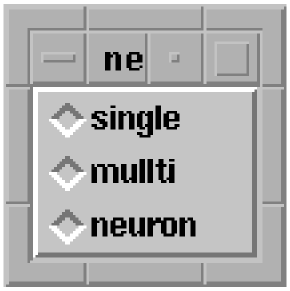

Figure 2.15: Net training strategy

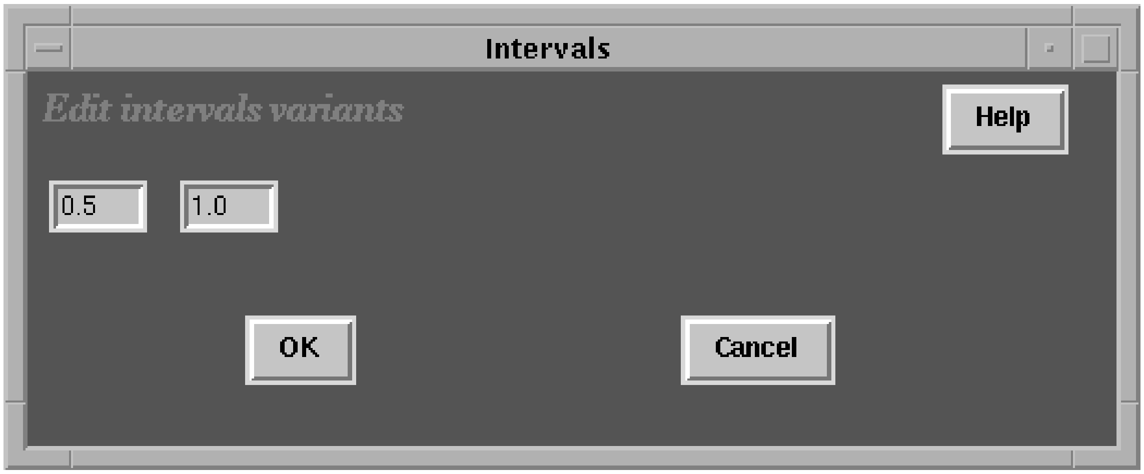

0.5 1.0

Figure 2.16: Net output intervals for different classes

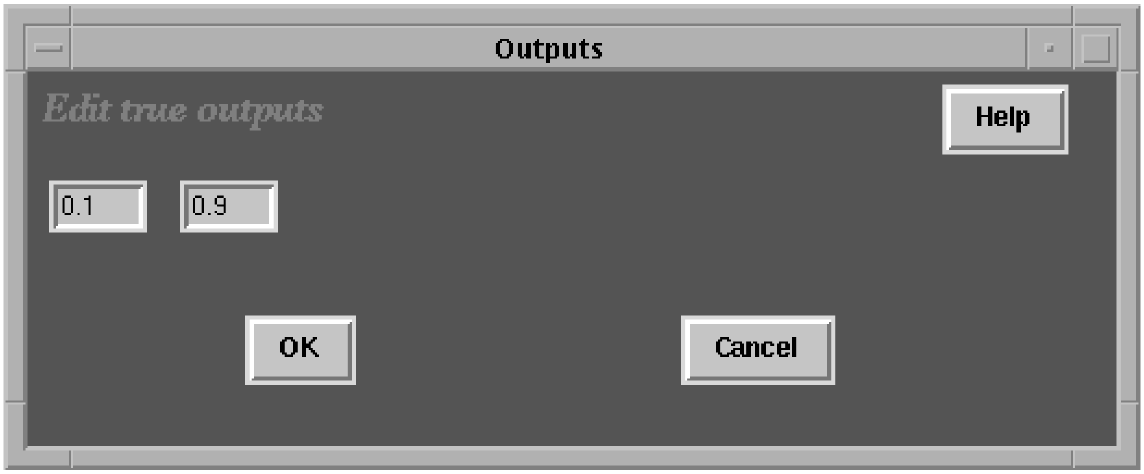

0.1 0.9

Figure 2.17: True outputs for different classes

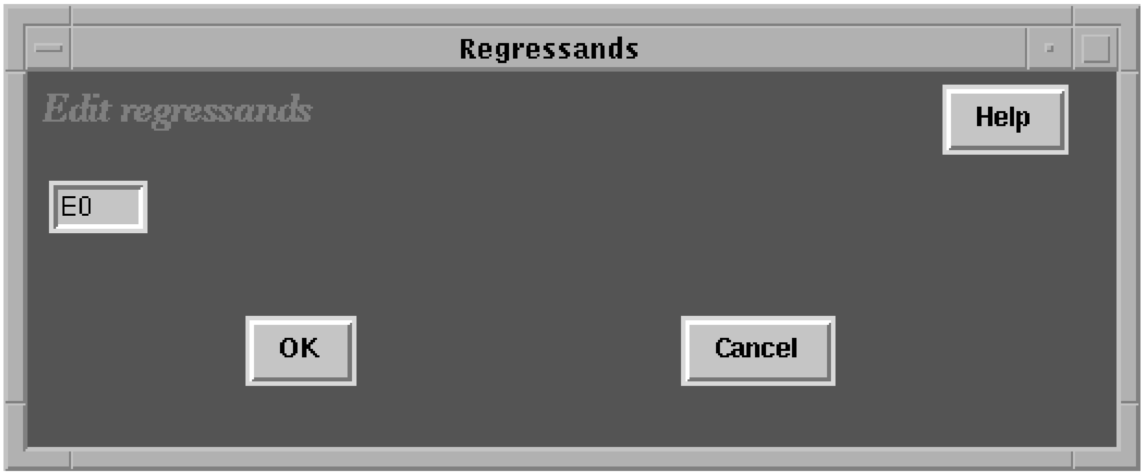

Edit regressands

E0

Figure 2.18: Regressands

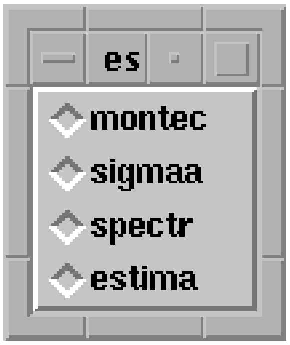

Figure 2.19: Quality function

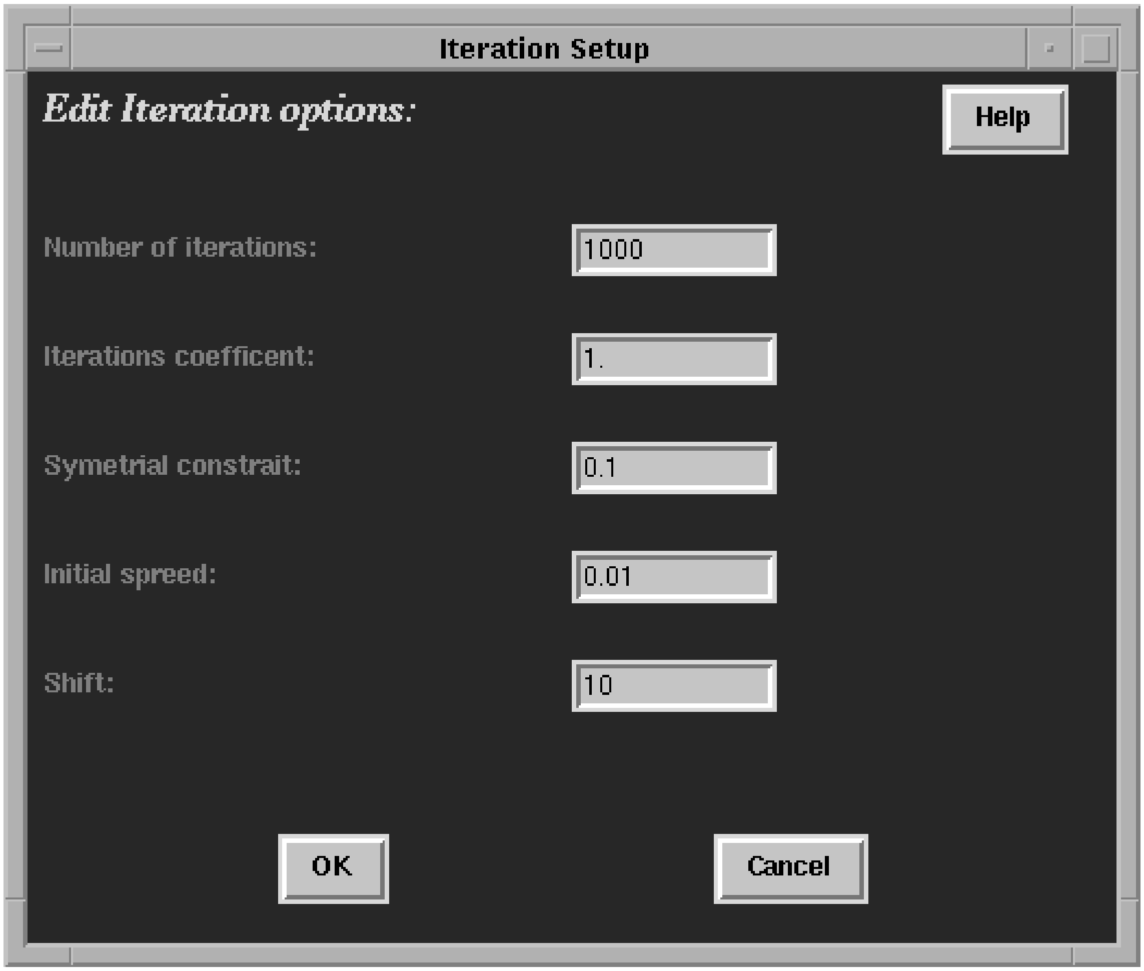

Iteration Setup

Edit Iteration options:

Number of iterations: 1000

Iterations coefficent: 1.

Symetrial constrait: 0.1

Initial spreed: 0.01

Shift: 10

Figure 2.20: Training initialization setup

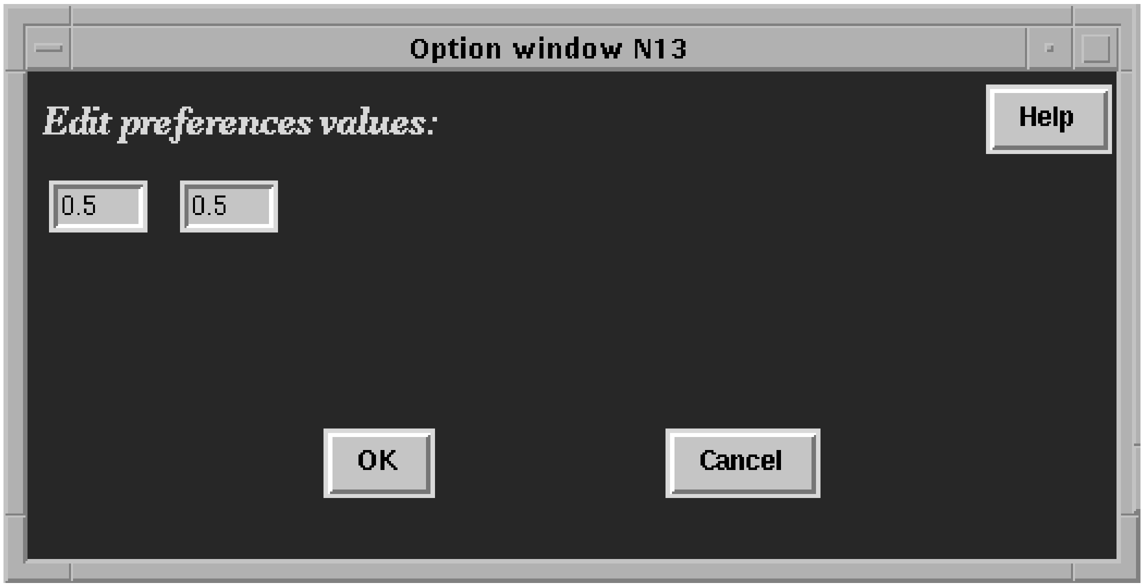

Option window N13

Edit preferences values:

0.5 0.5

Figure 2.21: Preference values

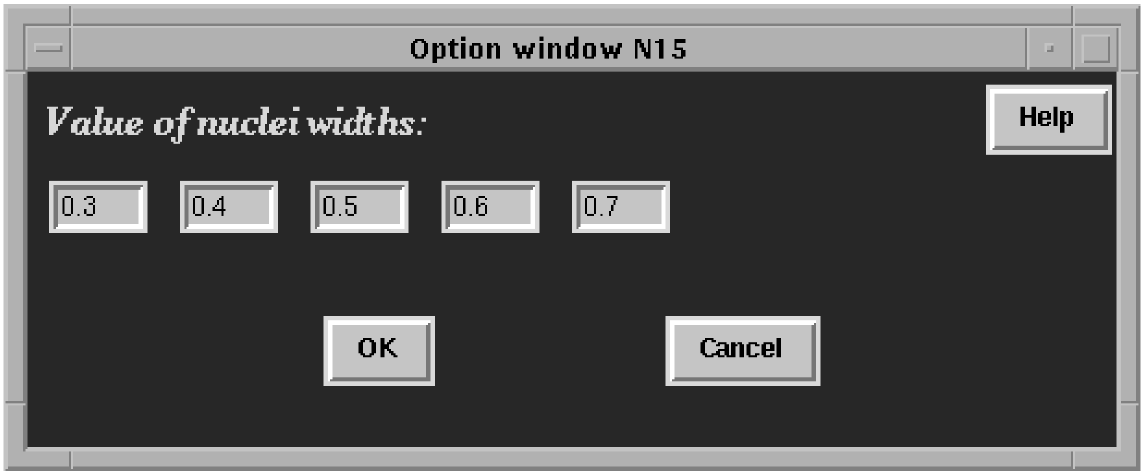

Option window N15

Value of nuclei widths:

0.3 0.4 0.5 0.6 0.7

Figure 2.22: Widths of Parzen kernels

2.9 DATA to drive ANI

After using the ANI graphical interface the following ASCII b.in file is created:

1. PARAMETER CONTROLS THE OUTPUT STREAM, (by selecting numbers from zero to 8, one can include various additional output information, to be printed into output file b.out, also permanently attached under mathematical number NT=2).
   DEBUG=
   2

2. NUMBER OF DIFFERENT DATA CLASSES TO BE HANDLED AND
   NUMBER OF BUTSTRAP REPLICAS (L and NBUT numbers):
   2, 100

3. TRAINING SAMPLES NAMES:
   KASCADE1000
   KASCADE1000

4. CONTROL(EXPERIMENTAL) SAMPLE NAME:
   KASCADE1000S

5. DUMP(ARCHIVE) SAMPLE NAME:
   NN-EST

6. PAW HBOOK NAME:
   b.hbook

7. TOTAL NUMBER OF VARIABLES IN DATA FILES:
   5

8. THE FIRST EVENT RELATIVE COORDINATES FOR EACH DATA FILE:
   0,500

9. TOTAL NUMBER OF EVENTS TO BE READ FROM EACH DATA FILE:
   500,500

10. FIRST EVENT COORDINATE and SIZE OF CONTROL (EXPERIMENTAL) DATA FILE:
    0,100000

11. STATUS (DENCURVE - producing numerous PAW plots, usually one dimensional case):
    NON

12. OPERATION MODE:
    (JMODE = DIMDIM, BHATA, ONE DIMEN., COVCOR, FWRITE, BETEST, ONE-LEAVE-OUT-, CLASSIFICATION, REGRO, BUTSTRAP, LEARNING, CLASSIFI, FAST, SUPERCUT, SOBOL-CUT, MULTI-CUT)
    LEARNING

13. THE TYPE OF DATA FILES (ASCII with header and weights, ASCII witout HEADER, OR PAW NTUPLES, (ACCESS = SEQUENTAL, SIMPLE, NOMAD):
    SEQUENTAL

14. DENSITY ESTIMATION MODE. Two general nonparametric modes are implemented, kernel density estimator and K nearest neghbours estimator.
    (JDEN = PARZ or KNN):
    PARZ

15. WEIGHTS IN REGRO MODE (JDIST = LINEAR, SQUARE, UNIFORM):
    UNIFORM

16. FORMAT OF SEQUENTAL INPUT (FORMAT1 ASCII string):
    (3F10.5)

17. NUMBER OF DIFFERENT A PRIORY PROBABILITIES AND LIST OF PROBABILITIES:
    (IAP number and AP array):
    3
    0.5, 0.5
    0.1,0.9
    0.01,0.99

18. RECONSTRUCT FIRST TYPE EVENTS PORTION?:
    RECONSTRUCTT

19. NUMBER AND VALUE OF NUCLEI WIDTHS (OR LIST OF NEAREST NEIGHBORS):
    (KCL number and F array)
    5
    0.3,0.4,0.5,0.6,0.7 15,25,50,100,150

20. MAXIMAL EXPONENT IN PARZEN DENSITY ESTIMATION AND STRANGNESS CRITERIUM IN BAYESIAN DECISION RULE:
    (expmax and strang):
    9000000.,0.00000000000000000001

21. NUMBER OF NEAREST NEGHBOURS FOR DIMDIM AND REGRO MODES, NUMBER OF PRINCIPAL COMPONENTS IF PCA MODE SELECTED (NEI=):
    17

22. VARIABLES TO BE PROCESSED (AMOUNT AND RELATIVE NUMBERS)
    (N number and NUMB array):
    2
    1,2

23. THE MINIMAL DIMENSION OF BEST VARIABLES SUBSET TO BE CHOOSEN BY BHATA SUBROUTINE (INTDIM=):
    1

24. LOWER BOUNDS OF VARIABLES (AMIN array):
    -9999999,-9999999

25. UPPER BOUND (AMAX array):
    9999999,9999999

26. Random generator used (genert = pseudo, or lp-tau - a uniform sieve in N-dimensions): In BETEST mode also RANNOR, NORRAN and NORMCO generators are used.
    pseudo

27. PARAMETERS OF PAW HBOOKS (FOR READ AND WRITE): (ntupw (r) - opening code; ntinw(r) - ntuple or histogram ID, MEMw(r) - memory size, IFOw(r) - hbook ID)
    1,10,100000,11
    0,20,1000000,22

28. DATA TRANSFORMATION TYPE (normalisation to 0-1 - renorm, principal component transformation -pca), :
    norenorm

29. NEURAL NET CONFIGURATION:N OF LAYERS, N OF NODES IN EACH LEYER. (LEYERS number, NODES array):
    3,1,3,1

30. N OF ITERATIONS, STEP VALUE, SIGMA CRITERIUM,
    INITIAL SPREED, RANDOM GENERATOR SHIFT (NITER, cf,sim,spread,ishift numbers):
    3000,0.1,0.02,88

31. SPEED (the power index for weighting the difference between actual and desired NN ootput).
    WSPEED (the power index for selecting event's weight variants) :
    1.,1.

32. QUALITY FUNCTION SYMMETRIZATION WEIGHTS (WIGHT array):
    0.5,0.5

33. SEARCH MODE (search = single - one dimensional search; MULLTI - all net parm. modificated simultaneously; neuron - all couplings and threshold of a randomly selected neuron)
    neuron

34. QUALITY FUNCTION TYPE (qualit = montec - training with M.C.; sigmaa - with ON/OFF pairs; estima - neural estimation:
    estima

35. QUALITY FUNCTION MODE, qtype = msd, (massa, kolm modes - now suspended)
    msd

36. MEMORY TYPE (memory = simple - no memorisation of better point during search; memory - the best changes are accumulated)
    bf memory

37. BEGIN RANDOM SEARCH FROM (begin = random point; or - better point, found in previous search cycles):
    random

38. STOP ITERATIONS IF QUALITY FUNCTION IS LESS THAN (stiter number):
    0.001

39. DECISION POINT (for 2 class case) (dpoint number):
    0.51

40. number of different partitionings of last neuron output (0-1) interval
    (analog of a priory probabilities for the neural decision making)
    and list of partitionings and goal functios for all classes.
    nipr number and part and goal arrays):
    2
    0.5, 1
    0.1,0.9
    0.1,1.
    0,0.6

41. MULTIDIMENSIONAL "BINS" NUMBER FOR FEATURE SPACE
    SCANNING (revealing of multidimensional nonlinear cluster shape),
    ndel number:
    1000

42. ESTIMATION MODE: NUMBER OF REGRESSANDS (ONE OR TWO)
    AND IT'S NAMES (ny number and numreg array):
    1
    MUON

Chapter 3

Statistical Inference in Cosmic Ray Physics

3.1 Nonparametric Inference

The scientific method is characterized by data classification, the study of their interrelations and relations to past experience, accumulated in various theories and hypotheses. Usually, it is impossible either to prove or to refute hypotheses by deductive method. The challenge is to draw sensible conclusions from noisy, discrepant information.

The main aspect of statistics is collection and interpretation of data, the interpretative aspect being the one that is now regarded as the essence of the subject [66]. The fundamental idea of statistics is that useful information can be obtained from individual small bits of data. An inductive method leads to empirical statements, that may be connected with theoretical ones by means of rational inductive conclusion rules [67].

The most natural and most general framework in which to formulate solutions to the physical inference in cosmic ray physics is a statistical one, which recognized the probability nature both of the physical processes of propagation of cosmic radiation through the atmosphere and the detectors, and - of the form in which data analysis results should be expressed.

However, it is very important to provide the scientist with objective criterion by which to judge the claims of hypotheses (models) under investigation (*problem solving strategy*). By model we mean a complete probability statement of what currently supposed to be known a priori about the mode of generation of data and of uncertainty about the parameters [68].

If this statement consists in the existence of an analytic distribution family, (like Poisson or Gaussian), appropriate to the problem in hand, we have prescribed parametric model. For such parametric models a well known concept of statistical inference consists in obtaining estimates of its parameters and verifying the validity of a chosen family [69].

3.2 Parametric Classification

The classification problem in parametric case (Newman-Pearson test) is traditionally described in terms of null and alternative hypothesis, critical and acceptance regions and level of significance [70]. The "best" critical region (the region of rejection of null hypothesis) is constructed by means of a Likelihood Ratio(LR):

$$LR(\mathbf{v}) \;=\; \frac{p(\mathbf{v}/\psi_1)}{p(\mathbf{v}/\psi_2)}, \tag{3.1}$$

each of two classes is defined by values of θ_i - the parameter of a prechosen analytic probability density function. $\mathbf{v}$ is a multivariate observation vector (point in multidimensional feature space) $p(\mathbf{v}/\psi_1)$, $(\mathbf{v}/\psi_2)$ - are conditional probability density functions describing distinct, mutually exclusive (non overlapping) and full $p(\mathbf{v}/\psi_1) + \; p(\mathbf{v}/\psi_2) = 1$ statements (null and alternate hypothesis).

The threshold value reflects the costs of consequences of statistical decision. Usually one select this value to keep on some constant minimal level error for one class, while maintaining to minimize the error of the other class.

For the K class case the $p(\psi)$ - will be chosen as a "true" class

$$\psi = argmax_{\psi_i} p(\mathbf{v}/\psi_i), i = 1, \ldots K. \tag{3.2}$$

If ψ takes infinite number of values from some metric space Ψ then we deal with an estimation problem and the Maximal Likelihood Estimate (MLE) is assymptotically unbiased and effective

$$\psi_{mle} = argmax_{\psi} \sum_{i=1}^{M} ln\; f(\mathbf{v}_i/\psi),\;\; \psi \;\subset\; \Psi. \tag{3.3}$$

where $\{\mathbf{v}_i\}$, $i = 1, M$ are the experimental events. The parametric estimation uses whole experimental sample set, instead of only one event in the classification problem, with the benefit of solving regression problem (parameter estimation) for all possible experimental situations. The analytical function $f(\mathbf{v}/\psi_{mle}) \;\equiv\; f(\mathbf{v})$ can be used for energy estimation, of course if the shape of particular functional family $f(\cdot)$ is known.

Although the results of analysis using parametric statistics usually are easy to present and understandable, it is very important to remember that any inferential conclusion based on parametric technique are not exactly valid unless every assumption is satisfied.

If these assumptions cannot be substantiated, or are discarded, or are not even known to the investigator, then the inference may be less reliable than a judicious opinion, or even arbitrary guess [4].

The parametric methods superimpose very restrictive assumptions on the nature of the population from which the sample is drawn. For example, the assumption of a normal distribution implies a continuous, symmetric, bell shaped distribution with infinite domain and a specific mathematical function. And statistical inference is exact for these sampling distributions only and may not even be close to the obtained one, if the population assumption comes to be incorrect.

3.3 Nonparametric Classification - Monte Carlo Statistical Inference

Usually, for experimental physics data analysis, the Likelihood Function cannot be written explicitly, and we deal with implicit, nonparametric models, for which no parametric form of underlying distribution is known, or can be assumed.

Nonparametric methods use much less stringent assumptions about population than those made in parametric statistics. Usually the underlying population distribution is assumed to be continuous only. Of course this assumption is rather mild comparing with the very specific assumptions made in parametric case.

Let us consider the stochastic mechanism $(\mathcal{A}, \mathcal{P})$ which generates the observations $\mathbf{v}$ in a multivariate feature space - $\mathcal{V}$, $\mathbf{v}$ is a d-dimensional vector of EAS parameters measured experimentally. We assume that observations are random and can be described by some conditional probability density function depending on the primary particle type. The feature space $\mathcal{V}$ covers possible acceptable values of EAS parameters including cuts on age and Ne parameter, etc...

The basic states space $\mathcal{A}$ consists of alternative models or classes (the alternative strong interaction models, or - different primary nuclei). The appropriate statistical model to describe this situation is the probability mixture model:

$$p(\mathbf{v}) = \sum_{k=1}^{L} P_k \; p(\mathbf{v}/\mathcal{A}_k). \tag{3.4}$$

And the main problem in EAS physics is to determine the proportions (frequencies) P_k of events in each category $\mathcal{A}_k$.

We don't know the full statistical description (conditional probability density functions $p(\mathbf{v}/\mathcal{A}_k)$ of how nature produces EAS from incident particles, nor the possibility to use particle beams outside the atmosphere to calibrate the installations, that is why, to determine the mutual probability measure on the direct product of $\mathcal{A}$ and $\mathcal{V}$ spaces the total Monte-Carlo simulation of the EAS development in the atmosphere and in detectors is performed, including experimental data registration and handling for alternative primary particles and possible strong interaction models in a wide energy range.

The set of d-dimensional $\mathbf{u}$ vectors obtained in simulations is an analog of the experimentally measured values of $\mathbf{v}$. But, as opposed to experimental data, it is known to which of the alternative classes each of these events belongs. These ”labeled” events include a priori information about dynamics of the EAS development and registration, which is given in a nonparametric form, in form of simulation trials.

The sequence $\{\mathbf{u}_i, \; t_j\}$, where $i = 1, M_j, \; j = 1, L, \; t-$ is the class index, is generated by a detailed Monte Carlo simulation program like CORSIKA and consists of L classes each containing M_j simulation trials.

This ”controlled” stochastic mechanism we denote by $(\mathcal{A}, \tilde{\mathcal{P}})$ and name training sample (TS). The training sample is the basis of all statistical procedures in applied Bayesian and neural approaches. Usually we denote a TS by $\mathcal{A}_k$ or explicitly by the primary group - P, O, ...,Fe.

The corresponding distribution mixture model takes the form:

$$\hat{p}(\mathbf{v}) = \sum_{k=1}^{L} \hat{P}_k \hat{p}(\mathbf{v}/\mathcal{A}_k) \tag{3.5}$$

Of course this substitution of unknown conditional densities $p(\mathbf{v}/\mathcal{A}_k)$ by their ”simulation” analog $\hat{p}(\mathbf{v}/\hat{\mathcal{A}}_k)$ is only valid if used model is adequate. And validation of the model remain the most crucial and yet unsolved problem in EAS data analysis.

Of course, for reliable estimation of conditional densities we'll need significant amount of training trials to cover all intrinsic variations of measurable EAS parameters and completely represent all categories (primary nuclei) .

Since both physical processes of particle production and those of registration are stochastic, only by careful measurement of probabilities we can gain an understanding of the EAS phenomena. We can't expect simple solutions, as multidimensional distributions of EAS parameters overlap significantly and any decision on primary particle type and it's energy will contain uncertainty.

The only thing we can require when classifying a distribution mixture is to minimize the losses due to incorrect classification to some degree and to ensure use of a priori information completely. Such a procedure is the *Bayes decision rule with nonparametric estimation of the multivariate probability density function.*

3.3.1 Bayesian Paradigm

The Bayesian approach of the statistical inference is a modification of the opinions of consistent experts (a-priori knowledge) in the light of new evidence and the Bayes theorem specifies how such modification should be made.

Moreover, as we believe, Bayesian a posteriori measures are only trustworthy and sensible measures of how the uncertainty about the phenomenon under investigation should be modified after new experimental data are achieved [3].

The Bayesian approach formalizes the account of all the losses connected with probable misclassification and utilizes all the differences of alternative classes [71]. The decision problem in a Bayesian approach is simply described in terms of the following probability measures defined on metric spaces:

- The space of possible states of nature $-\mathcal{A} \equiv (p, \alpha, O, N, Fe)$ - groups of primary nucleis;
- The space of possible statistical decisions – $\tilde{\mathcal{A}} \equiv (\tilde{p}, \tilde{\alpha}, \tilde{O}, \tilde{N}, \tilde{Fe})$ where $\tilde{p}, \ldots \tilde{Fe}$ are the decisions that the examined event is caused by a primary proton, or..., iron nuclei;
- Cost (losse) measure $c_{\mathcal{A}\tilde{\mathcal{A}}}$, or $c_{A_iA_j}$, or in simple notion c_{ij}. This measure is defined on the direct product of nature states and decision spaces $(\mathcal{A} \otimes \tilde{\mathcal{A}})$. All losses, connected with definite statistical decision $\mathcal{A}_\rangle$ are equal to

$$\mathcal{C}_i = \sum_{j=1}^{L} c_{ij}, \quad i, j = 1, L. \tag{3.6}$$

At correct classification of primary particles into "proton"and "iron" classes the losses are equal to zero

$$c_{Fe\tilde{Fe}} = c_{p\tilde{p}} = 0, \tag{3.7}$$

or for problem of background rejection in TeV gamma-ray astronomy

$$c_{\gamma\tilde{\gamma}} = c_{h\tilde{h}} = 0. \tag{3.8}$$

If we missclassify the signal event, we decrease the efficiency of γ-event registration. If we attribute hadronic images to γ-ray ones, we increase the background contamination. As we expect a significant excess of background against signal, we are interested in a strong background rejection. So, it is therefore reasonable to take the non symmetric loss function for this case

$$c_{\gamma\tilde{h}} = 0.9,\ \ c_{h\tilde{\gamma}} = 0.1. \tag{3.9}$$

For elemental composition studies one can take uniform a priori losses function

$$\mathcal{C}_p = \mathcal{C}_\alpha = \mathcal{C}_O = \mathcal{C}_N = \mathcal{C}_{Fe} = 0.2 \tag{3.10}$$

- Event (measurement, feature) space $\mathcal{V}$ - a set of measurable characteristics of EAS, Cherenkov image parameters etc....
- The prior measure $P_A \equiv (P_p, P_{Fe} \ldots)$.
- Conditional densities (Likelihood functions):

$$\{\hat{p}(\mathbf{v}/p),\ \{\hat{p}(\mathbf{v}/\alpha),\ \{\hat{p}(\mathbf{v}/O),\ldots\}. \tag{3.11}$$

These density functions are estimated by means of training samples obtained in simulation trials with different primaries.

Multivariate probability density estimation is a fundamental problem in data analysis, pattern recognition and artificial intelligence. The estimation of the conditional (on particle type) density on the basis of a collection of simulations is also a key problem in cosmic ray and high energy physics.

3.3.2 Bayesian Decision Rules

The Nonparametric Bayesian decision rule takes the form

$$\tilde{\mathcal{A}} = \eta(\mathbf{v},\mathcal{A},\tilde{\mathcal{P}}) = argmax_i\{\mathcal{C}_i\hat{p}(\mathcal{A}_i/\mathbf{v})\},\ i = 1,\ldots,L. \tag{3.12}$$

where c_i is the losses connected with $\tilde{\mathcal{A}}$ decision , $\hat{p}(\mathcal{A}_i/\mathbf{v})$ is the nonparametric estimates of the a posteriori density, connected with conditional ones by Bays theorem:

$$\hat{p}(\mathcal{A}_i/\mathbf{v}) = \frac{\hat{P}_i\hat{p}(\mathbf{v}/\mathcal{A}_i)}{\hat{p}(\mathbf{v})}. \tag{3.13}$$

And finally, substituting the a posteriori densities by the conditional ones we get the Bayesian decision rule in the form

$$\tilde{\mathcal{A}} = argmax_i\{\mathcal{C}_i P_i \hat{p}(\mathbf{v}/\mathcal{A}_i)\},\ i = 1,\ldots,L. \tag{3.14}$$

As one can easily see from above formulae, the Bayesian statistical decision is dependent on multiplicator $\mathcal{C}_i$ P_i therefore we can't separate the influence of losses (cost) measure and prior measure on decision made. Changes in losses can be compensated in changes in prior to keep constant the Bayesian decisions. We think, that it is reasonable to treat $\mathcal{C}_i P_i$ as single entity and denote it as a priori losses.

The robust Bayesian inference claims that after considering repeated evidence, the initial used prior distribution can't influence the a posteriori distribution heavily [3].

So, the choice of prior distribution isn't of critical importance for fraction estimation, because of the very big volumes of experimental data overwhelming the initial prior knowledge.

For the investigation of the influence of the chosen value of the a priori losses on the classification results, the statistical decision are made simultaneously for different alternative variants of a priori losses. Examining the, so called, "influence curves" obtained with different losses, one can select the preferable regime of estimator operation. For example, it is possible to select the desired ratio of background rejection and signal detection efficiency.

In ANI package provision is made to avoid statistical decision if all classes are very far from experimental events (outliers problem). If

$$\hat{p}(\mathbf{v}/\mathcal{A}_i) \ < ST \ for \ all \ i = 1, \ldots K, \tag{3.15}$$

then the outliers report is send to output stream. ST is, so called, Strangeness criteria, usually set to very small number.

Conditional densities are estimated by the TS $(\mathcal{A}, \tilde{\mathcal{P}})$ using one of many nonparametric methods available, L is the number of classes.

The Nonparametric Likelihood Ratio for classes $\mathcal{A}_1$, $\mathcal{A}_2$ and experimental event $\mathbf{v}$ can be represented as

$$LR(\mathbf{v}) \ = \ \frac{\hat{p}(\mathbf{v}/\mathcal{A}_1)}{\hat{p}(\mathbf{v}/\mathcal{A}_2)}. \tag{3.16}$$

Usually for comparison purposes we 'll use the sampling mean of Log Likelihood ratio.

The nonparametric Log-likelihood function for $k-th$ class has the form:

$$\mathcal{L}_k = \sum_{i=1}^{M} ln \ \hat{p}(\mathbf{v}_i/\mathcal{A}_k), k = 1, L, \tag{3.17}$$

where M is number of experimental events. The negative of Log Likelihood function is calculated in ANI, therefore the smaller values will correspond to most probable model.

3.3.3 Nonparametric Probability Density Estimators

To estimate conditional densities, we used Parzen and KNN methods [75, 77, 78, 79, 80, 81, 82, 83, 84] with automatic parameter (kernel width - for Parzen estimate, and number of neighbor - for KNN estimate) adaptation [85].

Several probability density values corresponding to different values of parameters are calculated simultaneously. Then the obtain sequence is ordered and the median of this sequence is chosen as final estimate (so called L-estimate). Depending on the intrinsic probability density in the vicinity of point $\mathbf{v}$, where the density is estimated, due to stabilizing properties of the median, each time the best estimate will be chosen [74].

The Parzen kernel probability density is estimated by:

$$\hat{p}(\mathbf{v}/\mathcal{A}_i) = \frac{\mid \Sigma_i \mid}{2\pi^{d/2} h^d} \sum_{j=1}^{M_i} e^{-r_j^2/h^2} \omega_j, \quad i = 1 \ldots, L, \ \ \sum_{j=1}^{M_i} \omega_j = 1 \tag{3.18}$$

where d is the feature space dimensionality, M_i is the number of events in the $i-$th TS, r_j is the distance from experimental event $\mathbf{v}$ to the $j-$th event of the TS in the Mahalanobis metric

$$r_j^2 = (\mathbf{v} - \mathbf{u_j})\Sigma_i^{-1}(\mathbf{v} - \mathbf{u_j}), \tag{3.19}$$

where Σ_i is the sampling covariance matrix of the class to which $\mathbf{u}_j$ belongs, ω_j are the event weights, h is the kernel width (parameter controlling the degree of the "smoothness" of an estimate).

The K nearest neighbors estimate (equal weight only are accepted) takes the form

$$\hat{p}(\mathbf{v}/\mathcal{A}_i) = \frac{k-1}{M_i V_\mathrm{k}(\mathbf{v})}, \tag{3.20}$$

where $V_\mathrm{k}(\mathbf{v})$ is the volume of a d-dimensional hypersphere containing the k nearest neighbors to the experimental event $\mathbf{v}$,

$$V_\mathrm{k}(\mathbf{v}) = V_\mathrm{d} \mid \Sigma_i \mid^{1/2} r_\mathrm{k}^d \, , V_\mathrm{d} = \frac{\pi^{d/2}}{\Gamma(d/2+1)}, \tag{3.21}$$

where r_k is the distance to the k-th nearest neighbor of $\mathbf{v}$, $\Gamma(.)$ is the gamma function. $\mid \Sigma_i \mid$ is the determinant of the covariance matrix of the class to which the K-th neighbor belongs.

3.3.4 Nonparametric Regression

As well as for density estimation, described in previous section, we use the K Nearest Neighbors and Parzen window for nonparametric regression. The choice of nonparametric methods for energy estimation is obvious: the a priori information about the shape of energy spectra in the "knee" region (ascribed both from measurements and existent models of particle generation and acceleration in interstellar media) predicts rather complicated character of spectra and change to different modes. Therefore we couldn't expect that any parametric family with not very large number of parameters will describe the data satisfactory.

So, also in the case of energy estimation, as for classification, the nonparametric methods only allow an event-by-event analysis of EAS data.

The method is based on the fact that the events close to each other in feature space $\mathcal{V}$ should have close to each other energies (geometric consistency hypothesis).

The Parzen regression energy estimate takes form

$$\hat{E}(\mathbf{v_j}) = \sum_i^{M_{TS}} C_i E_i \tag{3.22}$$

where

$$C_i = \frac{\mid \Sigma_i \mid}{2\pi^{d/2} h^d} e^{-r_{ij}^2/h^2} \omega_i. \tag{3.23}$$

Here, r_{ij} is the distance from the observable $\mathbf{v}_j$ to the i-th point of the TS $\mathbf{u}_i, \omega_i$ is the training event weight.

The Parzen estimate is calculated for different prechosen values of kernel widths h. The median of the estimates sequence is used as final estimate.

The KNN regression (again only for equal weights) energy estimate takes slightly different form

$$\hat{E}(\mathbf{v_j}) = \sum_{i}^{K} C_i E_{[i]} \tag{3.24}$$

$$\sum_{i}^{M_{TS}} C_i = 1 \tag{3.25}$$

where $E_{[i]}$ stands for the sequence of energy values of K nearest to $\mathbf{v_j}$ neighbors of TS. C_i coefficients are inverse proportional to distance (or square distance) between $\mathbf{v_j}$ and $\mathbf{u}_i$

The KNN estimate is also calculated for different prechosen values of K. The median of the estimates sequence is used as final estimate.

3.3.5 Bayes Error Estimation

The classification methods, like all the statistical ones, include a procedure quality test as a necessary element. This stage is also necessary for the determination of the frequencies of the probability mixture (3.5).

The most natural measure for quality test is the error probability which depends on both the degree of overlapping of alternative multivariate distributions and the decision rule being used (Bayes decision rules provides minimal error as compared to any other decision rule using the same features):

$$R^B = E\{\theta[\eta(\mathbf{v}, \mathcal{A}, \mathcal{P})]\} = \int \mathbf{v} p(\mathbf{v}) d\mathbf{v}, \tag{3.26}$$

where

$$\theta[\eta(\mathbf{v}, \mathcal{A}, \mathcal{P})] = \begin{cases} 0 & \text{, for correct classification,} \\ 1 & \text{, otherwise} \end{cases} \tag{3.27}$$

The mathematical expectation is taken over the whole $d-$dimensional feature space $\mathcal{V}$. In other words the Bayes error is a measure of the overlapping of alternative distributions in the feature space $\mathcal{V}$, e.g. the expected proportion of the "incorrect" classification. Since we do not know to which class experimental vectors belong, we obtain an estimate of $\hat{R}^B$ via the TS:

$$\hat{R}^B = E\{\frac{1}{M_{TS}} \sum_{i=1}^{M_{TS}} \theta[\eta(\mathbf{u}_i, \mathcal{A}, \tilde{\mathcal{P}})]\}, \tag{3.28}$$

i.e. we classify the $\{\mathbf{u}_i\}, i = 1, M_{TS}$ and check the correctness of the classification over the index of the class $t_j, j = 1, L$. The expectation is taken over all possible samples of volume M_{TS}.

However, as numerous investigations have shown (e.g.,[72]), this estimate is systematically biased and hence, a one-leave-out-for-a-time estimate is preferable

$$\hat{R}^e = \frac{1}{M_{TS}} \sum_{i=1}^{M_{TS}} \theta\{\eta(\mathbf{u}_i, \mathcal{A}, \tilde{\mathcal{P}}_{(i)})\}, \tag{3.29}$$

where $(\mathcal{A}, \tilde{\mathcal{P}}_{(i)})$ is a TS with a removed i-th element, which is classified and then "returned" to the sample. This estimate is unbiased and has an essentially smaller m.s. deviation compared with other estimators[73]. The advantage of $\hat{R}^e$ is especially notable when the feature space has a high dimensionality.

Note, that we have the possibility to estimate the error probability of various types by classifying various TS classes - $\{\mathbf{u}_i, t_j\}, j = 1, L$.

By R^e_{ij} (or simply R_{ij}) we denote the probability of classifying the $i-$th class events as belonging to the $j-$th class (misclassification). By R_{ii} the "true" classification probability will be denoted. For EAS classification according to 5 primary groups, each element of the "classification matrix" have to be determined, using the Bayes risk estimate (3.29).

$$\begin{pmatrix} R_{p\to p} & R_{p\to\alpha} & R_{p\to o} & R_{p\to si} & R_{p\to fe} \\ R_{\alpha\to p} & R_{\alpha\to\alpha} & R_{\alpha\to o} & R_{\alpha\to si} & R_{\alpha\to fe} \\ R_{o\to p} & R_{o\to\alpha} & R_{o\to o} & R_{o\to si} & R_{o\to fe} \\ R_{si\to p} & R_{si\to\alpha} & R_{si\to o} & R_{si\to si} & R_{si\to fe} \\ R_{fe\to p} & R_{fe\to\alpha} & R_{fe\to o} & R_{fe\to si} & R_{fe\to fe} \end{pmatrix}$$

This matrix presents accumulate a priori knowledge on the possibility of data classification into 5 categories. If all diagonal elements are greater than 0.6 (and therefore - the sum of all non diagonal elements in each line is less than 0.4), you can expect unambitious results of fraction estimation after reconstruction procedures explained in next section.

The overall index reflecting the "goodness" G of features used is following index of separability

$$G = \left(\prod_{i=1}^{L} R_{ii} \right)^{1/L}. \tag{3.30}$$

This averaged product of diagonal elements represents the "mean" probability of true classification into one of L categories. This index, of course, is directly connected with Bayes error.

3.3.6 Fraction Estimation

Now let us estimate the a posteriori fraction of various classes in the distribution mixture.

The best estimate of the a posterior fraction [8] (in case of a uniform a priori information and absence of systematic errors) is the empirical fraction

$$P^e_i = \frac{M_i}{M_{tot}}, \tag{3.31}$$

where, M_i is the number of events classified by the Bayesian decision rule (3.12) as belonging to the class $\mathcal{A}_i$, M_{tot} is the total number of events. With account of classification errors the corrected fraction (proportion) can be obtained as the solution of the following set of linear equations:

$$\sum_{k=1}^{L} \hat{P}_k R_{ki} = P^e_i, i =, 1, \ldots L. \tag{3.32}$$

where $\hat{P}_k$ is the estimate of the proportions P_k of the distribution mixture (3.4).

The accuracy of the estimates is defined by the TS size and number of control data as well as by the value of the Bayes risk, which represents the "quality" of discrimination with the chosen feature subset.

Note, that the set (3.32) is a poorly defined system and at large values of classification errors the solutions of the set are unpredictable and hence, the choice of a feature combination providing a high percentage ($\geq 60\%$) of correct classification is a necessary preliminary stage.

For classification in two categories (for example "heavy" –Fe, and "light" – p nuclei) the system of two equations can be easily solved explicitly:

$$P_{Fe} = \frac{P^e_{Fe} - R_{p,Fe}}{1 - R_{p,Fe} - R_{Fe,p}}, \quad P_p = 1 - P_{Fe}. \tag{3.33}$$

3.3.7 The Bootstrap Procedure

As we have shown in the previous section, to estimate the proportion of various nuclei in the primary flux, beside classification of experimental data by a TS, it is also necessary to calculate the misclassification rates R_{ij}. The accuracy of the obtained nuclear fraction is a function of both accuracies of classification and the determination of R_{ij}.

The possibility to decrease the bias and variance of the estimates of misclassification rates (3.32) was discussed in [28], where it was demonstrated that it is possible to improve the accuracy of the estimates, if the TS size is large, and, therefore we can obtain the estimate of (3.29), dividing the training sample to independent subsamples.

Unfortunately, time consumption per model event generation increases abruptly with primary particle energy and the TS size is rather small for high energy events.

Thus, the problem of an efficient use of the information contained in training samples is very important for cosmic ray physics, since samples corresponding to the highest energies are very limited and also the classical sampling models (statistical moments, etc…) do not allow to extract the whole information carried by a sample.

Of the greatest importance is also the estimation of the statistical errors of obtained fractions of different primary nuclei. The limited number of simulation didn't allow to calculate the errors of obtained fractions explicitly.

We propose to use the advanced resampling methods for fraction error estimation. The resampling methods of statistical error estimation were widely used since the last two decades. An efficient procedure actively developed in both applied and theoretical aspects is the bootstrap method [87] which lies in replication of the initial sample many times by means of random sampling with replacement.

Thus the obtained in such way conditionally independent bootstrap-replicas stand for independent samples from the general population (under the condition of sufficiently large size of the initial sample) and can be used for statistical error estimation [88]. In fact, the bootstrap method substitutes the unknown general population by a single sample.

The theoretical basis of the bootstrap method is the analog of the Central Limit Theorem (CLT) proved in [89]:

$$P\{\sqrt{B}(\mu_* - \mu_M) < tS_M \mid v_1, \ldots, v_M\} \rightarrow \mathcal{N}(t), \tag{3.34}$$

when $M,\ B \rightarrow \infty$ and $v_1, \ldots, v_M$ are independent, identically distributed (IID) random quantities, $\mathcal{N}(t)$ is a standard Gaussian distribution and t is it's quantile, μ_M and S_M are estimates of the first and the second statistical moments,

$$\mu_* = \sum_{j=1}^{B} \mu_j^b / B, \quad \mu_j^b = \sum_{i=1}^{M} v_i^{(j)} / M \tag{3.35}$$

μ_j^b is the $j-th$ bootstrap replica's mean, μ_* is the bootstrap first moment.

Moreover, analogies between sampling and the bootstrap are valid also for many other statistics. Referring to [90], we shortly summarize the main idea of the new method: a new procedure - the bootstrap-moments (denoted by μ_* and σ_*) are introduced, which in many cases substitute the statistical moments calculated according to a distribution function (in most cases of interest - unknown).

Of course, the analytical calculation of the bootstrap moments is usually impossible. However, and here lies much of the strength of the bootstrap approach, these quantities may be computed, to any desired level of accuracy, by a Monte Carlo simulation [90].

Returning to the problem of distribution mixture coefficient estimation we consider two ways of bootstrap procedure incorporation:

- to obtain the bootstrap estimate of the misclassification coefficients R_{*ij} and empirical ratio $P^e_{*\ i}, \ \ i = 1, L$, then reconstruct the fraction according to (3.32).

- carry out procedure of fraction estimation using each bootstrap replica, obtaining B bootstrap estimates for the fraction $\hat{P}_{*\ i} \ \ (i = 1, L, \ j = 1, B)$.

The second way is preferable, due to the possibility of explicit calculation of procedure systematic error and therefore - to evaluating the m.s.e. for obtain fraction estimates.

By several bootstrap replicas we calculate the bootstrap expectation $\hat{\mathbf{P}}_*$ and the bootstrap standard deviation (m.s.e.) of the mixture coefficients $\hat{\mathbf{P}}$, which will be used as final estimates of the fraction of different nuclei groups in the primary flux.

3.4 The Neural Classification Technique

The basic computing element in a multi layered Feed-Forward Neural Network (FFNN) is a node (formal neuron). A general i-th node recieves signals from the outputs of the all neurons of the previous layer:

$$\mathrm{IN}_i^{l+1} = T_i + \sum_{j=1}^{\mathrm{NODES}(l)} W_{ij}^l \times \mathrm{OUT}_j^l, \qquad i = 1, \mathrm{NODES}(l+1), \ \ l = 1, L-1. \tag{3.36}$$

where the threshold T_i and connection strengths (weights) W_{ij}^l are parameters associated with the node i, l is the layer index, L is the total number of layers, NODES(l) is the number of neurons in the l-th layer and OUT_j^l is the output of the j-th neuron in l-th layer. The index j corresponds to the higher layer and the index i to the next layer.

The output of the neuron is assumed to be a simple function of it's input, usually it is formed by the, so called, nonlinear sigmoid function:

$$\mathrm{OUT}_i^l = \frac{1}{(1 + e^{-\mathrm{IN}_i^l})}, \qquad i = 1, \mathrm{NODES}(l), \ \ l = 2, L. \tag{3.37}$$

where IN_i^l is the input of the i-th neuron in the l-th layer.

The multidimensional feature, entering the first layer are translated from input through hidden layers to the output nodes. Therefore FFNN provides the mapping of a complicated input signal to the class assignments.

For classification purposes this mapping takes a special form with aim to "shift" different classes of TS from each other as much as possible.

Therefore the "goal" output $\mathrm{OUT}^{goal}(k)$ for events of the k-th category could be chosen as follows:

$$\mathrm{OUT}^{goal}(k) = \frac{k-1}{K-1}, \qquad k = 1, K. \tag{3.38}$$

where K is total number of classes. Of course it is possible to define another set of "goal" values.

In the case of two classes, i.e. signal and background events, the "goal" outputs, as one can easily see, are equal to zero and one. The actual events classification is performed by comparing the obtained output value with the "goal" one. We expect, that the data flow passing through the trained net will be divided in two clusters concentrated in the opposite regions of the $(0, 1)$ interval. Choosing an appropriate point in this interval (the so-called decision point c), the classification procedure can be defined: an event with an output greater or equal than the decision point is attributed to the background class, while all the other events - to the signal class:

$$\mathrm{OUT}(\mathbf{v}) \begin{cases} < c & , \mathbf{v} \text{ is classified as signal,} \\ \geq c & , \mathbf{v} \text{ is classified as background,} \end{cases} \tag{3.39}$$

where $\mathrm{OUT}(\mathbf{v})$ is the output node response for a particular experimental measurement $\mathbf{v}$. This decision rule is a Bayesian decision rule; therefore the output signal of a properly trained feed forward neural net is an estimate of the a posteriori probability density [91].

For the multi-way classification one can define a set of nonoverlapping intervals in $(0-1)$. This set, along with the chosen "goal" values, will determine the mapping of net output into class labels.

The figure of merit to be minimized is simply the discrepancy of apparent and target outputs over all training samples (so called classification score):

$$Q = \sum_{k=1}^{K} \sum_{j=1}^{M_k} \left(\mathrm{OUT}(k) - \mathrm{OUT}^{\mathrm{goal}}(k) \right)^2 \tag{3.40}$$

where $\mathrm{OUT}_j(k)$ is the actual output value for the j-th training event, belonging to the k-th class, and the $\mathrm{OUT}^{\mathrm{goal}}(k)$ is the target value for the k-th class output, where K is number of categories and M_k is the number of events in the k-th training set.

In many cases of interest it is preferable (and possible) not to use the simulations at all. If the calibration of experiment with background cosmic radiation, as in case of atmospheric Cherenkov telescopes is available, a new model-independent quality function can be determined.

Searches for discrete gamma-ray sources consisted in the detection of an abundance ($N_{\mathrm{on}} - N_{\mathrm{off}}$) of events coming from the direction of a possible source (N_{on}) as compared with the control measurement, when pure background is registered (N_{off}). As the expected fluxes are very weak (the signal to background ratio not exceeding 0.01), one should always answer the following question: is the detected abundance a real signal or only a background fluctuation? The measure of statistical significance used in gamma-ray astronomy is the P-value of the Student statistical test (σ) [92]:

$$\sigma = \frac{N_{\text{on}} - N_{\text{off}}}{\sqrt{N_{\text{on}} + N_{\text{off}}}}. \tag{3.41}$$

The greater σ, the lesser the probability that the detected excess is due to background fluctuation. The equipment construction and the development of new data handling methods have the purpose to enlarge the value of σ. After selecting the "gamma-like" events from raw data (both from the ON and OFF samples), the criterion takes the form:

$$\sigma = \frac{N^{\star}_{\text{on}} - N^{\star}_{\text{off}}}{\sqrt{N^{\star}_{\text{on}} + N^{\star}_{\text{off}}}}, \tag{3.42}$$

where $N^{\star}_{\text{on}}, N^{\star}_{\text{off}}$ are the numbers of events "surviving" after the cut.

As the new objective function just this expression is used instead of the classification score (3.40). After executing all ONN, OFF samples, the σ value is calculated each time by means of "survived" (classified as signal) events.

3.4.1 Neural Estimation

The same FFNN with different quality function are used for primary energy and mass estimation. The following function have to be minimized

$$Q = \sum_{j=1}^{M} \omega_j \left(\text{OUT}(\mathbf{u}_j) - \text{OUT}^{\text{true}}(\mathbf{u}_j)\right)^2, \tag{3.43}$$

where, $\mathbf{OUT}(\mathbf{u}_j)$ is the vector output of the FFNN last layer and the $\mathbf{OUT}^{\text{true}}(\mathbf{u}_j)$ is the vector of parameters used in simulation (primary mass and energy of of "pseudo-experimental" event with $\mathbf{u}_j$. ω_j is the event weight (usually the highest energy events get higher weight).

The quadratic metric is used as measure of discrepancy of actual "and" true regression function values:

$$\text{OUT}(\mathbf{u}_j) - \text{OUT}^{\text{true}}(\mathbf{u}_j) \;=\; \alpha(\widehat{mass}(\mathbf{u}_j) - mass(\mathbf{u}_j))^2 + (1-\alpha)(\hat{E}(\mathbf{u}_j) - E(\mathbf{u}_j))^2 \tag{3.44}$$

The α coefficients are changing during training cycles to provide stable and reliable recovery of both energy and mass.

3.4.2 Net Training

Two main scenarios of net training are implemented in ANI.

- The deterministic mode: the multidimensional quasi-random sieves are used for scanning of the net parameter space. Positioning the sieve center at the previously found best point, and subsequently decreasing sieve size, we'll arrive to the best net.

- The random search algorithm use pseudo-random numbers to select the particular net node and randomly change all it's weights. If new weights bring an improvement of quality function, then this change survives, and a new random search step is performed, in opposite case the changes are subtracted and another random step is made from the previous point.

The total number of searching net parameters equals:

$$NTOT = \sum_{l=2}^{L} NODES(1) + \sum_{l=1}^{L-1} NODES(l)NODES(l+1). \qquad (3.45)$$

The random change (addition, or subtraction) Δ_i is selected on the $i-th$ iteration of search procedure in the following way

$$\Delta_i = STEP\ f(Q_{i-1})\ (RNDM\ -\ 0.5), \qquad (3.46)$$

where RNDM - is randomly distributed in the (0 - 1) interval, $f(Q_{i-1})$ – is the power function, controlling the random step size during reaching the global minimum and STEP is normalizing factor.

Also complementary search modes can be used:

- Single mode - single parameter is randomly chosen and randomly changed;

- Multi mode - all net parameters simultaneously are randomly changed.

It is possible to combine different search modes. Each will start from the best point reached in a previous search. Changing modes and search parameters helps to escape the local minima region and finally obtain desired solution.

3.4.3 Genetic Algorithms

As we've described in the previous section, the net training (search of global minima) is a very time-consuming procedure with no guarantee to find the unique best point in multidimensional (dimensionality may be 100 and more) net parameters space.

To fasten this process, the genetic approach is proposed. Starting from a "pool" of "good" solutions, obtained with different searching scenarios starting from different initial points we determine the "genetic" operations on it.

Each solution is represented by a "chromosome" – collection of gene (each gene consists of a singe neuron parameters). The main genetic operations are "crossing-over" – exchange of of randomly chosen neurons in randomly chosen chromosome, and mutation – rare process of the random changing the single "allele".

Then the evolution started (of course the rules of forming of the next generations have to be defined) and "fitness survival" mechanism is triggered.

We'll demonstrate in the ANI testing chapter, that some of "offsprings" demonstrate better characteristics than "parents".

The genetic module is a separate program written in C for UNIX by S.Chilingarian.

3.4.4 Net Topology

As for many other nonparametric techniques, for FFNN training it is very difficult to find an appropriate method for net parameter determination (e.g. the number of nodes and layers).

Of course, you can form the initial "pool" from networks with different topologies, and leave evolving population to find the best one. But this approach seem to be too complicate, due to numerous variants and possibilities.

Instead the "Occam" principle is used. Starting from minimal configuration (single hidden layer with 3-5 neurons), then increase net, check for improvement and stop when no more improvement take place.

It is worth to mention, that you can't use very complicated nets, if training samples are limited in size. The empirical rule requires as minimum 10 training events for each net parameter. Therefore you can't use more than the simplest net (4::3::1) if your training sample consists of 100 events and you try to make 3-way classification of 4-dimension EAS measurables.

3.4.5 Stopping Rules

Usually, the net training iterations canceled when the value of quality function is stabilized, and no more improvement takes place. Or, when the requested maximal number of iterations has been reached. Then the obtained set of net parameters can be used for experimental data classification.

But, there always is the danger of "over training" (especially for small training sets) . The obtained network will very good describe the particular training set, but not the required overall dependence. So, the "training" error could be minimized, but the "generalization" error, obtained with the same net, but with an independent sample can give a rise of classification errors. Therefore, in each step of training it is important to check the results with an independent sample and stop training when the "generalization" error starts to increase.

3.5 KNN Algorithm of Fractal Dimension Estimation

The basic approach to dimensionality analysis lies in characterizing physical systems by the invariant probability measure singularities [93]. To do this, let us determine the scaling of moments of the random quantity $p_{\mathrm{i}}(l)$ of order q at scale l:

$$C_{\mathrm{q}}(l) \equiv < p_{\mathrm{i}}(l)^q > \equiv \sum_{i=1}^{N(l)} p_{\mathrm{i}}(l)^{q+1} \sim l^{\phi(q)}, \;\; \phi(q) = q d_{\mathrm{q\text{-}1}}, \tag{3.47}$$

where d_{q} are the Renyi dimensions (generalized dimensions) determined for $-\infty < q < \infty$. At $q = -1$, the relation (3.47) determines the capacity dimension $d_{\mathrm{F}} = d_0$, at $q = 0$ the information dimensionality d_1 and at $q = 1$ the correlation dimension d_2.

The estimates of the Renyi dimensions are defined as a slope connecting some values of $\{l_{\mathrm{i}}\}$ with the corresponding values of $\{C_{\mathrm{q}}(l_{\mathrm{i}})\}$ in a double-logarithmic scale.

While the formal definition of the generalized dimension must be given in the limits of very small scales and of infinite numbers of points in the distribution, in practical applications only a limited amount of events is accessible, so only a finite scale can be considered. In fact, if we cover the distribution with boxes that are too small, most of them will contain just one particle or moreover no at all.

Therefore, the direct Renyi dimension calculation besides that it is rather time-consuming and there are no instructions regarding the choice of the box-size $\{l_\mathrm{i}\}$. Algorithms based on nearest neighbor information (KNN-algorithms) are much more efficient than the box-counting algorithms and they introduce a natural scale - the sample-averaged distance to NN:

$$\overline{R}_\mathrm{k}\ , k = 1, 2, \ldots M - 1, \tag{3.48}$$

where M is the total number of events in the sample. Using the ergodic theorem one can make a replacement [94, 95]:

$$\sum_{i=1}^{N(l)} p_\mathrm{i}\ (l)^{q+1} \sim \sum_{j=1}^{M} \tilde{p}_\mathrm{j}\ (l)^{q} \simeq Q_\mathrm{l} \tag{3.49}$$

where $\tilde{p}_\mathrm{j}$ is the probability to find the point of the studied set not in the box of size l, but inside the hypersphere of radius l, centered at some other point of the studied set and Q_l is the total number of q-tuples within this sphere. For the $\overline{R}_\mathrm{k}$ sequence the scaling relation takes the form:

$$Q_{\overline{R}_\mathrm{k}} \sim \overline{R}_\mathrm{k}^{\phi(q)} \tag{3.50}$$

For $q = 1$ (correlation dimension) the number of q-tuples is simply equal to the number of the sample events within l-spheres, and the left-hand side of (3.50)is equivalent to the mean number of the sample points inside a hyper-sphere with radius equal to the average distance to the K-th neighbor, i.e. is equal to the number k, so:

$$k \sim \overline{R}_\mathrm{k}^{d_2}. \tag{3.51}$$

Hence, the modified algorithm defines d_2 as a slope of the k-dependence of $\overline{R}_\mathrm{k}$ in a double-logarithmic scale.

Note that the obtained dimensionality is not in any way connected with the regions where singularities of the probability measure arise, i.e. it is impossible to recover the spatial structure of the multi-fractal support by the d_q spectrum. That is why we believe that the local dimensionality may be useful in separating the space regions where considerable fluctuations of the invariant probability measure are observed.

Apart from sample averaging, there is also one more way to get a linear equation for dimension determination [96]. We can determine the same procedure as described above not for the sample averaged distances, but for the actual distances to the nearest neighbors of each point in the sample.

For this, one must choose the series $\{k_\mathrm{j}\}$ such, that the density estimates are very close to each other and hence, the dependence of $\hat{p}_\mathrm{k}(v)$ on k can be ignored. Following these chosen $\{R_{k_\mathrm{j}}(v_\mathrm{i})\}$ values and the corresponding $\{k_\mathrm{j}\}$ values, one can estimate the local dimension at a point v_i.

The moda of the histogram of the local dimensionalities usually points on the value of global one, but local inhomogeneities of the sample can also be readily seen from the histogram as local pikes.

Chapter 4

ANI Testing (Gaussian Data)

4.1 Bayesian Analysis

4.1.1 Density Estimates

To check the ANI density estimation modes we use samples from multivariate Gaussian populations with different means (0 - for the first class and 1 - for the second) and equal variances (1 for both classes). We compare the theoretical value of the Bayes error, which for Gaussian distributions is directly related to the Mahalonobis distance (3.19) between first statistical moments of two classes:

$$R^B = \Phi(-r_{mah}/2), \tag{4.1}$$

where Φ is the cumulative standard Gaussian distribution function. For univariate Gaussian population many theoretical results exists on the closeness of estimated and true probability density function ([76]). The two main measures used to describe this closeness are the L_1 metric – L_2 metric (the integrated mean square error)

$$L_1 = \int E(\mid \hat{p}_m(v) - p(v) \mid) dv \tag{4.2}$$

$$L_2 = \int E(\hat{p}_m(v) - p(v)^2) dv \tag{4.3}$$

Where $\hat{p}_m$ is nonparametric density estimate obtain by implementing one of nonparametric density estimators (3.18,**??**) with a sample of m events. From the figure (4.1)one can see the density curves corresponding to the different smoothing parameters (bandwidths) overlayed onto the standard Gaussian density ([86]).

For the small kernel width $h = 0.1$ the estimated is discreet, for the width - $h = 0.7$ – *oversmoothed*. There is a number of notions for "optimal" kernel width ([76]), for samples from Gaussian populations, for example

$$h = 1.66M^{-1/5} \tag{4.4}$$

This equation is valid only if Mahalonobis metric is used. As one can easily calculate, the optimal kernel width increase from 0.41 for sample size $M = 1000$, to - 0.67 for sample size $M = 100$. For multivariate Gaussian distributions, of course, one have to have take greater values.

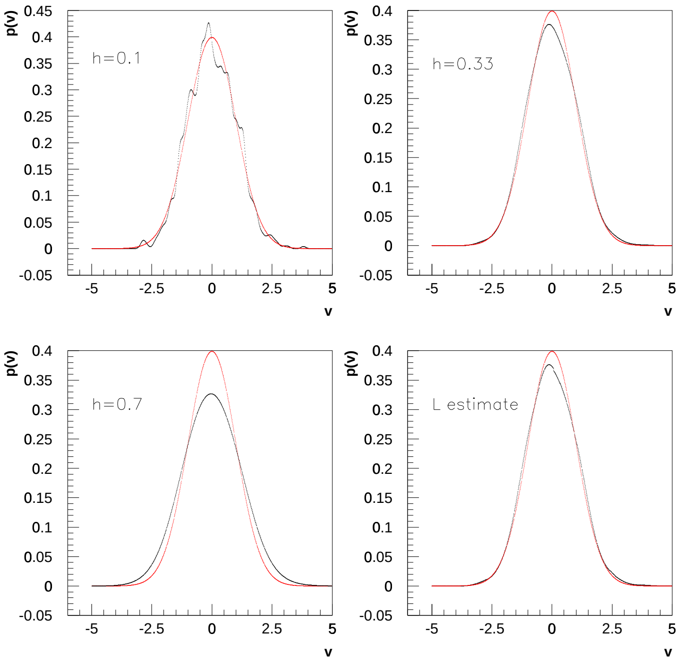

Figure 4.1: Parzen density estimates of standard normal distribution

The "optimal kernel" and adaptive estimates (L-estimate) show better approximation, compared with estimates with fixed parameters. Note, that the L-estimate didn't use very specific a priory information on distribution function shape, as "optimal kernel" estimate, therefore it is robust and can be used for samples taken from distributions, which analytic shape is unknown (common case in experimental data analysis). The sequence of fixed kernels, used for constructed of L-estimate, should cover some wide interval depending, of course, on the available sample size.

To check the density estimator we calculate the probability integral for several independent samples from standard Gaussian population:

$$\int \hat{p}(v)dv \tag{4.5}$$

As one can see from the figure 4.2, the distribution is very compact approaching 1 from the left (the bottom Darbu sum), proving the correct normalization of the estimated densities (3.18).

The results of L-estimator check are summaries in Table 4.1. The densities were estimated in 51 points uniformly distributed in (-5 +5) interval. The $L1$ and $L2$ measures were calculated for samples from standard Gaussian population. The Bayes risk estimates were done for samples from standard Gaussian and Gaussian with mean 1 and variance 1, according to (3.29).

The densities were calculated simultaneously for 7 kernel widths (from 0.2 to 0,8).

Corresponding Bayes errors and L1, L2 measures as well as first and second statistical moments, were calculated for each from 1000 trials of independent samples of size 10, 25,

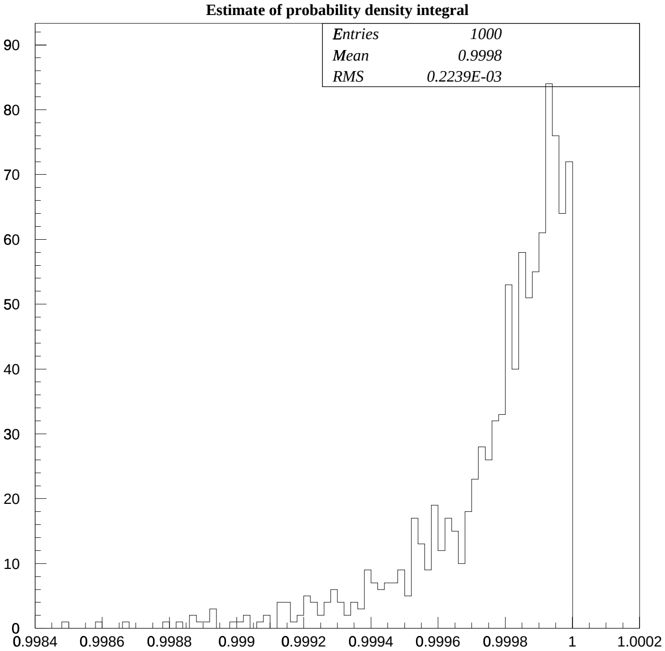

Figure 4.2: The histogram of "probability integrals"

Table 4.1: *The quality check of Parzen density estimator, samples from Gaussian populations N(0,1)-N(1,1), L-estimator*

MxB	mean		variance		R^e	$L1$	$L2$
10	0.002	0.996	1.437	1.463	0.332 ± 0.210	0.345 ± 0.150	0.0310 ± 0.024
x	-0.050	0.978	1.340	1.330	0.325 ± 0.190	0.340 ± 0.140	0.0310 ± 0.024
1000	-0.004	0.998	1.400	1.430	0.332 ± 0.200	0.340 ± 0.140	0.0300 ± 0.023
25	-0.008	0.995	1.144	1.139	0.317 ± 0.140	0.240 ± 0.100	0.0154 ± 0.013
x	-0.033	0.978	1.080	1.080	0.320 ± 0.140	0.250 ± 0.100	0.0166 ± 0.012
1000	-0.005	0.990	1.140	1.140	0.317 ± 0.145	0.240 ± 0.100	0.0155 ± 0.012
100	-0.002	0.994	1.031	1.033	0.317 ± 0.074	0.141 ± 0.050	0.0058 ± 0.0041
x	-0.003	0.966	0.980	0.980	0.314 ± 0.080	0.153 ± 0.048	0.0065 ± 0.0042
1000	-0.006	0.948	1.030	1.030	0.312 ± 0.071	0.141 ± 0.050	0.0057 ± 0.0040
400	-0.004	1.000	1.010	1.001	0.308 ± 0.060	0.083 ± 0.024	0.0021 ± 0.0013
x	-0.030	0.965	0.960	0.960	0.310 ± 0.050	0.097 ± 0.028	0.0026 ± 0.0014
100	-0.000	0.990	1.000	1.010	0.310 ± 0.055	0.089 ± 0.032	0.0023 ± 0.0015
1000	-0.001	0.996	1.001	0.992	0.310 ± 0.100	0.062 ± 0.028	0.0012 ± 0.0008
x	-0.035	0.959	0.950	0.950	0.310 ± 0.100	0.077 ± 0.033	0.0016 ± 0.0010
10	-0.004	0.998	0.990	1.000	0.310 ± 0.100	0.064 ± 0.025	0.0011 ± 0.0005

100; 100 trials for - 400; and 10 trials for - 1000. Rather well agreement with other estimators reported in ([82, 15]), demonstrates the consistence and unbiasness of density estimators used in ANI.

4.1.2 The Bootstrap Statistical Moments

To check the validity of bootstrap approach we test the biasness of bootstrap moments using samples from the standard distribution $N(0, 1)$; the sample size varied between 25 and 1000, the number of bootstrap replicas in a series was from 10 to 1000.

The mean was calculated for each bootstrap replica according to (3.35), and for each bootstrap series - the bootstrap estimate of the mean μ_* and - mean standard deviation - $\delta_* = \sigma_*/M$, was evaluated. The results of investigations, which present in table 4.2, illustrate the validity of "butstrap" CLT (3.34) and consistency of using of the bootstrap moments.

Although the mathematical theorems were proved for the asymptotic cases $M,\ B \to \infty$ even with small sample sizes and rather small numbers of bootstrap replicas $(M, B = 50)$, the obtained bootstrap estimates coincide with sampling statistical moments with reasonable precision. Of course, enlarging of sample size and bootstrap replicas number improves the accuracy significantly.

4.1.3 Distribution mixture coefficients estimation

The bootstrap fraction estimator (see section 3.3.7) was checked by a pilot Monte Carlo study of 2-way classification with samples from Gaussian population $N(0, 1)$ and $N(1, 1)$. For comparing the "bootstrap errors" of "reconstructed" proportion with expected from usual sampling procedures we make a mixture "experimental" sample from both samples in $0.2 - 0.8$ proportion, therefore the fraction of "first type" events in mixture was 0.2. The empirical fraction estimate P_1^e and the error matrix R^e were calculated using the Bayesian nonparametric procedures (3.31 and 3.29). Then the "true" fraction $\hat{P}_1$ was calculated according to (3.32 and 3.33).

The sample averaged values of all 3 estimates was obtained with independent random samples from the same Gaussian populations. They are denoted in the table by brackets <>.

The bootstrap estimates are denoted by $*$ symbol.

The examples of particular run are presented in ANI outputs section (5.3).

In table 4.3 100 events were used for training and 1000 for classification, 10 bootstrap samples was simulated. The dimensionality was varied from 1 to 4.

Table 4.4 represents results for 1000 event training and the same 1000 for classification and 10 bootstrap replicas.

The last table 4.5 represents 2 big butstrap trials 1000 for 100 training and 100 for 1000. Only dimensionality 4 was used.

As it is seen from the tables, especially for the big sampling and bootstrap replicas values, the bootstrap fraction estimates along with m.s.e. estimates are in consistence with sampling estimates.

Although, a more detailed Monte Carlo simulations are required for definite conclusions after quantitative comparisons.

Table 4.2: *Bootstrap expectations and bootstrap standard deviations of sampling statistics*

	B	10	50	100	200
	$E\{\mu_* - \mu_M\}$	-0.0152	0.0031	-0.0048	-0.0003
M=25	$\sigma\{\mu_* - \mu_M\}$	0.0639	0.0251	0.0174	0.0160
δ_{25}=0.2	$E\{\delta_*\}$	0.1891	0.1974	0.1929	0.1977
	$\sigma\{\delta_*\}$	0.0560	0.0300	0.0031	0.0028
	$E\{\mu_* - \mu_M\}$	-0.0024	-0.0023	0.0003	-0.0001
M=50	$\sigma\{\mu_* - \mu_M\}$	0.0402	0.0227	0.0149	0.0097
δ_{50}=0.1414	$E\{\delta_*\}$	0.1481	0.1398	0.1396	0.1395
	$\sigma\{\delta_*\}$	0.0286	0.0182	0.0167	0.0154
	$E\{\mu_* - \mu_M\}$	-0.0171	-0.0010	-0.0004	-0.0008
M=100	$\sigma\{\mu_* - \mu_M\}$	0.0323	0.0152	0.0101	0.0066
δ_{100}=0.1	$E\{\delta_*\}$	0.0897	0.0959	0.1000	0.0988
	$\sigma\{\delta_*\}$	0.0212	0.0107	0.0097	0.0086
	$E\{\mu_* - \mu_M\}$	0.0038	-0.0017	0.0001	0.0000
M=200	$\sigma\{\mu_* - \mu_M\}$	0.0231	0.0107	0.0082	0.0048
δ_{200}=0.0707	$E\{\delta_*\}$	0.0593	0.0692	0.0694	0.0700
	$\sigma\{\delta_*\}$	0.0154	0.0078	0.0063	0.0049
	$E\{\mu_* - \mu_M\}$	-0.0018	0.0007	0.0004	0.0003
M=500	$\sigma\{\mu_* - \mu_M\}$	0.0115	0.0072	0.0040	0.0032
δ_{500}=0.0447	$E\{\delta_*\}$	0.0430	0.0452	0.0442	0.0446
	$\sigma\{\delta_*\}$	0.0095	0.0043	0.0033	0.0024
	$E\{\mu_* - \mu_M\}$	0.0038	0.0001	0.0002	0.0003
M=1000	$\sigma\{\mu_* - \mu_M\}$	0.0079	0.0050	0.0030	0.0022
δ_{1000}=0.032	$E\{\delta_*\}$	0.0322	0.0317	0.0316	0.0315
	$\sigma\{\delta_*\}$	0.0073	0.0033	0.0022	0.0017

Table 4.3: Fraction estimation, M=100; B=10

N	1	2	3	4
R^B	0.309	0.240	0.193	0.159
Index	0.632	0.719	0.788	0.825
R^e	0.285	0.280	0.205	0.165
P_1^e	0.367	0.338	0.297	0.285
$\hat{P}_1$	0.162	0.183	0.206	0.219
R_*^e	0.295 ± 0.094	0.264 ± 0.075	0.221 ± 0.045	0.173 ± 0.072
P_{*1}^e	0.394 ± 0.096	0.340 ± 0.045	0.277 ± 0.041	0.270 ± 0.038
$\hat{P}_{1*}$	0.132 ± 0.165	0.193 ± 0.078	0.263 ± 0.022	0.203 ± 0.039
$< R^e >$	0.325 ± 0.098	0.252 ± 0.082	0.221 ± 0.082	0.177 ± 0.029
$< P_1 >$	0.355 ± 0.103	0.393 ± 0.077	0.324 ± 0.057	0.311 ± 0.039
$< \hat{P}_1 >$	0.184 ± 0.075	0.156 ± 0.087	0.220 ± 0.033	0.173 ± 0.063

Table 4.4: Fraction estimation, M=1000; B=10

N	1	2	3	4
R^B	0.309	0.240	0.193	0.159
Index	0.700	0.767	0.813	0.839
R^e	0.300	0.233	0.187	0.159
P_1^e	0.367	0.338	0.297	0.285
$\hat{P}_1$	0.162	0.183	0.206	0.219
R_*^e	0.300 ± 0.044	0.231 ± 0.029	0.187 ± 0.029	0.159 ± 0.023
P_{*1}^e	0.376 ± 0.043	0.348 ± 0.018	0.301 ± 0.020	0.291 ± 0.018
$\hat{P}_{*1}$	0.163 ± 0.029	0.189 ± 0.020	0.205 ± 0.014	0.217 ± 0.008
$< R^e >$	0.310 ± 0.029	0.250 ± 0.019	0.200 ± 0.025	0.164 ± 0.018
$< P_{*1}^e >$	0.405 ± 0.030	0.342 ± 0.025	0.329 ± 0.024	0.309 ± 0.020
$< \hat{P}_1 >$	0.194 ± 0.040	0.191 ± 0.040	0.186 ± 0.035	0.199 ± 0.019

Table 4.5: Fraction estimation, N=4, B=100, 1000

N=4	100x1000	1000x100
R^B	0.159	0.159
Index	0.825	0.839
P_1^e	0.260	0.285
$\hat{P}_1$	0.156	0.219
R^e	0.165	0.159
R_*^e	0.171 ± 0.073	0.160 ± 0.019
P_{*1}^e	0.270 ± 0.042	0.287 ± 0.015
$\hat{P}_{*1}$	0.205 ± 0.051	0.215 ± 0.012
$< R^e >$	0.170 ± 0.062	0.165 ± 0.021
$< P_1^e >$	0.312 ± 0.052	0.304 ± 0.020
$< \hat{P}_1 >$	0.208 ± 0.051	0.202 ± 0.023

4.1.4 Bayesian Mapping

Bayesian decision rule (3.12) is defined in each point of feature space $\mathcal{V}$, and for each point the definite decision is made (of course each point $\mathbf{v} \subset \mathcal{V}$ have to have the ”physical” meaning, visa-versa the outliers selection rule (3.15) will be triggered).

The $\mathbf{v}$ points attributed for one and the same category usually form, so called, ”clusters” - compact regions in $\mathcal{V}$. The shape of this regions can be highly nonlinear and ever disconnected. On the figure 4.3 we can see distinct clusters corresponding to samples from 2-dimensional Gaussian population with means 1, 5, 7. Variances of all classes are equal to 1, 1000 events for each class were used.

As the sample means are rather far from each other, the clusters get definite shape to contain as much events from particular class, simultaneously rejecting events from the other classes. The spheric shape of edge clusters is explained by the spheric symmetry of 2 dimensional uncorrelated Gaussian population, the middle class variables are correlated, and therefore second cluster points (superimposed on the figure) had an elliptic shape.

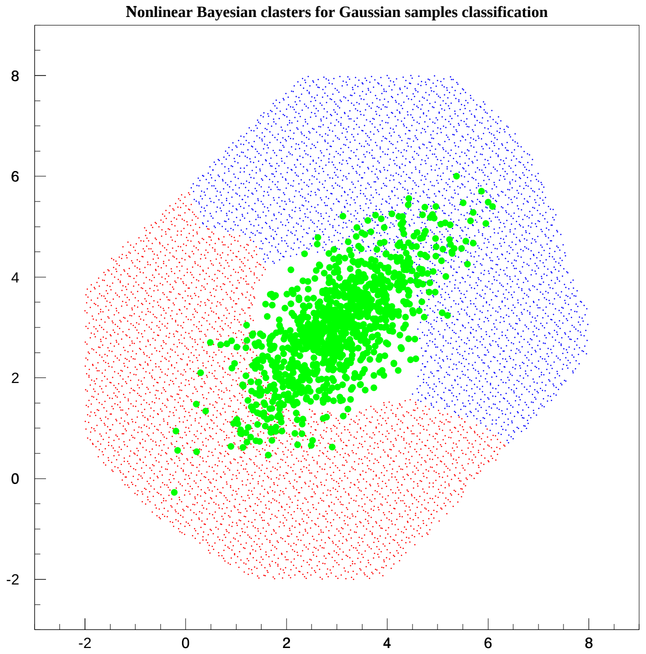

Figure 4.3: The Bayes clusters for samples from Gaussian populations with different means

On the figure 4.4 the clusters corresponding to the two samples from the one Gaussian population are presented. Very complicated form of cluster is explained by the sampling random fluctuation.

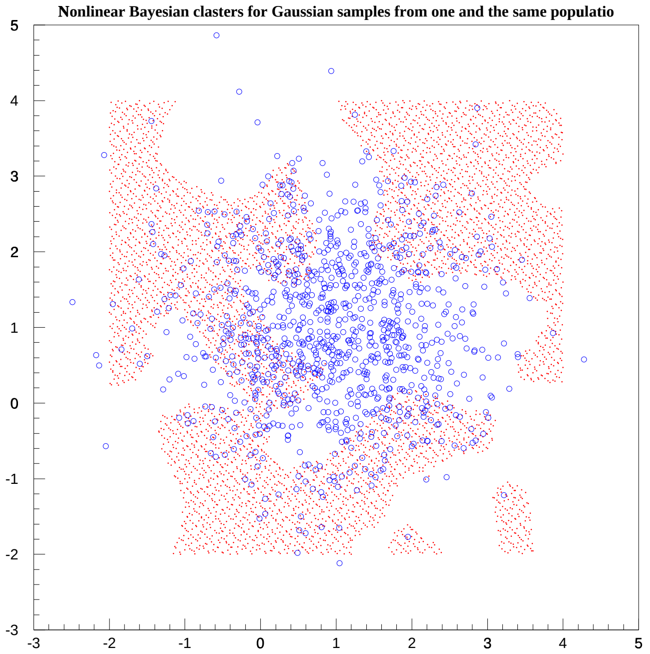

Figure 4.4: The Bayes clusters for samples from Gaussian populations with same means

4.2 Artificial Neural Networks Models

4.2.1 Neural Clusters

We use the 2:4:2:1 feedforword network for detecting the 2-dimensional clusters with radial symmetry. Training samples consists of two classes of 450 uniform distributed "background" events. The 50 "signal "events generated according to 2-dimensional radial symmetric Gaussian population with mean - 0.5 and σ - 0.03 were added to one of background samples.

The goal of algorithm is to find a 2-dimensional cluster maximizing the objective function (3.41), e.g. containing as much as possible "signal" events, and rejecting the background events.

Figure (4.5) presents the results of Sobol sieves search strategy (see section 3.4.2). A is size of pseudo-random sieve.

After obtaining several trained networks, the obtain "chromosome" where used as a "pool" for genetic algorithm. The "fittest descent" strategy after several generations of offsprings, as one can see from figure 4.6 improves situation. Both "mutations" and "crossovers" increase σ values.

4.2.2 Whipple Crab Detection

The best discrimination technique used in the WHIPPLE Observatory is the multidimensional cuts (*supercuts*) method proposed in ([37]) and then improved in ([30]) (four Cherenkov image parameters were used). The method consists of a posterior selection of the best gamma-

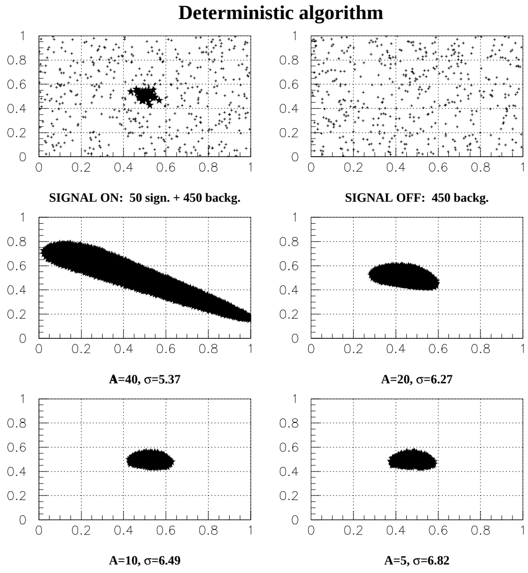

SIGNAL ON: 50 sign. + 450 backg.

SIGNAL OFF: 450 backg.

A=40, σ=5.37

A=20, σ=6.27

A=10, σ=6.49

A=5, σ=6.82

Figure 4.5: Deterministic Search

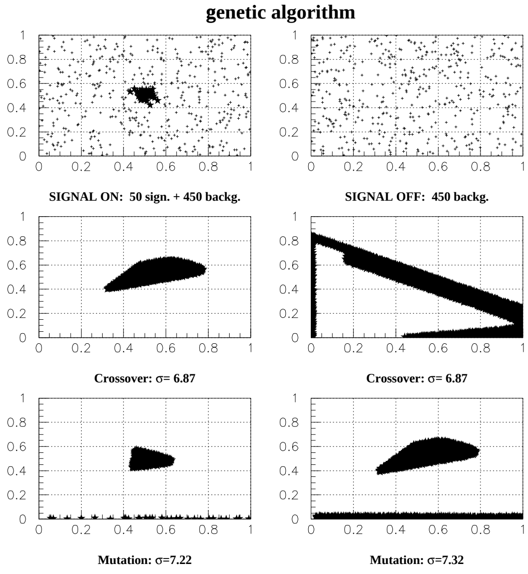

SIGNAL ON: 50 sign. + 450 backg.

SIGNAL OFF: 450 backg.

Crossover: σ= 6.87

Crossover: σ= 6.87

Mutation: σ=7.22

Mutation: σ=7.32

Figure 4.6: Genetic Search

cluster (multidimensional box), containing "gamma-like" events. The particular coordinates of the box were selected to maximize the σ value on the 1988-1989 Crab nebula observation data base (65 ON, OFF pairs $\sim 10^6$ events) ([29]) . By implementing the supercuts method, the initial σ value was enlarged from 5(raw data) to 34.

The parameters of the Cherenkov image, used for background rejection reflect the inherent differences in angular size and shape from two types of images (WIDTH, LENGTH) and differences in the image orientation (MISS, ALPHA), the estimate of impact parameter of particle - DIST; the dispersion parameter (CONC) of the images have also been used. A single parameter can be defined which combines the shape and orientation criterion - AZWIDTH.

We use a simple 4::5::1 neural net to select the better nonlinear shape of the gamma-cluster. The net was trained on experimental ON&OFF events.

For Neural analysis were used the same variables as for Supercut analysis: WIDTH, LENGTH, DIST, ALPHA. The comparison of different background suppression methods one can see from the table 4.6, where DIFF= $N^{\star}_{\mathrm{on}} - N^{\star}_{\mathrm{off}}$ is the estimate of the signal, DIFF$/N^{\star}_{\mathrm{off}}$ - is the estimate of the signal to noise ratio, $\frac{N^{\star}_{\mathrm{off}}}{N_{\mathrm{off}}}$- is the estimate of background suppression by used technique.

Table 4.6: WHIPPLE Crab detection, 1988-1989

	$N^{\star}_{\mathrm{on}}$	$N^{\star}_{\mathrm{off}}$	σ	DIFF	DIFF$/N^{\star}_{\mathrm{off}}$	$\frac{N^{\star}_{\mathrm{off}}}{N_{\mathrm{off}}}$
Raw	506255	501408	4.8	4847	0.01	
AZWIDTH	14622	11389	20.4	3233	0.28	0.0227
WEDGE cut ([37])	6017	3381	27.2	2636	0.78	0.0067
SUPERCUT ([30])	4452	1766	34.3	2686	1.52	0.0035
NEURAL 4::5::1	6278	2858	35.8	3420	1.20	0.0057

The neural nonlinear cluster is much less restrictive than supercut and ever AZWIDTH cut. More "intelligent", smooth nonlinear shape of γ-cluster ensures the significant enhancement of signal detection efficiency along with very high rejection of background.

Chapter 5

ANI Testing (KASCADE Data Analysis)

A. Chilingarian, H. Rebel, M. Roth, A. Vardanyan

5.1 The Simulation Procedure

All statistical decisions and procedures are correct within the prechosen model. Thus a realistic simulation is the key problem of any physical inference in indirect experiments. Extensive air shower investigations are a classical example of such a situation. An adequate consideration of detector response and an identical reconstruction of experimental and simulated data are necessary steps of data analysis.

The first simulation data base of the KASCADE experiment fulfilling the above requirements is available since recently, and we use specific EAS parameters, like the numbers of electrons/photons (N_e) and truncated number of muons ($N_{\mu^{tr}}$) and the age (S_{30}) parameter as input for data analysis.

The physical meaning of these variables will not be discussed, we only mention that the procedures of their use are identical for experimental data and simulations. It is also very important to say that hypotheses about lateral distributions of muons and electrons at very small and large distances are not of influence.

The simulations of the EAS development in the atmosphere was done with the CORSIKA code (version 5.2: VENUS and QGS models) .

For the calculation of the full detector response function the GEANT CERN package was used. The parameters of simulated showers were reconstructed with the same programs as experimental ones.

The measured EAS parameters by KASCADE are as follows in the table 5.1:

As one can see from the figure 5.1 the overlapping of shower parameters corresponding ever to more distinct classes (proton and iron initiating primaries) is rather big and one can't expect reliable classification of primaries according to the single EAS features.

In the multidimensional features space, as one can see from the figure 5.2 the differences between proton and iron samples could be detected. Therefore, the detailed examination of all EAS characteristics and their correlations will allow to find a subset of features to be used for experimental data classification.

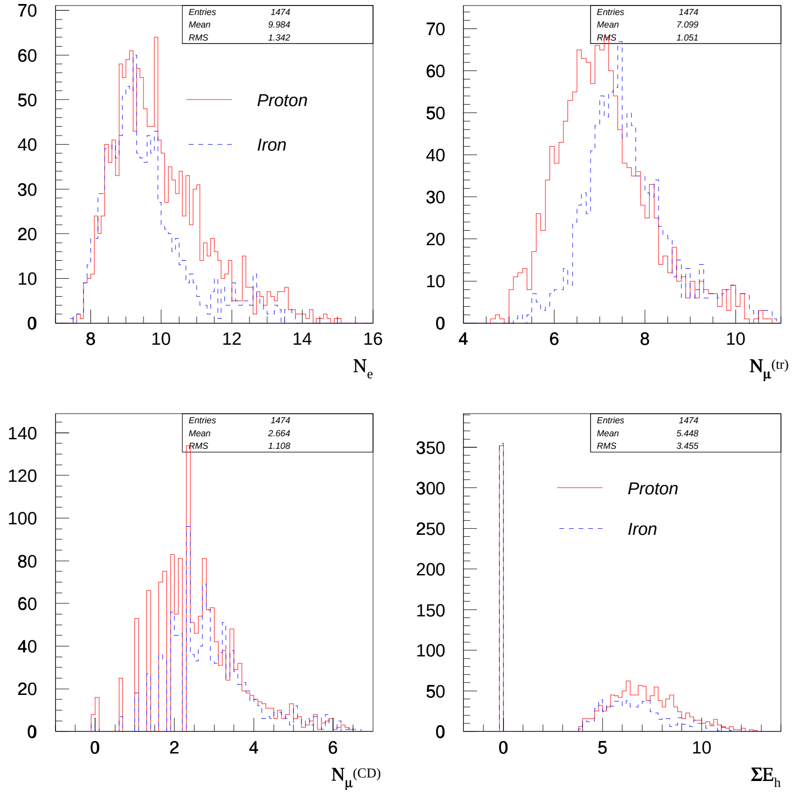

Figure 5.1: Features distribution for proton and iron

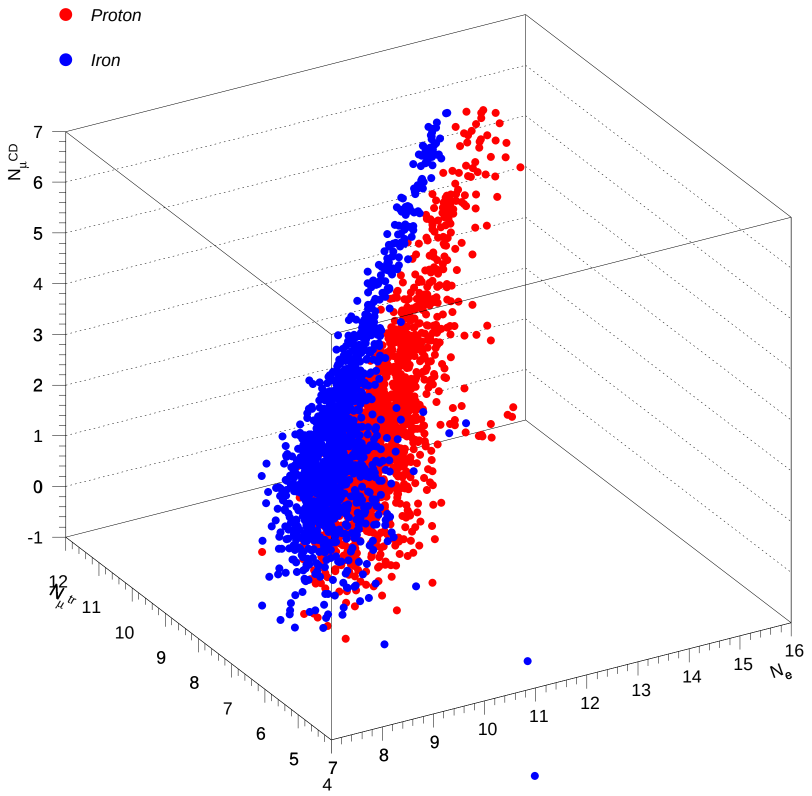

Figure 5.2: Proton and iron events distribution in 3 dimensional space of features

Table 5.1: EAS features detected by KASCADE experiment

N_e	Number of electrons in EAS
N_μ^{tr}	Truncated number of muons (number of muons in the range of 40 to 200m)
S_{30}	Shower age associated with a Molier radius 30m
N_μ^*	Number of muons in central detector
N_h	Number of hadrons
E_h^{max}	The sum of energy of most energetic hadrons
E_{sum}	Total energy of hadrons

5.2 Validation of Models

5.2.1 Comparison of the Single EAS variables

First of all we've to examine the variables to select primary mass discriminants and varibles corralated with the primary energy. We use for this purposes simulated events, for which the "true" values of mass and energy are known. For all measurable EAS variables we calculate the P-values of following statistical tests:

- Student's t-test

  $$t = \frac{\mu_1 - \mu_2}{\sqrt{\sigma_1^2 + \sigma_2^2}};$$

  where the μ_1, σ_1 and μ_2, σ_2 are the mean values and the standard deviations of the first and second class respectively.

- Kolmogorov-Smirnov D-test

  $$D = supremum_v |F_1(v) - F_2(v)|;$$

  were $F_1(v)$ and $F_2(v)$ are the cumulative probability function for first and second class (model) respectively. $(F(v) = \frac{N(v_i<v)}{N(v)})$

- Mann-Whitney U-test

  $$U = \frac{T_1}{M1} - \frac{T_2}{M2};$$

  were the T_1 and T_2 are the sum of ranks of events from first and second samples respectively, and M1, M2 - are the number of events in samples. The rank is the number of particular event in ordered sequence of events (so called variation sequence).

5.2.2 Correlation analysis

The correlation analysis was done to select the best pairs of variables for distinguishing between classes.

Table 5.2: *P-values of statistical tests for proton and iron for different models: t - Student, D - Kolmogorov-Smirnov, U - Mann-Whitnay*

QGS	t	D	U	VENUS	t	D	U
N_e	3.177	2.747	4.996	N_e	2.869	3.161	5.778
N_μ^{tr}	12.601	6.026	12.723	N_μ^{tr}	10.274	4.282	9.403
S_{30}	17.160	7.489	17.294	S_{30}	20.415	8.314	19.473
N_μ^*	7.207	3.452	7.132	N_μ^*	5.650	2.031	3.872
N_h	0.673	1.647	2.811	N_h	2.265	3.335	5.848
$maxE_h$	5.564	3.066	6.144	E_{max}	3.612	2.402	4.458
$sumE_h$	2.478	3.126	3.985	E_{sum}	3.457	3.140	6.174

Table 5.3: *Correlation matrix for QGS data*

	Mass	E_0	N_e	N_μ^{tr}	S_{30}	N_μ^*	N_h	$maxE_h$	$sumE_h$
Mass	1.00	0.21	-0.03	0.27	0.32	0.15	-0.03	-0.11	-0.07
E_0	0.21	1.00	0.92	0.95	-0.25	0.94	0.78	0.53	0.73
N_e	-0.03	0.92	1.00	0.90	-0.43	0.93	0.85	0.62	0.81
N_μ^{tr}	0.27	0.95	0.90	1.00	-0.23	0.93	0.78	0.52	0.72
S_{30}	0.32	-0.25	-0.43	-0.23	1.00	-0.33	-0.39	-0.33	-0.38
N_μ^*	0.15	0.94	0.93	0.93	-0.33	1.00	0.86	0.60	0.82
N_h	-0.03	0.78	0.85	0.78	-0.39	0.86	1.00	0.70	0.95
$maxE_h$	-0.11	0.53	0.62	0.52	-0.33	0.60	0.70	1.00	0.73
$sumE_h$	-0.07	0.73	0.81	0.72	-0.38	0.82	0.95	0.73	1.00

Table 5.4: *Correlation matrix for Venus data*

	Mass	E_0	N_e	N_μ^{tr}	S_{30}	N_μ^*	N_h	$maxE_h$	$sumE_h$
Mass	1.00	0.18	-0.06	0.18	0.33	0.09	-0.05	-0.09	-0.07
E_0	0.18	1.00	0.91	0.95	-0.24	0.94	0.80	0.52	0.76
N_e	-0.06	0.91	1.00	0.90	-0.40	0.93	0.89	0.60	0.85
N_μ^{tr}	0.18	0.95	0.90	1.00	-0.24	0.92	0.81	0.51	0.76
S_{30}	0.33	-0.24	-0.40	-0.24	1.00	-0.32	-0.41	-0.28	-0.40
N_μ^*	0.09	0.94	0.93	0.92	-0.32	1.00	0.86	0.57	0.83
N_h	-0.05	0.80	0.89	0.81	-0.41	0.86	1.00	0.65	0.95
$maxE_h$	-0.09	0.52	0.60	0.51	-0.28	0.57	0.65	1.00	0.68
$sumE_h$	-0.07	0.76	0.85	0.76	-0.40	0.83	0.95	0.68	1.00

5.2.3 Probability Distances

Another important measure of the separability of two samples is the *Bhattacharya distance*, which takes the form:

$$Bhata = \frac{1}{8}(\mu_2 - \mu_1)^T \left(\frac{\Sigma_1 + \Sigma_2}{2}\right)^{-1} (\mu_2 - \mu_1) + \frac{1}{2}\ln\frac{|\frac{\Sigma_1+\Sigma_2}{2}|}{\sqrt{|\Sigma_1||\Sigma_2|}}$$

where the μ_i and Σ_i are the expected vector and covariance matrix of i-th class. The first term of this equation is the *Mahalanobis distance* and the last term is the so called correlation distance.

$$R_{Mahal} = (\mu_2 - \mu_1)^T \left(\frac{\Sigma_1 + \Sigma_2}{2}\right)^{-1} (\mu_2 - \mu_1)$$

$$R_{Corr} = \ln\frac{|\frac{\Sigma_1+\Sigma_2}{2}|}{\sqrt{|\Sigma_1||\Sigma_2|}}$$

We select the best subsets of EAS features according the Bhattacharya distance

Table 5.5: *The best feature subsets according to the Bhatacharya distance*

	2 best		next best			worst	
QGS	N_e	N_μ^{tr}	N_μ^*	S_{30}	$sumE_h$	N_h	$maxE_h$
VENUS	N_e	N_μ^{tr}	S_{30}	N_μ^*	$sumE_h$	N_h	$maxE_h$

5.2.4 KASCADE Experimental Data

2371 events of central calorimeter and array data and 450000 events of array data only were available for analysis. The events were selected within $15 - 20°$ zenith angle range (the simulations were done for this angles).

To check homogeneity of data we divide experimental data to 3 parts and make multiple comparisons with techniques described above. Also the negative Log likelihood function value $\mathcal{L}$ (3.17) and estimate of Bayesian error R^e (3.29) were calculated.

	$\mathcal{L}$	$R_{Mahal.}$	$R_{Bhata.}$	$R_{corr.}$	R^e
1 class	2.911	0.011	0.007	0.024	0.479
2 class	2.803	0.029	0.021	0.069	0.466

Table 5.6: Exp. data homogeneity test, features used: N_μ^{CD}, E_h^{sum}

The homogeneity check for array and calorimeter data one can find in tables 5.6, 5.7, 5.8, 5.9. All tests demonstrate rather good agreement with the each other and prove the homogeneity of experimental data samples.

	$\mathcal{L}$	$R_{Mahal.}$	$R_{Bhata.}$	$R_{corr.}$	R^e
1 class	4.434	0.129	0.038	0.086	0.429
2 class	4.289	0.056	0.041	0.135	0.453

Table 5.7: Exp. data homogeneity test, features used: N_e, N_μ^{tr}, N_μ^{CD}, E_n^{sum}

	$\mathcal{L}$	$R_{Mahal.}$	$R_{Bhata.}$	$R_{corr.}$	R^e
1 class	1.428	0.002	0.000	0.000	0.490
2 class	1.425	0.001	0.000	0.000	0.494

Table 5.8: Exp. data homogeneity test, features used: N_e, N_μ^{tr}

Table 5.9: *One dimensional tests of exp. data: t - Student, D - Kolmogorov-Smirnov, U - Mann-Whitnay*

	t	D	U
N_e	1.816	1.114	1.433
N_μ^{tr}	0.080	0.823	0.570
N_μ^*	1.595	1.118	1.776
E_h^{sum}	1.418	0.407	1.358

5.2.5 QGS and VENUS Comparison

To compare CORSIKA different strong interaction models, one have to have the same mass composition and energy distribution in experimental and simulated data, to avoid mass depended differences.

The mass composition of primary cosmic radiation in low energy region (bellow $2{*}10^{15}$ eV) is measured by direct methods and the following proportion of different nucleus is assumed to be true [62]: *H – 24%*; *He – 31%*; *O – 21%*; *Si – 12%*; *Fe – 12%*.

To avoid energy spectrum based differences we choose rather narrow energy interval. The truncated muon interval (in logarithmic scale) $7.82 \leq N_\mu^{tr} \leq 9.21$ is corresponding to the $6 * 10^{14} \leq E_0 \leq 2 * 10^{15}$ eV.

Thus, we construct simulation samples from VENUS and QGS models with this proportion of primaries and in the mentioned energy range. The selection was made by N_μ^{tr} in both, Monte Carlo and experimental data.

Both models are very close to experimental data (see tables 5.11 and 5.10), but all tests give a bit preference to the VENUS model. On the colored map 5.3 one can see the regions of preference with experimental data superimposed and VENUS forms a more compact cluster compared with QGS.

5.2.6 The KASCADE Classification Matrices

The examination of classification matrix and it's index (3.30) gives clues for understanding the discriminative power of different EAS measurables for composition estimation.

The value greater than of 0.6 are still allow for solving the system of equation (3.32) . For the lower values the solutions didn't converge and fraction couldn't be reconstructed. Therefore we have to find appropriate variables, or reduce the number of classes. Only balance between expected classification errors and number of classes used, will allow to obtain reasonable and reliable estimates of the fraction.

Table 5.10: Comparison of exp. data with VENUS and QGS models

	$\mathcal{L}$	R_{Bhata}	R^e
QGS	1.2036 ± 0.01	0.023 ± 0.001	0.456 ± 0.01
VENUS	1.1818 ± 0.01	0.014 ± 0.001	0.469 ± 0.02

Table 5.11: One dimensional tests for models and experiment

VENUS	t	D	U	QGS	t	D	U
N_e	0.916	2.312	0.901	N_e	3.369	3.004	4.368
N_μ^{tr}	3.199	1.450	2.653	N_μ^{tr}	4.609	2.632	4.787

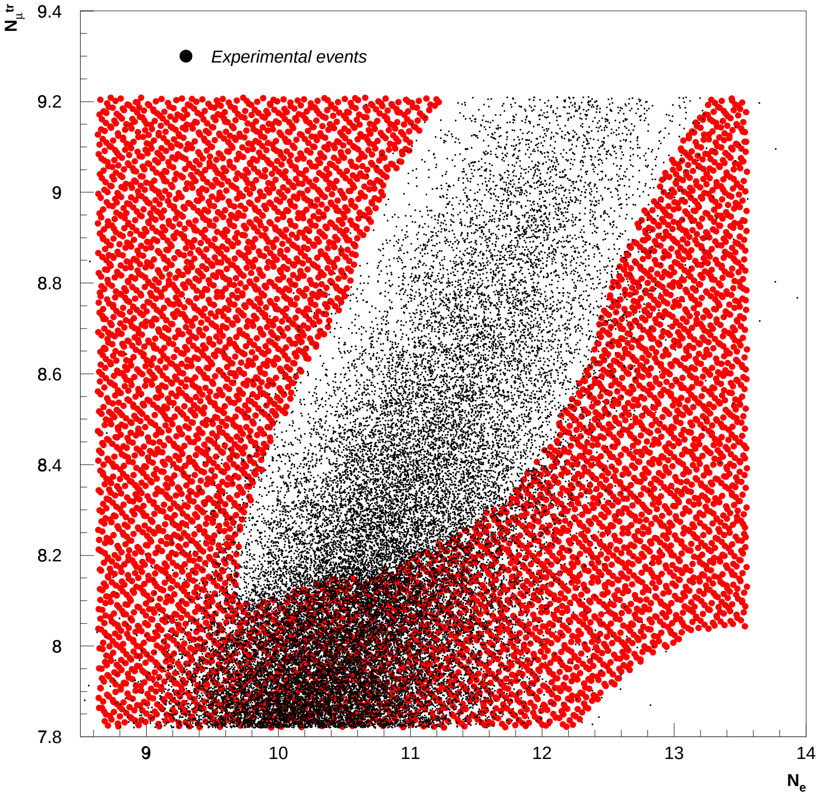

Figure 5.3: QGS (red area) and VENUS (white area) clusters and experimental events distribution in N_e, N_μ^{tr} space

As one can see from tables (5.13), (5.12), (5.14), present status of a priori knowledge accumulated in M.C. models and represented in training samples, didn't support the attempts to make 5-way classification even for all available features.

Table 5.12: Calorimeter data, features used N_{μ}^{CD}, E_h^{sum}

0.5833	0.1172	0.0260	0.1777	0.0958
0.4211	0.1194	0.0244	0.2490	0.1861
0.3126	0.1138	0.0121	0.2701	0.2914
0.3362	0.1017	0.0276	0.2845	0.2500
0.3005	0.0863	0.0216	0.2311	0.3606

Table 5.13: Array data, features used N_e, N_{μ}^{tr}

0.5148	0.2620	0.1024	0.0565	0.0643
0.3240	0.2979	0.1846	0.0885	0.1050
0.1185	0.1803	0.2340	0.1721	0.2951
0.0707	0.1064	0.1942	0.1958	0.4330
0.0445	0.0659	0.1006	0.1362	0.6527

Table 5.14: KASCADE data, features used N_e, N_{μ}^{tr}, N_{μ}^{CD}, E_h^{sum}

0.4785	0.3085	0.1323	0.0438	0.0368
0.2678	0.3863	0.1943	0.0766	0.0750
0.0558	0.1932	0.2903	0.2200	0.2407
0.0367	0.1247	0.2311	0.2506	0.3570
0.0368	0.0706	0.1544	0.1471	0.5912

The situation with 3-way classification is much better, as we need much less a priori information, comparing with classification into 5 nuclei groups. As we can see from tables (5.16), (5.15), (5.17), even array information only allows to resolve the distribution mixture (3.4). The calorimeter information significantly increase the expected fraction reconstruction accuracy.

The 2-way classification in "heavy" and "light nuclei can be done with greater accuracy. See tables (5.19), (5.18), (5.20)

The information concern 5,3 and 2 -way classifications for KASCADE different parts is summarized in table (5.21), where the separability indexes are presented.

Table 5.15: 3-way classification by N_μ^{CD}, E_h^{sum}

$$\begin{vmatrix} 0.5749 & 0.2712 & 0.1539 \\ 0.3443 & 0.3319 & 0.3239 \\ 0.2167 & 0.2976 & 0.4857 \end{vmatrix}$$

Table 5.16: 3-way classification by N_e, N_μ^{tr}

$$\begin{vmatrix} 0.6831 & 0.2595 & 0.0574 \\ 0.2132 & 0.4849 & 0.3019 \\ 0.0919 & 0.3078 & 0.6003 \end{vmatrix}$$

Table 5.17: 3-way classification by N_e, N_μ^{tr}, N_μ^{CD}, E_h^{sum}

$$\begin{vmatrix} 0.7108 & 0.2419 & 0.0473 \\ 0.1777 & 0.5176 & 0.3048 \\ 0.0779 & 0.2559 & 0.6662 \end{vmatrix}$$

Table 5.18: 2-way classification by N_μ^{CD}, E_h^{sum}

$$\begin{vmatrix} 0.665 & 0.335 \\ 0.246 & 0.754 \end{vmatrix}$$

Table 5.19: 2-way classification by N_e, N_μ^{tr}

$$\begin{vmatrix} 0.863 & 0.137 \\ 0.088 & 0.912 \end{vmatrix}$$

Table 5.20: 2-way classification by N_e, N_μ^{tr} N_μ^{CD}, E_h^{sum}

$$\begin{vmatrix} 0.865 & 0.135 \\ 0.076 & 0.924 \end{vmatrix}$$

Table 5.21: Separability index for KASCADE

	Index-5	Index-3	Index-2
CD	0.154	0.462	0.708
ARRAY	0.341	0.584	0.887
ARRAY+CD	0.38	0.626	0.894

5.2.7 Colored Nuclear maps

It is of greatest importance to divide initial feature space according to different primaries. Each decision rule maps $\mathbf{v_i}$,(or $\mathbf{u_i}$) events to one of 3 nuclei groups. Visa-versa, each nuclei group is mapped by decision rule (3.12) to the definite region of feature space $\mathcal{V}$.

By examining of such "nuclear maps" we can make insight to the possibility of defining the type of particular nuclei and about expected misclassification to the other nuclear groups.

Overlaying the experimental data on the colored nonlinear "masks" we can visualize the Bayesian decision procedure.

The different masks, for various variables, two energy regions and 2 strong interaction models are posted below.

The colored maps are corresponded to 2 - and 3-way classifications, directly corresponding to the R^e estimates and tables from the previous section.

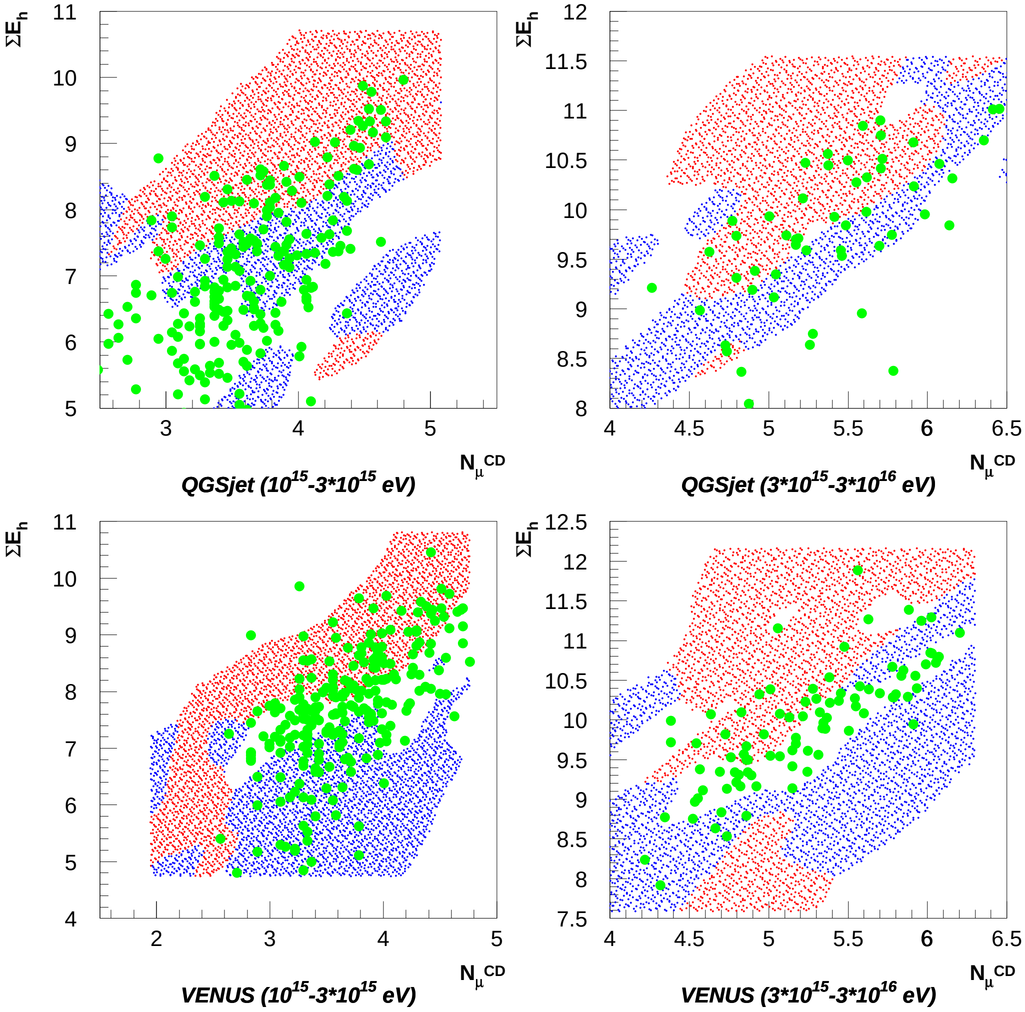

Figure 5.4: 3-way map, calorimeter information. Green points represent oxygen MC data.

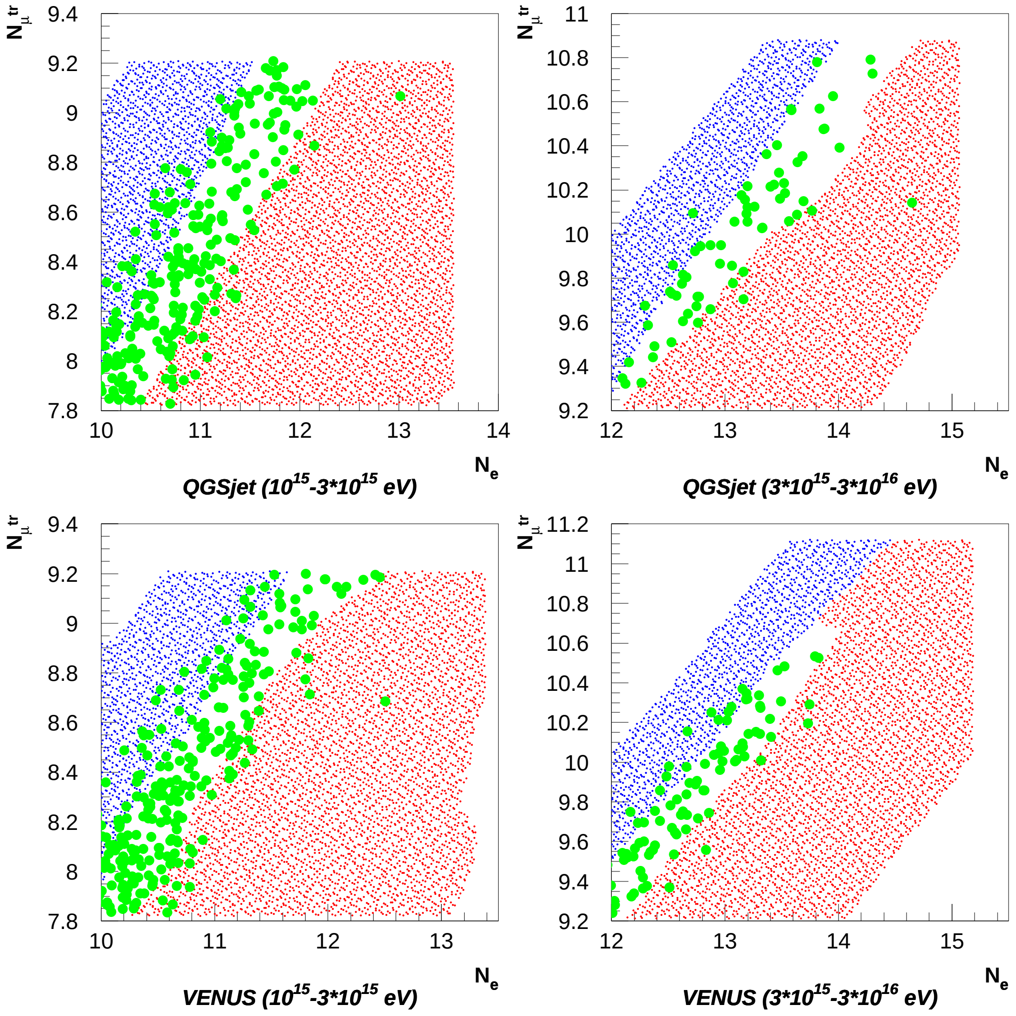

Figure 5.5: 3-way map, array information. Green points represent oxygen MC data.

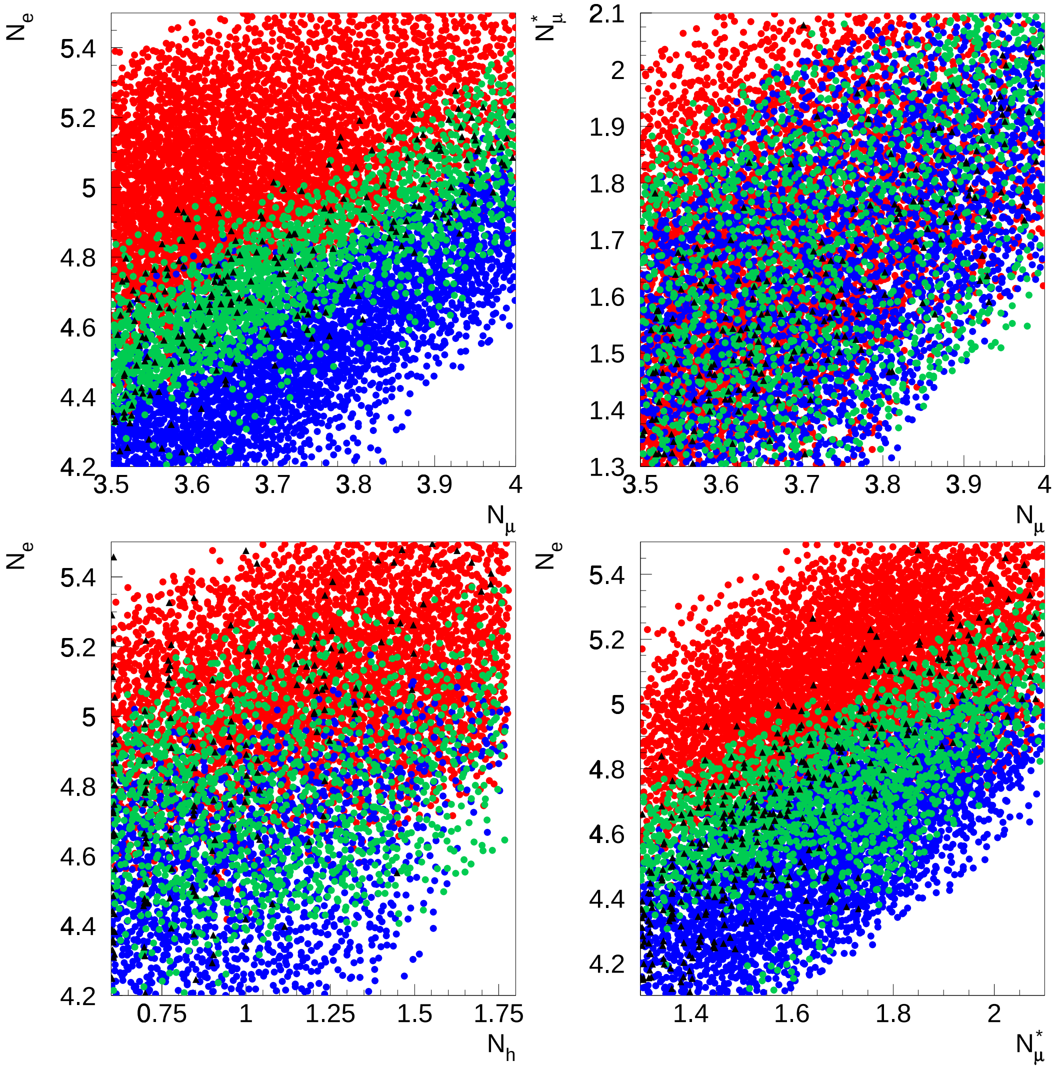

Figure 5.6: QGS model: 3-way map, array information. p_p ≡red, p_O ≡green, p_{Fe} ≡blue. Black triangles represent oxygen MC data. $E_{MC} \in [1 \times 10^{15}, 3 \times 10^{15}]$eV

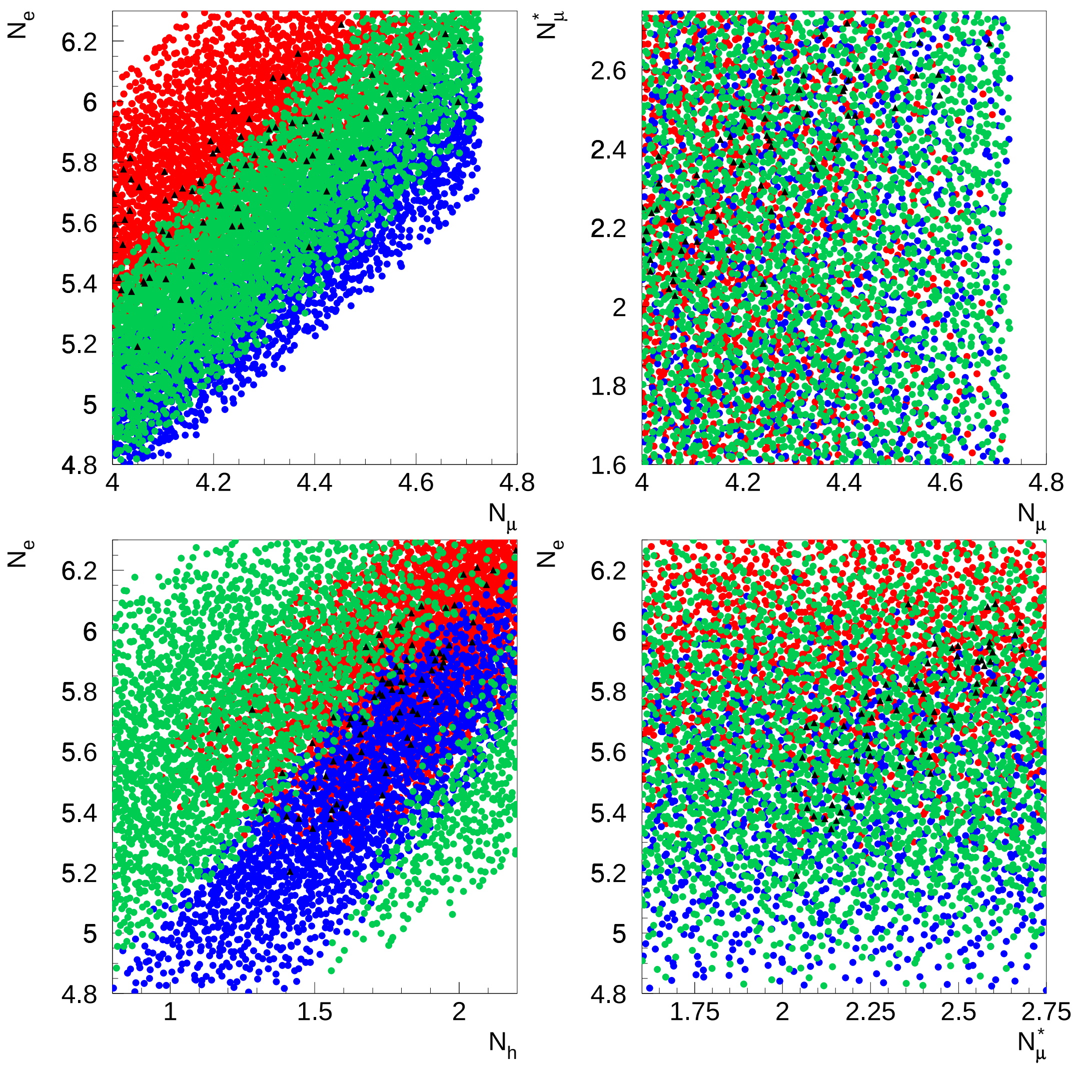

Figure 5.7: QGS model: 3-way map, array information. p_p ≡red, p_O ≡green, p_{Fe} ≡blue. Black triangles represent oxygen MC data. $E_{MC} \in [3 \times 10^{15}, 3 \times 10^{16}]$eV

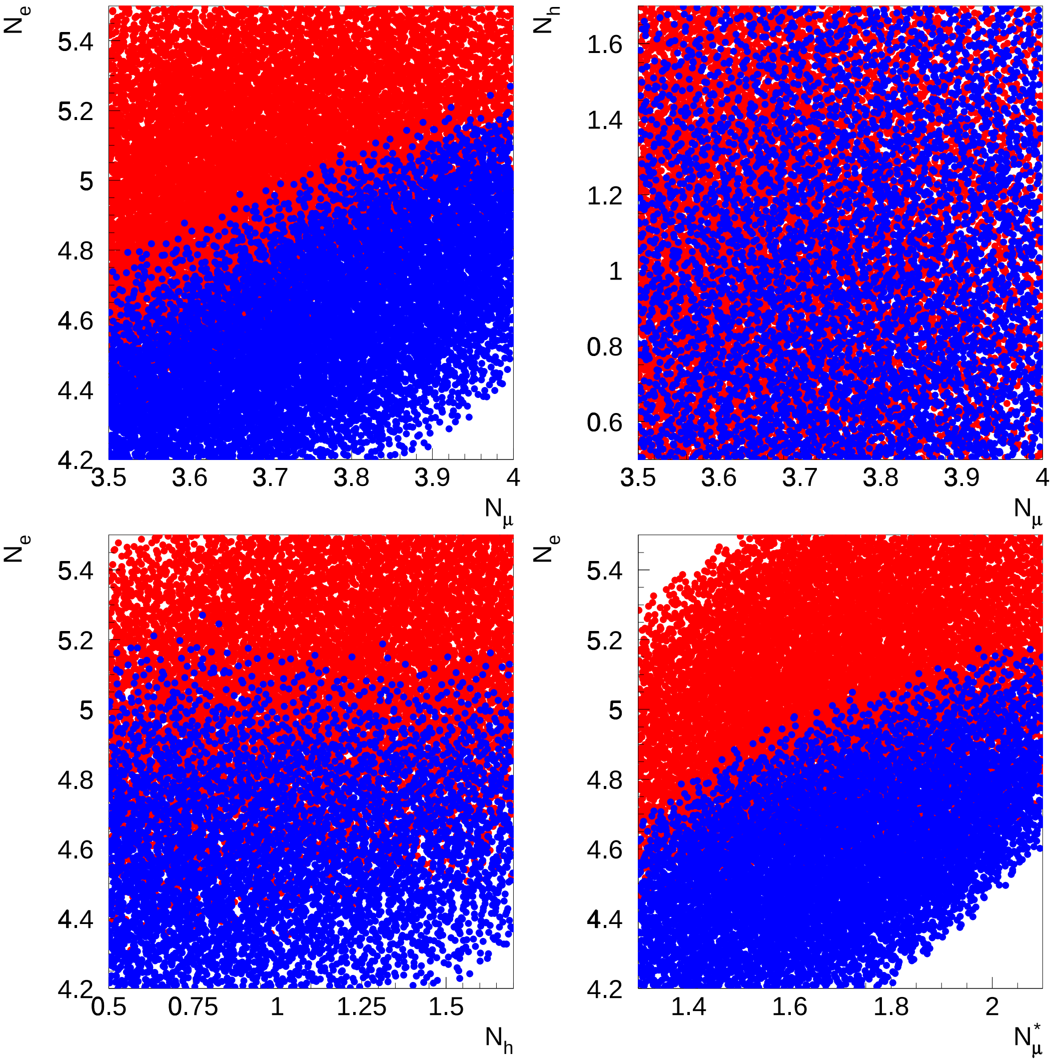

Figure 5.8: VENUS model: 2-way map, array information. p_p ≡red, p_{Fe} ≡blue. $E_{MC} \in [1 \times 10^{15}, 3 \times 10^{15}]$eV

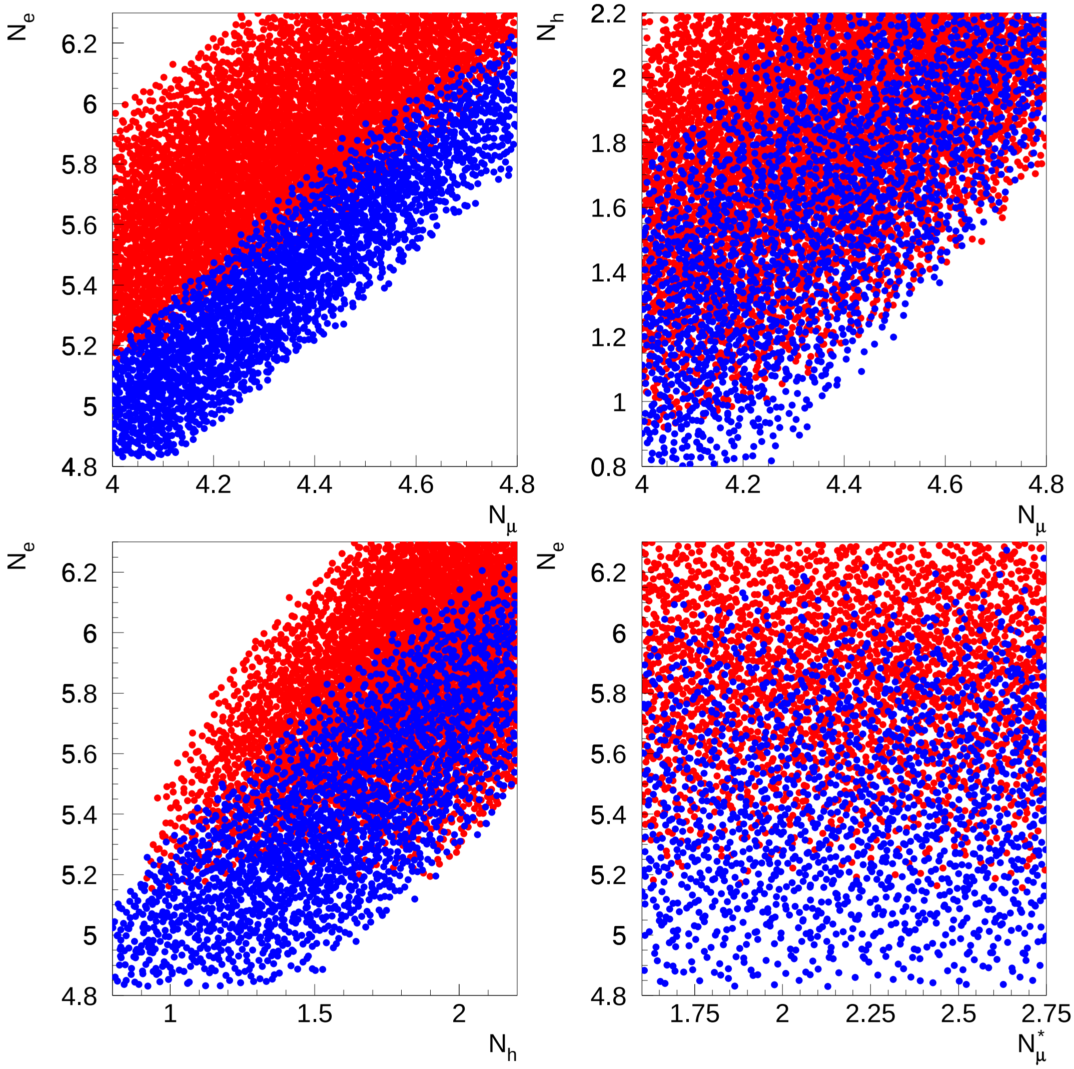

Figure 5.9: VENUS model: 2-way map, array information. p_p ≡red, p_{Fe} ≡blue. $E_{MC} \in [3 \times 10^{15}, 3 \times 10^{16}]$eV

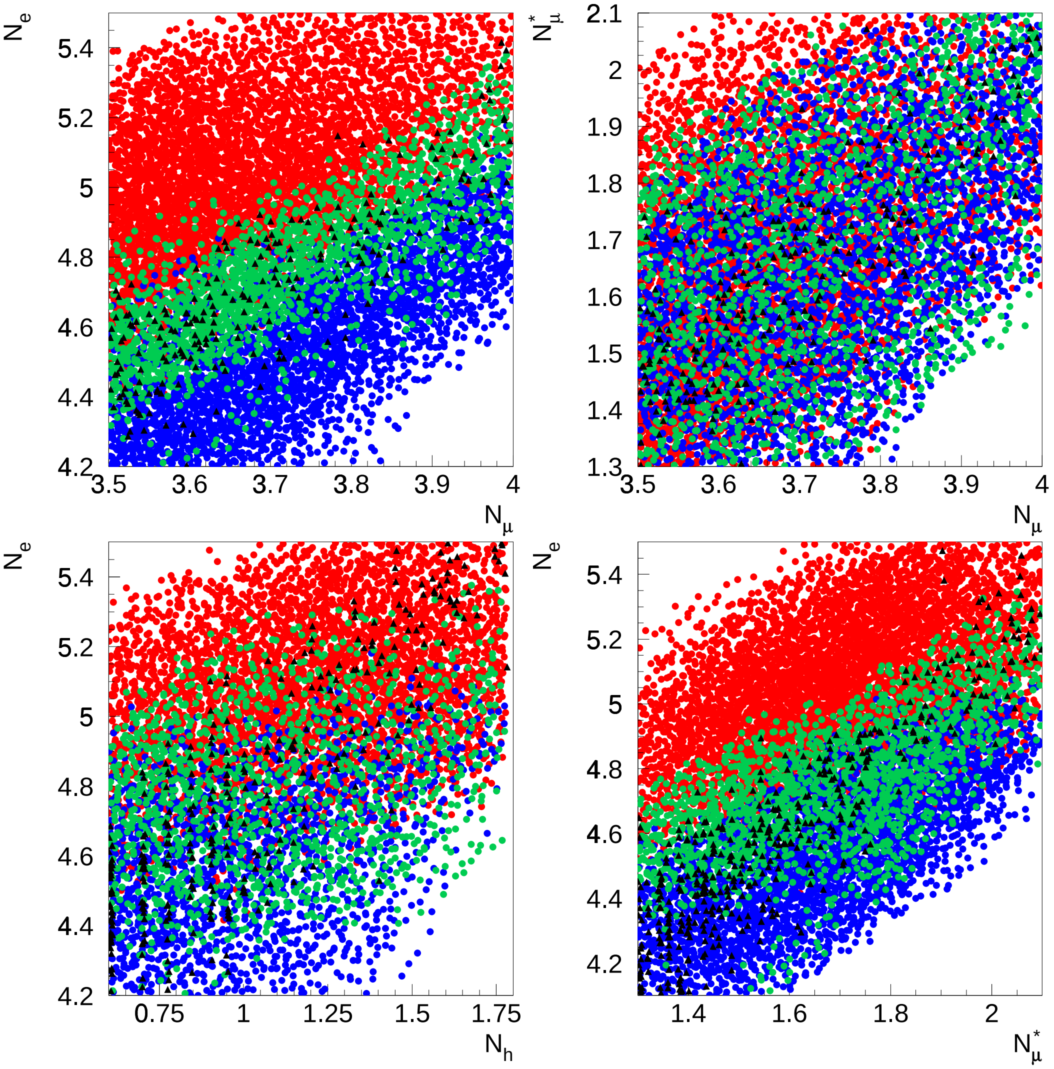

Figure 5.10: VENUS model: 3-way map, array information. p_p ≡red, p_O ≡green, p_{Fe} ≡blue. Black triangles represent oxygen MC data. $E_{MC} \in [1 \times 10^{15}, 3 \times 10^{15}]$eV

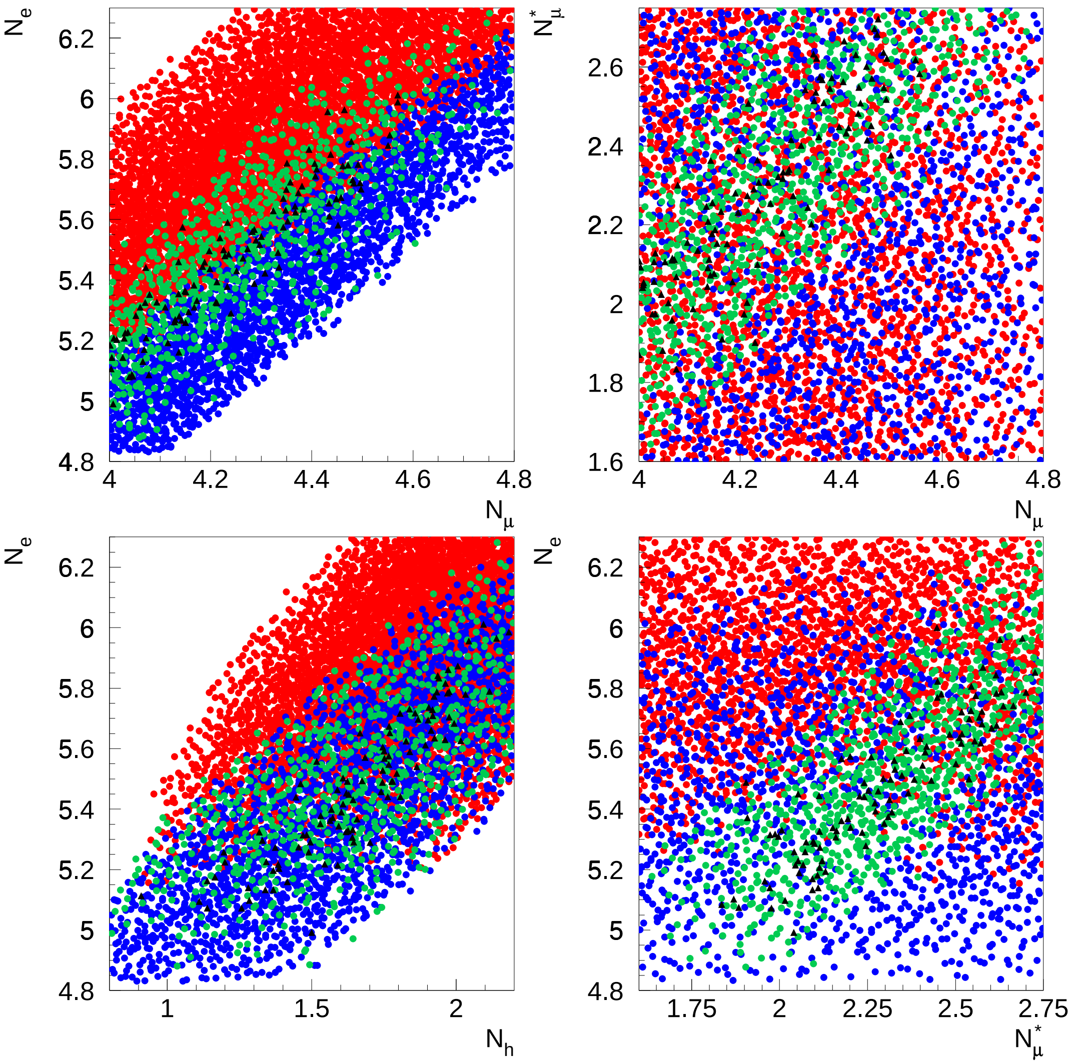

Figure 5.11: VENUS model: 3-way map, array information. p_p ≡red, p_O ≡green, p_{Fe} ≡blue. Black triangles represent oxygen MC data. $E_{MC} \in [3 \times 10^{15}, 3 \times 10^{16}]$eV

5.2.8 Fraction Estimation

The KASCADE data fraction estimation was done in 5 energy bins using both calorimeter and array variables and both QGS and VENUS models. The bootstrapization procedure allows for method error estimation and, by combining results obtained by alternative models –the model error could be estimated. The steady tendency of heavier composition above the ”knee” is detected for all variables used in analysis and for both models. Although the luck of simulations and experimental data for the highest energies didn't support yet more firm conclusions.

Figures (5.12 and 5.13) and tables demonstrate the obtained results on the elemental composition energy dependence.

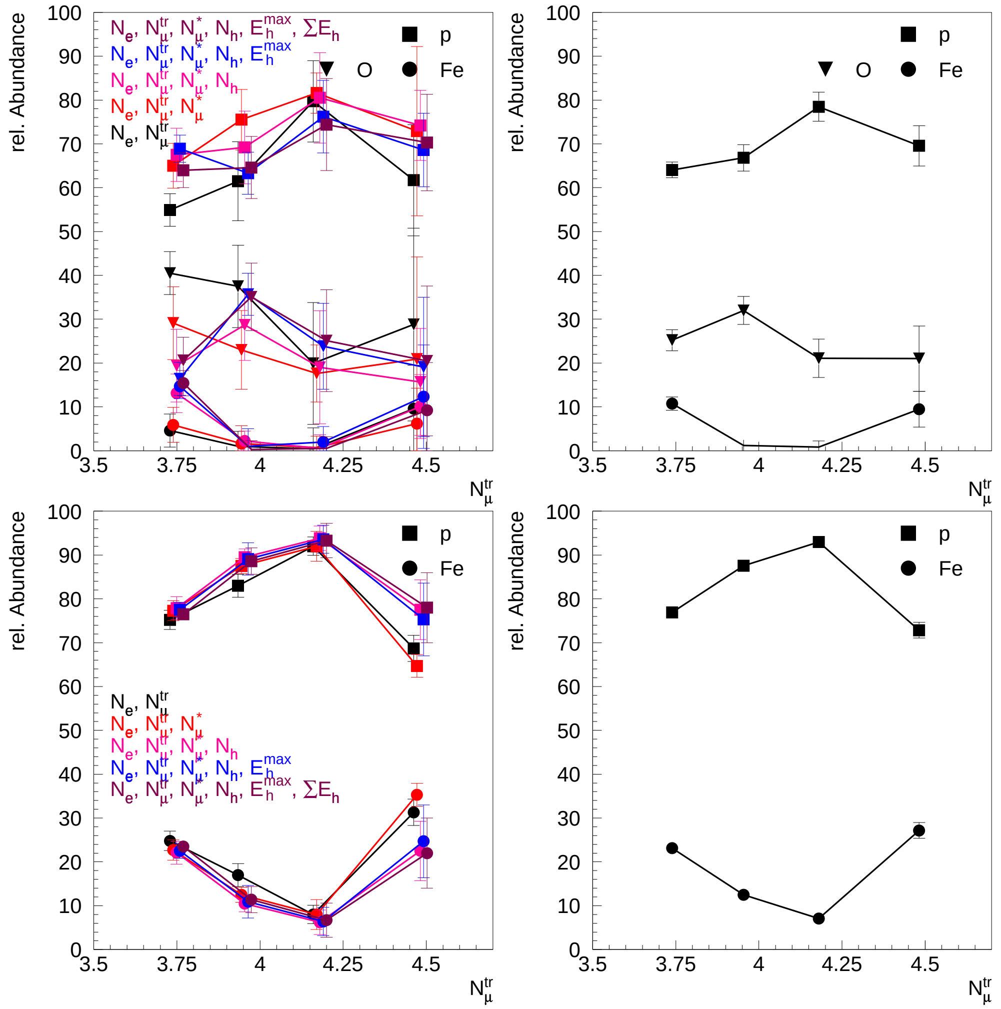

Figure 5.12: VENUS model: Reconstructed classification results using two (p, Fe) (lower graphs) and three (p, O, Fe) (upper graphs) classes for different sets of parameters.

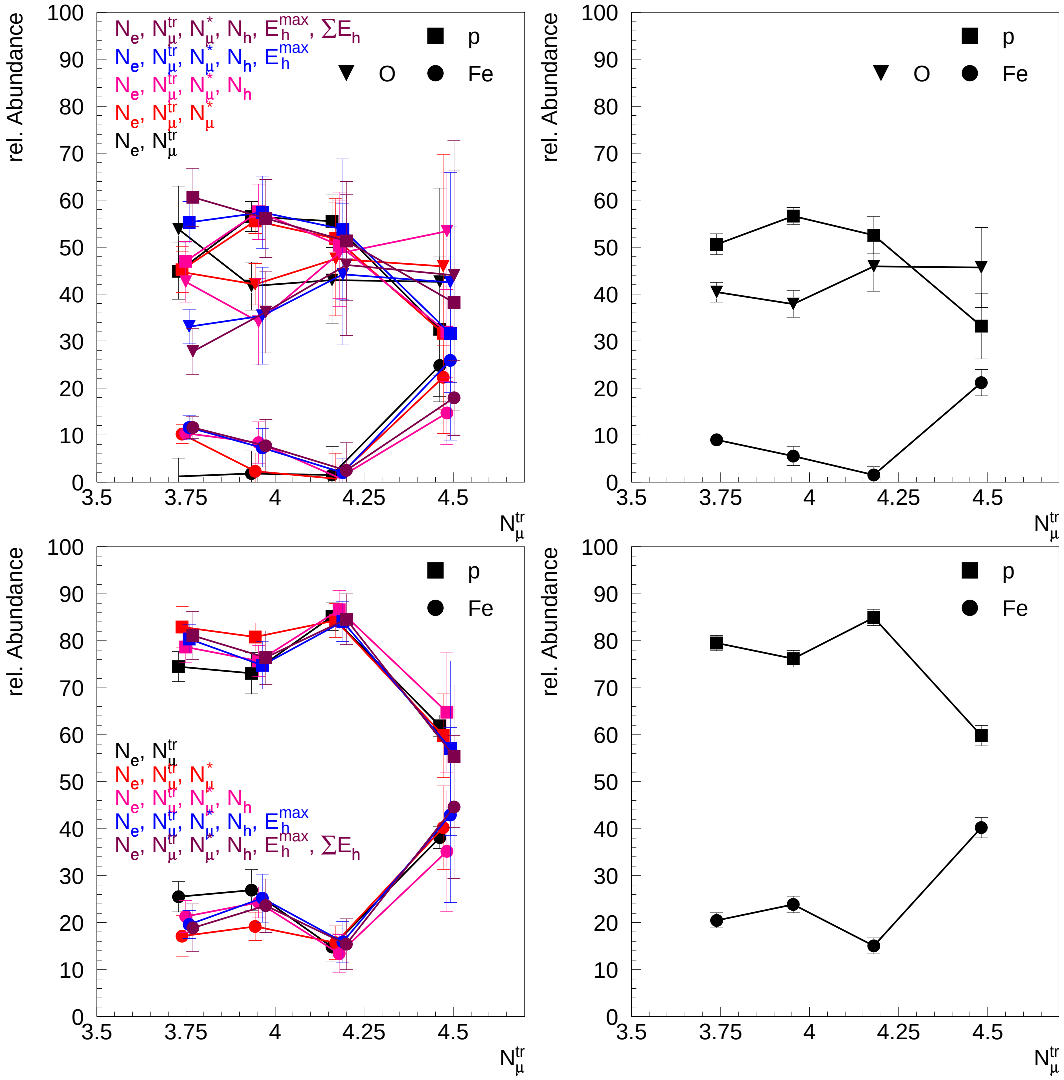

Figure 5.13: QGS model: Reconstructed classification results using two (p, Fe) (lower graphs) and three (p, O, Fe) (upper graphs) classes for different sets of parameters.

Table 5.22: $4.1 \leq lg_{10}\ N_\mu^{tr} \leq 4.4$, M_{TS}=150, M_{exp}=64

	%	stat. err.	meth. err.	model err.
P	52	±6	±2	±12
O	44	±3	±5	±12
Fe	4	±2	±2	±0.5

Table 5.23: $lg_{10}\ N_\mu^{tr} \geq 4.4$, M_{TS}=120, M_{exp}=20

	%	stat. err.	meth. err.	model err.
P	51	±11	±6	±18
O	33	±11	±10	±11
Fe	16	±8	±5	±6

Table 5.24: $4.1 \leq lg_{10}\ N_\mu^{tr} \leq 4.4$, M_{TS}=150, M_{exp}=64

	%	stat. err.	meth. err.	model err.
P	66	±11	±3	±7
Fe	34	±11	±3	±6

Table 5.25: $lg_{10}\ N_\mu^{tr} \geq 4.4$, M_{TS}=120, M_{exp}=20

	%	stat. err.	meth. err.	model err.
P	88	±5	±1	±3
Fe	12	±5	±1	±4

Table 5.26: $3.39 \leq lg_{10}\ N_\mu^{tr} \leq 3.65$, M_{TS}=555, M_{exp}=68420 (array)

	%	stat. err.	meth. err.	model err.
P	51	±0	±6	±6
O	42	±0	±11	±9
Fe	7	±0	±7	±1

Table 5.27: $3.65 \leq lg_{10}\ N_\mu^{tr} \leq 3.85$, M_{TS}=215, M_{exp}=56100 (array)

	%	stat. err.	meth. err.	model err.
P	51	±0	±6	±6
O	48	±0	±11	±7
Fe	1	±0	±7	±1

Table 5.28: 3.85 $\leq lg_{10}\ N_\mu^{tr} \leq$ 4.1, M_{TS}=140, M_{exp}=20400 (array)

	%	stat. err.	meth. err.	model err.
P	56	±0	±6	±6
O	44	±0	±11	±4
Fe	0	±0	±7	±2

Table 5.29: 4.1 $\leq lg_{10}\ N_\mu^{tr} \leq$ 4.4, M_{TS}=135, M_{exp}=7540 (array)

	%	stat. err.	meth. err.	model err.
P	63	±0	±8	±11
O	33	±0	±14	±12
Fe	4	±0	±8	±4

Table 5.30: $lg_{10}\ N_\mu^{tr} \geq$ 4.4, M_{TS}=110, M_{exp}=2285 (array)

	%	stat. err.	meth. err.	model err.
P	46	±1	±10	±12
O	46	±1	±14	±11
Fe	8	±0	±6	±8

5.3 The Examples of ANI Outputs

```
RUN BEGINS AT 26/04/98 12.39.06

ANALYSIS AND NONPARAMETRIC INFERENCE (ANI-98)
```

The platform is DEC Alppa workstation, 600 MHz CPU speed.
Revised version, May 1998, Karlsruhe.

```
JOB MODE - ONE-LEAVE-OUT-
```

Classification matrix calculation (3.29),
3.18.

```
JOB STATUS - noDENCURVE

DENSITY ESTIMATIORN MODE: PARZ
```

One of two available density estimators: PARZ or KNN

```
MAXIMAL EXPONENT 0.4000E+03
```

Maximal possible power index of exponent.

```
STRANGE EVENTS SELECTION, DENSITY < 0.1000E - 34
```

Bayes strengeness criterium (3.15).

```
Number of BOOTSTRAP replicas 10
```

Usually greater than 50, See (3.35)

```
Number of VARIABLES 3
```

Size of variables subset, $\mathbf{u}, \mathbf{v}$ dimensionality.

```
CONTROLE (EXPERIMENTAL) SAMPLE:

n01 REL. COORDINATES: 9800 1000 Selected: 0
```

From file **n01** 1000 events are read starting from 9800,
200 - from Gaussian population N(0,1), and 800 from -
N(1,1), those the fraction of "first type" events in
"experimental" sample is 0.2.

```
TRAINING SAMPLE:
n01 REL. COORDINATES: 1000 1000 Selected: 1000

n01 REL. COORDINATES: 11000 1000 Selected: 1000
```

The "pure" cases - samples from Gaussian populatios
N(0,1) and N(1,1), in file n01 there are 10000 five-dimensional
events of both kinds, any events could be selected.

```
Minimal and Maximal values of Training Sample

-0.2899E + 01 < X1 < 0.4073E + 01

-0.4220E + 01 < X2 < 0.3916E + 01

-0.4360E + 01 < X3 < 0.4432E + 01
```

Extremal values of each variable of selected samples.

```
SUPERIMPOSED BOUNDARIES:

-0.5000E + 01 < X1 < 0.5000E + 01

-0.5000E + 01 < X2 < 0.5000E + 01

-0.5000E + 01 < X3 < 0.5000E + 01

-0.5000E + 01 < X4 < 0.5000E + 01

-0.5000E + 01 < X5 < 0.5000E + 01
```

Selective "cuts" for each "measured" variable.
Restrictions on the $\mathcal{V}$ feature space

```
ONE-LEAVE-OUT- TEST OVER TRAINING SAMPLE

class  0.90  1.00  1.20  1.40  1.50  1.60  2.00 summ  ada

1 > 1  0.799 0.798 0.796 0.794 0.791 0.788 0.769 0.796 0.794
1 > 2  0.201 0.202 0.204 0.206 0.209 0.212 0.231 0.204 0.206

2 > 1  0.181 0.177 0.175 0.168 0.166 0.164 0.145 0.175 0.168
2 > 2  0.819 0.823 0.825 0.832 0.834 0.836 0.855 0.825 0.832
```

The parameters of the Parzen density estimator (kernel widths).
The **summ** is the mean estimate, **ada** - the L estimate -
median of ordered sequence of estimates.
Seven kernel widths are used.

Each row of this matrix represents the "classification" matrix
obtained with Bayes dicisicion rule (3.12) with
particularkernel width.

```
RUN FINISHS AT 26/04/98 12.39.21 CPU TIME 0.1512E+02
```

RUN BEGINS AT 26/04/98 12.39.30

ANALYSIS AND NONPARAMETRIC INFERENCE (ANI-98)

Experimental data classification.
Comparisons of exp.data with theoretical models.

JOB MODE - CLASSIFICATION

Minimal and Maximal values of Exp. Data
$-0.3161E+01 < X1 < 0.4054E+01$
$-0.3583E+01 < X2 < 0.3875E+01$
$-0.2320E+01 < X3 < 0.4420E+01$

Calculated extremal values of experimental data.

MEAN OF LOG-LIKELIHOOD RATIO (first/second)

$-0.501 - 0.457 - 0.383 - 0.325 - 0.302 - 0.281 - 0.217 - 0.360 - 0.329$

Calculated according (3.16), negative values
corresponds to the 2 class preference, positive - to the 1.

LOG-LIKELIHOOD FUNC. - exp. according to theor. models

class 0.90 1.00 1.20 1.40 1.50 1.60 2.00 *summ ada*

$1 > 1$ 5.162 5.171 5.227 5.324 5.384 5.449 5.741 5.308 5.332
$1 > 2$ 4.668 4.718 4.846 4.999 5.082 5.168 5.524 4.948 5.003

Negative of (3.17), the smallest values are
correspond to the best model.

MEAN VALUES OF BAYES ERROR AND PR. DISTANCES

R MAHALO R BHATA R CORR BAYES

1.548 0.204 0.041 0.267

Sampling estimates of probability distances
between experimental and model data (3.19), (3.26).

BAYSIAN CLASSIFICATION OF CONTROL SAMPLE

class 0.90 1.00 1.20 1.40 1.50 1.60 2.00 *summ ada*

$1 > 1$ 0.309 0.309 0.306 0.298 0.296 0.292 0.280 0.305 0.297
$1 > 2$ 0.691 0.691 0.694 0.702 0.704 0.708 0.720 0.695 0.703

Empirical fraction estimation by implementing Bayes ,
decision rules (3.31), $\mathbf{P}^e$

RECONSRUCTED PROPORTION OF 1 TYPE EVENTS

0.207 0.213 0.211 0.208 0.208 0.205 0.216 0.209 0.206

Reconstructed proportion of first type events (3.33),

$\hat{\mathbf{P}}$

SEPARABILITY MEASURE

0.654 0.657 0.657 0.661 0.660 0.659 0.657 0.657 0.661

THE ESTIMATED PROPORTIONS (CERM RQN PROGRAM)

class 0.90 1.00 1.20 1.40 1.50 1.60 2.00 *summ ada*

$1 > 1$ 0.207 0.213 0.211 0.208 0.208 0.205 0.216 0.209 0.206
$1 > 2$ 0.793 0.78 70.789 0.792 0.792 0.795 0.784 0.791 0.794

The solution of linear equations system (3.32).

RUN FINISHS AT 26/04/98 12.39.38 CPU TIME 0.7967E+01

```
RUN BEGINS AT 26/04/98 12.39.49

ANALYSIS AND NONPARAMETRIC INFERENCE (ANI-98)
```

Bootstrapisation of Bayes risk, classification rates and fraction estimates. Obtaining of fraction errors.

```
JOB MODE - BUTSTRAP

MEAN OF ONE-LEAVE-OUT-TEST

class  0.90  1.00  1.20  1.40  1.50  1.60  2.00 summ ada

1 > 1  0.804 0.804 0.801 0.797 0.792 0.789 0.773 0.801 0.796
1 > 2  0.196 0.196 0.199 0.203 0.208 0.211 0.227 0.199 0.204

2 > 1  0.183 0.182 0.180 0.174 0.171 0.167 0.157 0.179 0.173
2 > 2  0.817 0.818 0.820 0.826 0.829 0.833 0.843 0.821 0.827
```

The same as in ”ONE-LEAVE-... mode, but averaged over B bootsrap replicas, see section (3.3.7).

R^e_*

```
BOOTSTRAPIZATION OF CLASSIFICATION

class  0.90  1.00  1.20  1.40  1.50  1.60  2.00 summ ada

1 > 1  0.309 0.310 0.305 0.301 0.299 0.297 0.286 0.305 0.301
1 > 2  0.690 0.690 0.695 0.699 0.701 0.703 0.713 0.695 0.699
```

The same as in ”CLASSIFICATION” mode, but averaged over B bootsrap replicas, see section (3.3.7).

$\hat{\mathbf{P}}^e_*$

```
VARIANCE OF ONE-LEAVE-OUT-TEST

class  0.90  1.00  1.20  1.40  1.50  1.60  2.00 summ ada

1 > 1  0.019 0.020 0.025 0.029 0.033 0.036 0.053 0.025 0.029
1 > 2  0.019 0.020 0.025 0.029 0.033 0.036 0.053 0.025 0.029

2 > 1  0.013 0.015 0.019 0.025 0.028 0.032 0.047 0.020 0.025
2 > 2  0.013 0.015 0.019 0.025 0.028 0.032 0.047 0.020 0.025
```

The m.s.d. of emphirical risk estimates.

```
CLASSIFICATION VARIANCE

class  0.90  1.00  1.20  1.40  1.50  1.60  2.00 summ ada

1 > 1  0.010 0.010 0.015 0.020 0.022 0.025 0.042 0.016 0.020
1 > 2  0.010 0.010 0.015 0.020 0.022 0.025 0.042 0.016 0.020
```

The m.s.e. of proportion estimates, see section.

```
BOOTSTRAP AVERAGE OF RECONSTRUCTED PROPORTION

class  0.90  1.00  1.20  1.40  1.50  1.60  2.00 summ ada

1 > 1  0.2040.2060.2010.2040.2060.2090.2100.2030.205
1 > 2  0.7960.7940.7980.7960.7940.7910.7900.7970.795
```

Reconstruction of fraction for each bootsrap replica then averaging
see section (3.3.6).

$\hat{\mathbf{P}}_*$

```
SDE OF RECONSTRACTED PROPORTIONS

class  0.90  1.00  1.20  1.40  1.50  1.60  2.00 summ ada

1 > 1  0.0110.0120.0120.0130.0150.0180.0130.0120.014
1 > 2  0.0110.0120.0120.0130.0150.0180.0130.0120.014
```

The m.s.e. of reconstructed proportions

```
PROPORTIONS (AVERAGED RISKS AND CLASSIFICATIONS)

class  0.90  1.00  1.20  1.40  1.50  1.60  2.00 summ ada

1 > 1  0.2040.2060.2020.2040.2070.2100.2100.2030.205
1 > 2  0.7960.7940.7980.7960.7930.7900.7900.7970.795
```

Recostructed fractions with bootstrap mean classification and risks.

```
RUN FINISHS AT 26/04/98 12.45.38 CPU TIME 0.7967E+04
```

Bibliography

[1] R. Schlaifer, Probability and Statiatics for Buseness Decisions, Mc.Graw-Hill, New York (1959).

[2] H.Raifa, R.Schlaifer, Applied Statiatical Decision Theory, Harvard Univ., Boston (1961).

[3] J.O.Berger, The Robust Bayesian Viewpoint, in Robustness of Bayesian analyses, ed. Kadane J.B., Elsevier Science Publishers, (1984).

[4] W.Edwards, H.Lindman, L.J.Savage, Bayesian Statistical Inference, in Robustness of Bayesian analyses, ed. Kadane J.B., Elsevier Science Publishers, (1984).

[5] K.Fukunaga, Introduction to Statistical Pattern Recognition, Academic Press, Harcourt Brace Jovanovich Publishers, (1990).

[6] J.N.Friedman, Data analysis techniques for high-energy physics, CERN Yellow Report, (1974).

[7] P.J.Diggle and R.J.Gratton, Monte Carlo methods for implicit statistical models, J.R.Statist. Soc.B, v. 46 (1984), 193.

[8] J.D.Hey, An Introduction to Bayesian Statistical Inference, Martin Robertson, (1983).

[9] P.Desesquelles Multivariate analysis in Nuclear Physics, Ann.Phys. FR., v. 20, (1995), 1.

[10] E.A.Thompson, Monte Carlo Likelihood in Genetic Mapping, Stat. Science., v.9, (1994), 355.

[11] A.A.Chilingarian, The review of data analysis methods for ANI experiment, Voprosi Atomnoj NAuki i Tekhniki, ser. tech. fiz. exp., v. 2 (8), Kharkov, (1981), 59.

[12] A.A.Chilingarian, The development of of Statistical methods in Cosmic Ray physics, Proc. 18 ICRC, v. 5, Bangalore, (1983), 524.

[13] N.Z.Akopov, Sv.Kh. Arutunian, A.A.Chilingarian, S.Kh.Galfayan, V.Kh.Matevosyan, M.Z.Zazyan, The design principle and structure of ANI data center, Preprint EPI 819(46), 1985.

[14] V.V. Avakyan, A.A,Chilingarian. et al, Bayesian identification of cosmic ray flux hadrons with TRD detector of PION installation, Preprint EPI 933(84), 1986.

[15] A.A.Chilingarian, Statistical decisions under nonparametric a prior information, Computer PhysicsCommunications, v. 54, (1989), 381.

[16] A.A.Chilingarian, H.Z.Zazyan, A bootstrep method of distribution mixture proportion determination Pattern Recognition Letters v.11, (1990), 781.

[17] A.A.Chilingarian, Development of data processing methods in HEP, from a Data Base to a Knowledge Base, Preprint EPI 1327 (22), 1991.

[18] A.A.Chilingarian, Statistical inference in cosmic ray physics, combined analysis of simulated and experimental data, Proc. 22 ICRC v.3, Dublin, (1991), 34.

[19] A.A.Chilingarian, Zazyan H.Z., On the possibility of investigation of the mass composition and energy spectra of PCR in the energy range $10^{15} - 10^{17}$ eV using EAS data, IL Nuovo Cimento v. 14C (6), (1991), 555.

[20] A.A.Chilingarian, H.Z. Zazyan, Experiments with particle bundels in cosmic ray physics. Determination of strong interaction parameters by a pattern recognition method, J. of Nuclear. phys. (russion) 54, (1991), 128.

[21] A.Chilingarian, S.Ter-Antonyan, A.Vardanyan, The comparison of Bayesian and Neural techniques in problem of classification to multiple categories, NIM, v. NIMA 1063, (1997) 230.

[22] G.Schatz , W.D.Apel, K.Bekk, E.Bollmann, H.Bozdog, I.M.Bancus, M.Brendle, J.N.Capdevielle, A.Chilingarian, K.Daumiller, P.Doll, J.Engler, M.Foeller, P.Gabriel, H.J.Gils, R.Glasstetter, A.Haungs, D.Heck, J.R.Hoerandel, K.H.Kampert, H.Keim, J.Kempa, H.O.Klages, J.Knapp, H.J.Mathes, H.J.Mayer, H.H.Mielke, D.Muehlenberg, J.Oehlschlaeger, M.Petcu, U.Raidt, H.Rebel, M.Roth, H.Schieler, G.Schmalz, H.J.Simonis, T.Thouw, J.Unger, B.Vulpescu, G.J.Wagner, J.Wdowczyk, J.H.Weber, J.Wentz, Y. Wetzel, T.Wibig, T.Wiegert, D.Wochele, J.Wochele, D.Wochele, J.Zabierowski, S.Zagromski, B.Zeitniz,

The KASCADE Experiment, Nucl.Phys.B (Proc.Suppl.) v. 60B, (1998) 151.

[23] A.A.Chilingarian, A.M.Dunaevski, et al, Multivariate analysis of Roentgen-Emulsion chamber data, 19 ICRC, v. 5, San-Diego, (1985), 392.

[24] S.Kh.Galfayan, A.A.Chilingarian, A.M.Dunaevski, M.Z.Zazyan, et al, Multiple comparisons of EAS and Roentgen-Emulsion chamber data with simulations, Izv. AN.SSSR., ser. fiz., 50(11) (1986), 2146.

[25] A.A.Chilingarian, S.Kh.Galfayan, M.Z.Zazyan, A.M.Dunaevski, et al, The upper boundary of of iron nuclei fraction in PCR obtained from PAMIR data, 20 ICRC, v.1, Moscow, (1987), 386.

[26] A.A.Chilingarian, S.Kh.Galfayan, M.Z.Zazyan, A.M.Dunaevski, et al, The new method of gamma-families analysis, 20 ICRC, v. 5, Moscow, (1987), 312.

[27] S.Kh.Galfayan, A.A.Chilingarian, A.M. Dunaevski, M.Z. Zazyan, et al, The iron nuclei in primary cosmic rays by gamma-families data, Izv. AN.SSSR., ser. fiz., v. 53, (1989), 280.

[28] A.A.Chilingarian, S.Kh.Galfayan et al, Upper boundary of iron nucleiin primary cosmic rays at $E > 10^{16} eV$ Lebedev Institute preprint 75, 1988.

[29] G.Vacanti, M.F.Cawley, et. al., Gamma-ray observations of the Crab Nebula at TeV energies, Astroph. J. 377, (1991), 467

[30] M.Punch, C.W.Akerlof, M.F.Cawley et.al., Supercuts: an improved method of selecting gamma-rays, Proc. 22 ICRC v.1, Dublin, (1991), 464.

[31] F.A.Aharonian, A.A.Chilingaryan, A.K.Plyasheshnikov, A.K.Konopelko, On the possibility for a higher efficiency of discrimination of gamma-rays from point sources by the pattern recognition method, Preprint YerPhI 1171(48), 1989.

[32] F.A.Aharonian, A.A.Chilingaryan, A.K.Plyasheshnikov, A.K.Konopelko, Analysis of the possibilities of suppression of the cosmic-ray background when detecting very high energy cosmic gamma-quanta by means of a system of Cherenkov gamma-telescopes with multichannel light receivers, Preprint YerPhI 1277(60), 1990.

[33] F.A.Aharonian, A.A.Chilingaryan, A.K.Plyasheshnikov, A.K.Konopelko, On the possibility of an improvement of background hadronic showers discrimination against gamma-ray coming from a discrete source by a multidimensional Cherenkov light analysis, 21 ICRC, v. 4, Adelaide, (1990), 246.

[34] A.A.Chilingarian, M.F.Cawley, Multivariate analysis of Crab Nebula Data, Wipple Collaboration internal report, Wipple Collaboration internal report, 5 July, 1990.

[35] F.A. Aharonyan, A.A.Chilingarian, et al, A multidimensional analysis of the Cherenkov images of air showers induced by very high energy gamma-rays and protons, NIM, v. A-302, (1991), 522.

[36] F.A.Aharonian, A.A.Chilingarian, A.K.Plyasheshnikov, A.K.Konopelko, Use of multidimensional analysis for classification of events registered by the system of Cherenkov gamma telescopes with multichannel light receivers, Izv. Akademii Nauk, USSR, Phys.(russion) v.55, (1991), 734.

[37] A.A.Chilingarian, M.F.Cawley, Application of multivariate analysis to atmospheric Cherenkov imaging data from the Crab Nebula, Proc. 22 ICRC v.1, Dublin, (1991), 460.

[38] A.A Chilingarian, Neural Net Classification of the gamma and proton images registered with atmospheric Cherenkov technique, random search learning in feed-forward networks, Proc. 22 ICRC v.1, Dublin, (1991), 540.

[39] A.A.Chilingarian, A.K.Konopelko, A.V.Plyasheshnikov, New algorithms for gamma-quanta energy estimation by the telescopes with Cherenkov light imaging facilities, Proc. 22 ICRC v.1, Dublin, (1991), 480.

[40] A.A.Chilingarian, On the methods of the enhancement of the reliability of the signal detection with Cherenkov Atmospheric techniques, Izv. AN (ser. phys. (in russian) v.57, (1993), 186.

[41] F.A.Aharonian, A.A.Chilingaryan, R.G.Mirzoyan, A.K.Plyasheshnikov, A.K.Konopelko, The system of imaging atmospheric Cherenkov telescopes: the new prospects for VHE gamma ray astronomy, Exp. Astr. v. 2, (1993), 331.

[42] A.A.Chilingarian, M.FCawley, Optimizing the non-linear gamma-ray domain in VHE gamma-ray astronomy using neural-network classifier, Proc. 24 ICRC, v.3, Rome, (1994), 742.

[43] A.A.Chilingarian, Neural classification technique for background rejection in high energy physics experiments, Neurocomputing, v. 6 , (1994), 497.

[44] A.A.Chilingarian, Detection of weak signals against background using neural network classifiers, Pattern Recognition Letters, v. 16, (1995), 333.

[45] A.A,Chilingarian, E.H.Sevinian, S.A.Chilingarian, The non-linear signal domain selection using a new quality function in neural net training, NIM, v. A 389, (1997), 242.

[46] A.Chilingarian, M.,Halpaap, H.J.Gils, H.Rebel, A Comparative study of EAS energy estimation methods, Proc. 24 ICRC, v.1, Rome, (1995), 391.

[47] H.Rebel, G.Volker, M.Foller, A.A.Chilingarian, Arrival time distributions from extensive air showers as signature of the mass composition of cosmic rays, J.Phys. v. G: 21, (1995), 451.

[48] A.A.Chilingarian, S.Ter-Antonyan, A.Vardanyan, M.Roth, J.Knapp, H.J.Gils, H.Rebel, On the nonparametric classification and regression methods for the multivariate EAS data analysis, Nuclear.Phys. B, v. 52B, (1997), 237.

[49] H.Rebel,M.Roth, J.Knapp, H.J.Gils,A.Chilingarian, S.Ter-Antonyan, A.Vardanyan, On the accuracy of the elemental composition determination on the mountain altitudes and sea level, Nuclear Phys. B., v. 52B, (1997), 240.

[50] I.M.Brancus, B.Vulpesku, H.Rebel, M.Duma, A.A.Chilingarian, Correlated features of arrival time and angle-of-incidence distributions of EAS muons, Astroparticle Physics, v. 7, (1997), 343.

[51] A.A.Chilingarian for KASCADE Collaboration, S.Ter-Antonyan, A.Vardanyan, How to infer the mass composition from EAS observations demonstarated with KASCADE data, 25 ICRC, v. 4, Durban, (1997), 105.

[52] M.Roth for KASCADE collaboration, S.Ter-Antonyan, A.Vardanyan, How to infer the primary energy spectrum from EAS observations demonstarated with KASCADE data, 25 ICRC, v. 4, Durban, (1997), 157.

[53] A.A.Chilingarian, S.Ter-Antonyan, A.Vardanyan, M.Roth, H.J.Gils, J.Knapp, H.Rebel, Energy Spectra and Elemental Composition Determination on Mountain Altitudes and Sea Level, Nucl. Phys. B. v. 60B (1988) 117.

[54] Capdevielle J.N. et al., 1992, KfK Report 4998, Kernforschungszentrum Karlsruhe. J.Knapp and D.Heck, 1993, KfK Report 5196B, Kernforschungszentrum Karlsruhe. D.Heck, J.Knapp, J.N.Capdevielle, G.Schatz, T.Thouw, 1998, FZKA Report 6019, Forschungszentrum Karlsruhe.

[55] J.Knapp, 1997, Rapporteur talk, Proc. 25 th ICRC, Durban , 1997 (in publication).

[56] S.G,Bayburina et al, Nucl.Phys. B v. 391, (1981)1.

[57] J.R.Ren, Phys. Rev. D v. 38, (1988), 1404.

[58] L.T.Baradzei et al, Nucl.Phys. v. B 370, (1992)365.

[59] T.K.Gaiser et al, Phys.Rev. v.D 47, (1993), 1919.

[60] N.Hayashida et al, Proc. 25 th ICRC, v. 6, (1997), 241.

[61] GEANT, 1993, CERN program library, CERN.

[62] A.A. Watson, Charged Cosmic Rays above 1 TeV, Rapporteur talk: 25 ICRC, Durban (1997).

[63] Jaynes E.T., in Foundations of Probability Theory, Statistics Inference and Statiustical Theories of Science, ed. W.L.Harper, C.A. Hooker, Dordrecht, Rewidel.

[64] W.H.Press, S.A.Teukolsky, et al., in Numerical Recipes in Fortran, chapter15.7, Cambridge Univ. Press.

[65] A Source Code Management System, user's guide and reference manual, version 1.46, CERN 1994.

[66] E.Lederman, Handbook of Applied Mathematics, Statistics, John Wiley and Sons, New-York, (1984).

[67] P.Hajek ,T.Havranek, Mechanizing Hypothesis Formation, Springer Verlag, Heidelberg, (1979).

[68] G.E.P.Box, The importance of practice in the development of statistics, Technometrics, 26 (1984), 1.

[69] E.A.Eadie, D.Drijard, F.E.James, M.Ross and B.Sadoulet, Statistical methods in experimental physics, North-Holland, Amsterdam, (1971).

[70] S.Zacks, The theory of statistical inference, John Wiley and Sons,New-York, (1977).

[71] D.V.Lindley, Bayesian statistics, Soc.for indust. and appl. math.,Philadelphia, (1978).

[72] G.T.Toussaint , Bibliography of misclassification, IEEE trans. on Information v.IT-20 (1974), 472.

[73] S.M.Snappin, J.D.Knoke, Classification error rate estimators evaluated by unconditional mean squared error, Technometrics, v.26 (1984), 371.

[74] B.Efron, Nonparametric standart errors and confidence intervals, Canadian J. Statist., v. 9 (1981), 139.

[75] L.Devroye, L.Gyorfi, Nonparametric density estimation. The L1 view, Jown Wiley and Sons, New-York, (1985).

[76] L.Devroye, Universal smothing factor selection in density estimation: theory and practice, Technical report, McGill Univ., (1997).

[77] M.Rosenblatt, Remarks on some nonparametric estimates of a density function, Ann. Math. Stat., v. 27, (1957), 832.

[78] E.Parzen, On estimation of a probability density function and mode, Ann. Math. Stat., v. 33, (1962), 1065.

[79] E.Fix, J.L.Hodges, Discriminatory analysis. Nonparametric discrimination, Consistency Properties Project 21-49-004, Report 4,USAF School of Aviation Medicine, Randolf Field, Texes, (1951).

[80] D.O.Lofsgaarden and C.D.Quesenberry, A nonparametric estimate of a multivariate density function, Ann. Math. Stat., v. 36, (1965), 1049.

[81] P.C.Mahalonobis, On the generalized distance in statistics, National Inst.of India, v. 2, (1936), 49.

[82] R.A.Tapia,J.R.Thompson, Nonparametric probability density estimation, The John Hopkins University Press, Baltimore and London, (1978).

[83] K.Fukunaga, D.Himmels, Bayes error estimation using Parzen and KNN procedures, v. PAMI9, (1987), 634.

[84] L.R.Rabiner, E.Levinson, A.E.Rozenberg and J.G.Wilpon, Speaker - independent recognition of isolated words using clustering techniques, IEEE trans. on Acoustics, Speech, Signal Processing, v. ASSP-27, (1974), 336.

[85] A.A.Chilingarian and S.Kh.Galfayan, Calculation of Bayes risk by KNN method, Stat. Problems of Control,Vilnius, v. 66, (1984), 66.

[86] Deutsche Bundesbank, 10 DM banknote, 1949-2001.

[87] B.Efron, Bootstrap methods, another look at the jacknife, Ann. Statist., v. 7, (1979), 1.

[88] A.K.Jain, R.C.Dubes and C-C.Chen, Bootstrap Techniques for error estimation, IEEE Trans., v. PAMI-9, (1987), 628.

[89] P.J.Bickel, D.A.Freedman, Some Asymptotic Theory for the Bootstrap, Ann. Stat. v.9, (1981), 1198.

[90] G.A.Young, Bootstrap: more than a stab in the dark? Stat. Science, v. 9, (1994), 382.

[91] D.W.Ruck, K.S. Rogers et al, The Multilayer Perceptron as an Approximation to a Bayes Optimal Discriminant Function, IEEE Trans. on Neural Networks v.1, (1990), 296.

[92] S.N. Zhang, D.Ramsden, Statistical data analysis for g-ray astronomy, Exp. Astronomy v.1, (1990), 158.

[93] C.Paladin, A.Vulpiani, Anomalous Scaling Laws in Multifractal Objects, Phys.Rep., v.156, No.4, (1987)

[94] K.Pawelzik, H.S.Shuster, Generalized dimensions an entropies from a measured time series, Phys.Rev.A, v.35, (1987) 481.

[95] J.G.Caputo, P.Atten, Metric entropy : an experimental means for characterizing and quantifying chaos, Phys.Rev.A, v. 35, (1987) 1311.

[96] K.W.Pettis, T.A.Baily, A.K.Tain, R.C.Dubes, An Dimensionality Estimator from Nearest Neighbour Information. IEEE Trans. on Pattern Anal. and Machine Intelligence, v. PAMI1, (1979), 25.